Evaluating the potential of improved spatial resolution for remote sensing of chlorophyll-a in coastal and inland waters

By

James Matthew Bramich

Bachelor of Engineering, Master of Arts (Hons), Graduate Diploma of Education,

Graduate Diploma of Applied Science (Marine Environment)

Institute of Marine and Antarctic Studies

Submitted in fulfilment of the requirements for the degree of

Doctor of Philosophy

University of Tasmania March 2019

Declaration of originality

This thesis contains no material which has been accepted for a degree or diploma by the University or any other institution, except by way of background information and duly acknowledged in the thesis, and to the best of my knowledge and belief no material previously published or written by another person except where due acknowledgement is made in the text of the thesis, nor does the thesis contain any material that infringes copyright.

Authority of access / Statement regarding published work

The publishers of the papers comprising chapter 2 hold the copyright for that content and access to the material should be sought from the respective journals. The remaining non-published content of the thesis may be made available for loan and limited copying and communication in accordance with the Copyright Act 1968.

Signed:

James M Bramich

Statement of Co-authorship

The following people and institutions contributed to the publication of work undertaken as part of this thesis:

Candidate: James Bramich, Institute of Marine and Antarctic Studies (IMAS), University of Tasmania

Author 1: Dr Christopher Bolch, University of Tasmania, Supervisor

Author 2: Dr Andrew Fischer, University of Tasmania, Primary Supervisor

Author details and their roles:

Paper 1, Bramich, J. M., Bolch, C. J., & Fischer, A. M. (2018). Evaluation of atmospheric correction and high-resolution processing on SeaDAS-derived chlorophyll-a: an example from mid-latitude mesotrophic waters. *International Journal of Remote Sensing*, *39*(8), 2119-2138

Located in chapter 2. Candidate was the primary author responsible for data collation, analysis and manuscript preparation. Author 1 and author 2 contributed to concept formalisation and development and editorial support.

We the undersigned agree with the above stated "proportion of work undertaken" for each of the above published (or submitted) peer-reviewed manuscripts contributing to this thesis:

Signed:	_____	_____
	Dr. Andrew Fischer	Prof. Craig Johnson
	Supervisor	Head of Centre
	Ecology and Biodiversity	Ecology and Biodiversity
	IMAS	IMAS
	University of Tasmania	University of Tasmania
Date:	9th April, 2019	8th May, 2019

Abstract

Remote estimation of the photosynthetic pigment chlorophyll-a (chl-a), which can be used as an indicator of algal biomass has numerous applications, including to assist in the detection and monitoring of algal blooms. Harmful algal blooms pose a threat to human and ecosystem health and are increasing globally. Algal blooms impact socially and economically important inland and coastal waters, they exhibit large spatial variability and effective monitoring regimes pose a challenge for water managers. Chapter 1 contains a discussion of how satellite remote sensing of chl-a can assist in the detection and monitoring of such blooms. Chl-a algorithms developed for oceanic waters can be confounded by dissolved organic matter and turbidity common to inland and nearshore waters. Such waters of interest are often too small to be resolved by satellite platforms initially designed for global ocean applications. This thesis examines the capability of platforms of varying spatial resolution to detect increases in algal biomass through the remote estimation of chlorophyll-a.

Chapter 2 contains an evaluation of the effectiveness of a high-resolution processing mode for Moderate Resolution Imaging Spectroradiometer (MODIS) derived chlorophyll-*a* retrieval algorithms in the coastal waters of Tasmania, Australia. Three aerosol correction models and chl-*a* retrieval algorithms were evaluated using both standard and high-resolution processing. Chl-*a* retrievals were evaluated in Bass Strait. Chlor_a, the default SeaDAS chl-*a* product, with the Management unit of the North Sea Mathematical models (MUMM) aerosol correction algorithm performed best (RMSE = 0.09 mg m^{-3}; MAPE = 34%; R^2 = 0.75). The fluorescence line height algorithm using Rayleigh corrected top of atmosphere reflectances (RMSE = 0.11 mg m^{-3}, MAPE = 41%, R^2 = 0.61) can provide an acceptable alternative in waters where full atmospheric

correction is problematic. High-resolution processing of MODIS imagery improved spatial resolution but reduced chl-*a* retrieval accuracy.

In Chapter 3, the capability of Landsat 8 operational land imager (OLI) was evaluated for detection and quantification of algal blooms in inland lakes. A partial least squares regression (PLSR) derived algorithm was calibrated and validated against *in-situ* chl-*a* estimates from Lake Trevallyn in Tasmania, Australia. The algorithm was developed against a calibration subset of the data and able to provide chl-a estimates strongly correlated with *in-situ* values when applied to the validation dataset (n = 10, NRMSEP = 21.6%; R^2 = 0.67; NSE = 0.53; bias = -0.03 μg/L). These results demonstrate the suitability of PLSR algorithms and Landsat 8 OLI imagery to complement the capability of *in-situ* instrumentation for local water quality monitoring applications.

The Sentinel 2 platform, with bands sampled to a spatial resolution of 20 m, was evaluated in Chapter 4. An improved semi-analytical model for chlorophyll-a (chl-a) retrievals was created by replacing a fixed chl-a specific absorption coefficient (*a**) with a variable model. This method was applied to three Sentinel 2 images taken over the Lake Erie's western basin correlating with an *in-situ* dataset of 24 samples. The improved algorithm produced chl-a retrievals with a 23% reduction in root mean squared error of prediction, an 85% reduction in bias and an increase in Nash-Sutcliffe efficiency of 7% over the default algorithm using a fixed *a** value. The resulting strong correlation between *in-situ* and estimated chl-a (r = 0.95) suggests that the Sentinel 2 platform could be effective in the detection and mapping of high biomass algal blooms.

In Chapters 2 to 4, clouds and the accuracy of atmospheric correction were identified as potential obstacles to the use of satellite platforms. Digital cameras found in mobile devices can be deployed below clouds and imagery is much less prone to atmospheric

effects. In chapter 5, chl-a retrieval algorithms were developed for the University of Maine's HydroColor app using partial least squares regression with band ratio inputs indicative of optically active water constituents. The app estimates remote sensing reflectance (R_{rs}) in the red, green and blue bands and derives turbidity and suspended particulate matter. The models were evaluated against a dataset of 49 HydroColor image sequences along with *in-situ* chl-a and turbidity measurements collected over a one-year period. The chl-a algorithm using the ratio of R_{rs}(blue)/ R_{rs}(green) was a poor predictor of *in-situ* chl-a (R^2 = 0.11; bias = 0.21 mg m^{-3}; NSE = -0.02). Adding inputs representing absorption due to CDOM and turbidity improved algorithm performance (R^2 = 0.56 to 0.60; bias = 0.11 to 0.15 mg m^{-3}; NSE = 0.39 to 0.46). The resulting algorithms appear capable of detecting relative changes in chl-a concentration, however would benefit from further development before being applied to active bloom detection and monitoring systems.

The outcomes of the research demonstrate that recently deployed satellite platforms, particularly Sentinel 2, have the capability to improve bloom detection and monitoring. Sentinel 2's 20m spatial resolution and 5-day revisit time could provide regular mapping of chl-a concentration in the many nearshore and inland waters that could not previously be resolved by platforms designed for global ocean applications. Such data could complement existing manual sampling regimes and *in-situ* instrumentation to identify blooms and further understand bloom dynamics. Digital cameras already have the potential to detect changes in chl-a concentration. If this can be further improved, then both regular and "on-demand" mapping of bloom areas could be performed using unmanned aerial vehicles at an even greater spatial resolution than available on satellite platforms.

Table of Contents

List of Tables

List of Figures

1 Introduction

1.1 Rationale

Chlorophyll-a (chl-a) is a photosynthetic pigment present in all organisms involved in primary production, including photosynthetic phytoplankton. Chl-a concentrations can therefore be used as an indicator of overall phytoplankton biomass. The ability to monitor the quantity and distribution of phytoplankton is of great importance to the scientific community for several reasons: photosynthesis plays a key role in the global carbon cycle, which has implications further understanding of climate change (Antoine, 2006), phytoplankton are the basis of marine food webs (Garrison, 2007) and, as phytoplankton growth is also dependent on nutrients such as nitrogen and phosphorus, chl-a levels can be used as an indicator of water quality in coastal and inland areas (Bricker et al., 2003). Furthermore, degradation of water quality can lead to harmful algal bloom (HAB) events.

HAB events occur when a sudden increase in the population of one or more species of microalgae, due to favourable growth conditions (Masó and Garcés, 2006), has a negative impact on human health, socioeconomic interests or the surrounding ecosystem (Anderson et al., 2012). HAB events may be either toxic or non-toxic. Toxic bloom events may lead to the contamination of shellfish, among other species, which pose severe threats to human health (Anderson et al., 2017, 2012; Ibelings et al., 2014; World Health Organization, 1999). Non-toxic events may have damaging ecosystem consequences such as oxygen depletion and food web disturbances (Masó and Garcés, 2006; Shen et al., 2012). In addition to the threats that HABs pose to public health, there are also economic costs associated with commercial fisheries, recreation and tourism and monitoring and management (Anderson et al., 2012; Hoagland et al., 2002).

Tasmania, Australia's southernmost state, illustrates many of these challenges. Its coastal and inland waters are of significant importance to the region. The commercial fishing sector alone is worth nearly $600 million per year and employs over two thousand people (Skirtun et al., 2012). Around the coasts, two marine dinoflagellates, *Gymnodinium catenatum* and *Alexandrium tamarense* are known to produce paralytic shellfish toxins (Negri et al., 2003). Shellfish farms in the Huon estuary suffer intermittent closures due to blooms of *G. catenatum* (Skerratt et al., 2002) and recreational rock lobster fisheries regularly close on much of the East coast due to *A. tamarense* (DPIPWE, 2013). Tasmania's inland waters are also susceptible to HABs. Lake Trevallyn, a hydroelectric storage reservoir in the state's north is a local source of drinking water and hub for recreational activities, both usages have been affected by blooms of *Anabaena circinalis*. Craigbourne Dam, a reservoir for rural irrigation in the south-east, has also seen blooms of *A. circinalis*, which prevent distribution of water resources (DPIF, 1997; Hydro Tasmania, 2014).

Reliable monitoring networks are necessary in reducing the economic and human health effects of harmful algal blooms (Masó and Garcés, 2006). Fixed monitoring stations with periodic water sampling are inadequate for HAB monitoring. Remote sensing technology can help with biomass quantification and bloom detection and mapping (Kutser, 2009) through the remote retrieval of chl-a (Anderson et al., 2017). Remote sensing of chl-a alone cannot distinguish less harmful from harmful blooms, but can assist water managers focus limited resources appropriately, thus development of algorithms for estimation of chl-a and subsequently algal biomass are a high research priority (Beck et al., 2016).

1.2 Chlorophyll-a retrieval

Remote estimation of ocean chl-a content is possible because its electromagnetic absorption and scattering characteristics are different to those of water. Remote sensing applications typically derive the water leaving radiance (L_w), radiance reflectance (ρ_w), or remote sensing reflectance (R_{rs}) and estimate concentrations of in water constituents based on band combinations of reflectance, or algorithms. Empirical algorithms are developed through statistical relationships of optically active constituents with remotely sensed spectral data, while analytical algorithms aim to determine constituent level by solving the radiative transfer equation. As physics based models can be used as regressors and some analytical algorithms make use of empirically derived constants, many algorithms are classified as either semi-empirical or semi-analytical (Odermatt et al., 2012). The relationship between the remote sensing reflectance and the inherent optical properties of the waterbody can be expressed by (Gitelson et al., 2008; Gordon et al., 1988):

$$R_{rs} \propto f \frac{b_b}{a + b_b} \qquad (1\text{-}1)$$

Where f is an empirical factor dependent on the geometry of the light field, a is the total absorption coefficient and b_b is the backscattering coefficient. Each term above is dependent on wavelength, λ, however this dependency is frequently omitted for readability. The total absorption and backscattering coefficients can in turn be expressed in terms of the contributions of the optically active constituents of water (Stramski et al., 2004):

$$\underline{a} = a_w + a_{ph} + a_{cdom} + a_d \qquad (1\text{-}2)$$

$$b_b = b_w + b_{ph} + b_{cdom} + b_d \qquad (1\text{-}3)$$

where the subscripts *w*, *ph*, *cdom* and *d* represent the contributions of water, phytoplankton, CDOM and detrital matter respectively.

Established empirical algorithms use band ratios between the blue part of the spectrum, where light is absorbed by chl-a, and the green, where it is reflected. These algorithms have been parameterised for multiple satellite platforms and are often collectively referred to as the ocean colour (OCx) algorithms (O'Reilly et al., 2000, 1998). The OCx algorithms provide adequate results in the estimated ninety-five percent of the world's oceans classified as case 1 waters. In case 1 waters, variations in the water leaving radiance signal are mostly correlated with concentrations of chl-a. In case 2 waters, factors such as the sea bottom, turbidity and coloured dissolved organic matter (CDOM) all affect the water leaving radiance signal (Morel and Prieur, 1977). Such waters include many inshore and coastal waters where chl-a retrieval algorithms based on blue/green ratios often perform poorly (Gilerson et al., 2009; Gin et al., 2002; Gohin et al., 2002) and can severely over-estimate chl-a levels (Darecki and Stramski, 2004; Dierssen, 2010; Gohin et al., 2002).

One alternative to blue/green algorithms is to utilise the chl-a fluorescence. The fluorescence line height (FLH) algorithm is an example of a spectral shape algorithm: one that measures a spectral peak or trough against a baseline established from neighbouring bands (Matthews and Odermatt, 2015; Wynne et al., 2008). FLH measures chl-a fluorescence peak height at approximately 685 nm and provides a linear indicator of chl-a concentration (Gower et al., 1999). The FLH algorithm may be applied to satellite imagery without full atmospheric correction (Gower and King, 2007). FLH has been shown to be well correlated with chl-a at concentrations up to 20 mg m^{-3} (Gower et al., 1999), however it has a smaller effective range, chl-a

concentrations up to 4 mg m^{-3}, in waters where the concentration of non-algal particles is greater than 5 mg m^{-3}. This decrease in effectiveness is due to the combined effects of CDOM and minerals that decrease photosynthetically available radiation and absorb the fluorescence signal within the water column (Gilerson et al., 2008, 2007). In cyanobacteria dominated waters, where much of the chl-a is in the non-fluorescing photosystem (Seppälä et al., 2007), FLH can be negative and forms the basis for the cyanobacteria index (Wynne et al., 2010, 2008).

Phytoplankton cause a peak in spectral reflectance near 700 nm due to minimal combined absorption due to water and phytoplankton (Gitelson, 1992; Gurlin et al., 2011). Dall'Ollmo and Gitelson (2005) use three wavelengths around this red edge peak to try to isolate absorption due to chl-a.. For each, wavelength, λ_1 is between 660 nm to 672 nm, λ_2 is between 700 nm and 710 nm and λ_3 is greater than 740 nm. Band selection is such that λ_1 is positioned for maximum absorption due to chl-a while λ_2 is chosen for minimal absorption, but near enough to λ_1 to predict absorption due to water and other constituents at λ_1. λ_3 is chosen in the near infrared (NIR) where total absorption at λ_3 is dominated by water and assumed to be constant (Dall'Olmo and Gitelson, 2005) leading to a three-band difference algorithm where:

$$R_3 = [R_{rs}^{-1}(\lambda_1) - R_{rs}^{-1}(\lambda_2)].R_{rs}(\lambda_3) \qquad (1\text{-}4)$$

R_3 has been calibrated to in-situ chl-a using both linear (Gitelson et al., 2008; Moses et al., 2009) and quadratic (Gitelson et al., 2009; Mishra and Mishra, 2012) models. This algorithm has also been the basis for algorithms using two (Gitelson et al., 2008; Gurlin et al., 2011) or four (Le et al., 2009) bands in the red and NIR.

Gons' (1999) semi-empirical algorithm uses three bands similarly located around the red edge reflectance peak do derive absorption due to chl-a and in turn chl-a concentration. The algorithm is based on the assumption that:

$$a_{ph}(\lambda) \approx a_{chl}(\lambda) \qquad (1\text{-}5)$$

and:

$$a_{chl}(\lambda) = C\, a^*(\lambda) \qquad (1\text{-}6)$$

where $a^*(\lambda)$ is the chl-a specific absorption coefficient at a given wavelength and C is the concentration of chl-a. He was able to derive the following formula for estimating chl-a using equations 1-7 and 1-8:

$$C = \frac{R(a_w(\lambda_2) + b_b) - a_w(\lambda_1) - b_b{}^p}{a^*(\lambda_1)} \qquad (1\text{-}7)$$

$$b_b = \frac{a_w(\lambda_3)\rho_w(\lambda_3)}{0.082Q - \rho_w(\lambda_3)} \qquad (1\text{-}8)$$

where R is the ratio of water surface reflectance (ρ_w) at each wavelength, a_w at all wavelengths is from (Buiteveld et al., 1994), p is an empirically derived constant and Q is a geometric factor dependent on the light field. Backscattering coefficient, b_b is assumed to be spectrally flat (Gons, 1999). A fully parametrised version of this algorithm is described in Chapter 4 (equations 4-2 and 4-3).

The algorithms that utilise red and NIR, or “red-edge” are less sensitive to CDOM (Gin et al., 2002; Gitelson et al., 2008; Gohin et al., 2002). However, such algorithms are not universally effective, Gons’ three band model (Gons, 1999; Gons et al., 2008, 2005, 2002) has been shown in different studies to both generally underestimate chl-a (Gurlin et al., 2011), or to overestimate at lower concentrations (Gitelson et al., 2008; Gons et

al., 2008). Other three band models in the red/NIR spectrum have been shown to be either inferior (Gurlin et al., 2011) or superior (Gilerson et al., 2010; Gitelson et al., 2011) to two band models. These discrepancies can be explained to some extent by the variation in the optical properties of the water bodies to which they have been applied. Chl-a specific absorption by phytoplankton is not constant and has been shown to vary according to algal type (Ahn et al., 1992), size (Ciotti and Bricaud, 2006) and concentration (Bricaud et al., 1995).

Analytic approaches to solving the radiative transfer equations include HydroLight (Mobley and Sundman, 2013), HYDROPT (Van Der Woerd and Pasterkamp, 2008) or spectral inversion techniques such as matrix inversion methods (Brando and Dekker, 2003; Campbell et al., 2011). Analytic approaches are in theory more transferable (Odermatt et al., 2012), however numerical approaches can be slow when applied to every pixel of a satellite image and both numerical and inversion methods require known specific inherent optical properties for the water body in question and accurate atmospheric correction (Brando and Dekker, 2003).

The above is not an extensive review of chl-a retrieval algorithms. The intention is not to review each of the algorithm types, but to describe the rationale behind algorithm development and illustrate some of the challenges faced. Those not covered to this point include artificial neural networks (Amanollahi et al., 2017; Guo et al., 2016; Schiller and Doerffer, 1999), partial least squares (Ali and Ortiz, 2016; Blix and Eltoft, 2018; Song et al., 2013) and various other approaches (Concha and Schott, 2016; Lim and Choi, 2015; Mishra and Mishra, 2012; Sakuno and Kunii, 2015). It is broadly acknowledged that most empirical algorithms will need to be regionally validated and/or tuned before they can be reliably applied to new water bodies (Dierssen, 2010;

Gilerson et al., 2010; Gin et al., 2002; Gitelson et al., 2008; Schiller and Doerffer, 1999) and that local specific inherent optical properties need to be determined before analytic approaches can be applied (Brando and Dekker, 2003; Campbell et al., 2011). To that end, further validation and enhancement of existing algorithms could be seen to advance the field of remote sensing.

1.3 Aims of this thesis

In the broad sense, remote sensing may include satellite platforms with coverage of large spatial scales down to hand held devices for the rapid detection of bloom conditions (Kutser, 2009). Satellite platforms typically used for oceanic remote sensing are limited in spatial resolution and are not able to resolve the vast majority of the worlds inland waters (Clark et al., 2017; Palmer et al., 2015; Verpoorter et al., 2014) while chl-a concentrations during cyanobacterial blooms can vary several orders of magnitude in a single pixel (Kutser, 2004). Smaller water bodies of importance include many drinking water reservoirs (Beck et al., 2016). The primary goal of this thesis is to investigate and improve the remote sensing of chl-a in inland and coastal waters in a way that may assist in the detection and monitoring of HABs. To this end the capabilities of platforms of several spatial resolutions will be evaluated on their potential for the remote sensing of chl-a, this will involve evaluation and calibration of existing algorithms as well as investigating the potential for new approaches:

- Chapter 2: The effect of high-resolution processing mode on chl-a retrievals will be investigated for the National Aeronautics and Space Administration's (NASA) moderate resolution imaging spectrometer (MODIS) platform.

- Chapter 3: A partial least squares regression (PLSR) type algorithm will be evaluated for the Landsat 8 operational land imager (OLI).
- Chapter 4: An improved version of Gons' (1999) semi-analytical chl-a retrieval algorithm will be validated against Sentinel 2 imagery.
- Chapter 5: PLSR will be used to develop a chl-a retrieval algorithm for the University of Maine's HydroColor app, which allows mobile devices such as phones and tablets to derive remote sensing reflectance from a sequence of images (Leeuw and Boss, 2018).

MODIS has bands with spatial resolutions of 250 m pixel^{-1}, 500 m pixel^{-1} and 1000 m pixel^{-1}. The bands designated for ocean colour monitoring have a spatial resolution of 1000 m pixel^{-1} (NASA, 2014). MODIS imagery can be processed to a spatial resolution of 250 m pixel^{-1} for all bands through interpolation (Franz et al., 2006), however the effect of such processing on the quality of chl-a retrievals has not been extensively evaluated. In chapter 2, we investigate the capability of high-resolution processing to improve monitoring of coastal waters by comparing the accuracy of chl-a retrievals using a variety of atmospheric correction and chl-a retrieval algorithms at both standard and high resolution.

With regards inland waters, this project has coincided with the launch of two medium resolution platforms: NASA and the United States Geographical Survey's (USGS) Landsat 8 operational land imager (OLI) and the ESA's Sentinel 2 multi spectral imager (MSI). Landsat 8 was launched in early 2013 just prior to the commencement of this project and has a native spatial resolution in most bands of 30 m pixel^{-1} (USGS, 2016). The Sentinel 2 constellation consists of two satellites equipped with MSI instruments. Sentinel 2A was launched in June 2015 and Sentinel 2B was launched in

March 2017. The MSI has bands with native spatial resolutions of 10, 20 and 60 m pixel^{-1} (ESA, 2018). Figure 1-1 (Bresciani et al., 2018) shows the relative positioning and spatial resolution of OLI and MSI bands and chapters 3 and 4 assess the capability of these platforms for the remote sensing of chl-a in inland waters.

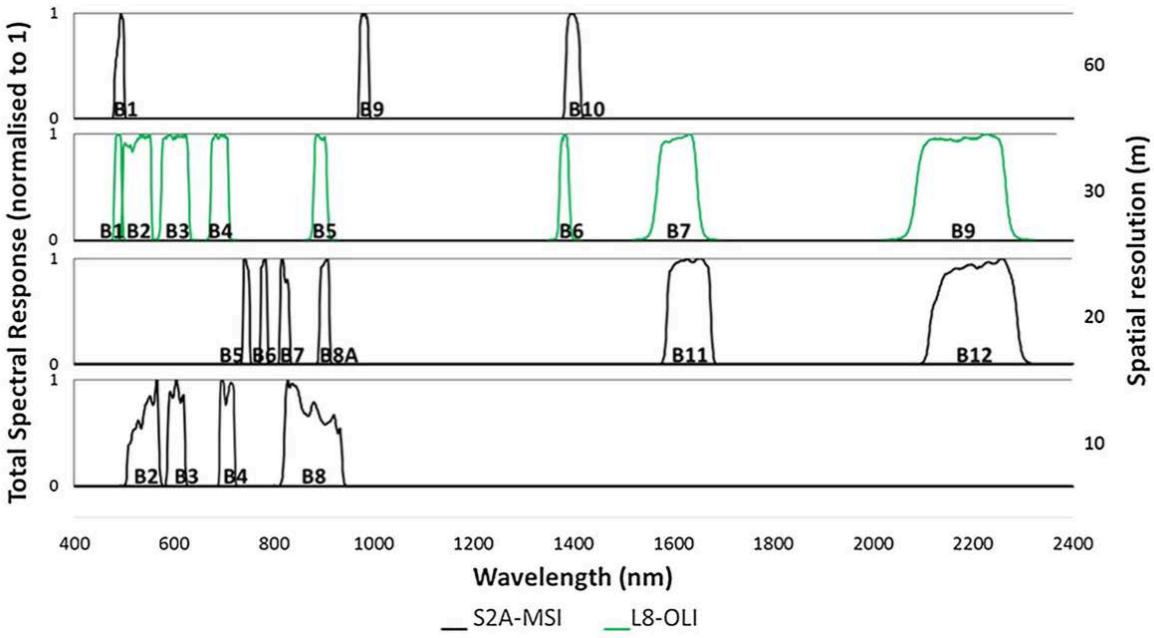

Figure 1-1: Band position and spatial resolution for Landsat 8 OLI and Sentinel 2 MSI (Bresciani et al., 2018)

Finally, in chapter 5, the utility of the built-in camera on an iPhone 5s is assessed using remote sensing reflectances collected using the HydroColor app (Leeuw and Boss, 2018). Should this platform provide useable estimates of chl-a, blooms and/or HABs could possibly be detected more quickly without the need for samples to be sent to the laboratory. As mobile devices and digital cameras are significantly less costly than hyperspectral imagers, this technology could enable unmanned aerial vehicles (UAV) as cost effective remote sensing platforms.

1.4 References

Ahn, Y.-H.H., Bricaud, A., Morel, A., 1992. Light backscattering efficiency and related properties of some phytoplankters. Deep Sea Res. Part A, Oceanogr. Res. Pap. 39, 1835–1855. https://doi.org/10.1016/0198-0149(92)90002-B

Ali, K.A., Ortiz, J.D., 2016. Multivariate approach for chlorophyll-a and suspended matter retrievals in Case II type waters using hyperspectral data. Hydrol. Sci. J. 61, 200–213. https://doi.org/10.1080/02626667.2014.964242

Amanollahi, J., Kaboodvandpour, S., Majidi, H., 2017. Evaluating the accuracy of ANN and LR models to estimate the water quality in Zarivar International Wetland, Iran. Nat. Hazards 85, 1511–1527. https://doi.org/10.1007/s11069-016-2641-1

Anderson, D.M., Boerlage, S.F.E., Dixon, M.B., 2017. Harmful Algal Blooms (HABs) and Desalination : A Guide to Impacts, Monitoring , and Management.

Anderson, D.M., Cembella, A.D., Hallegraeff, G.M., 2012. Progress in Understanding Harmful Algal Blooms: Paradigm Shifts and New Technologies for Research, Monitoring, and Management. Ann. Rev. Mar. Sci. 4, 143–176. https://doi.org/doi:10.1146/annurev-marine-120308-081121

Antoine, D., 2006. Global- and Ocean-scale primary production from satellite observations. Remote Sens. Mar. Environ. Man. Remote Sens. 85–147.

Beck, R., Zhan, S., Liu, H., Tong, S., Yang, B., Xu, M., Ye, Z., Huang, Y., Shu, S., Wu, Q., Wang, S., Berling, K., Murray, A., Emery, E., Reif, M., Harwood, J., Young, J., Nietch, C., Macke, D., Martin, M., Stillings, G., Stump, R., Su, H.,

2016. Comparison of satellite reflectance algorithms for estimating chlorophyll-a in a temperate reservoir using coincident hyperspectral aircraft imagery and dense coincident surface observations. Remote Sens. Environ. 178, 15–30. https://doi.org/10.1016/j.rse.2016.03.002

Blix, K., Eltoft, T., 2018. Evaluation of Feature Ranking and Regression Methods for Oceanic Chlorophyll-a Estimation. IEEE J. Sel. Top. Appl. Earth Obs. Remote Sens. 11, 1403–1418. https://doi.org/10.1109/JSTARS.2018.2810704

Brando, V.E., Dekker, A.G., 2003. Satellite hyperspectral remote sensing for estimating estuarine and coastal water quality. Geosci. Remote Sensing, IEEE Trans. 41, 1378–1387.

Bresciani, M., Cazzaniga, I., Austoni, M., Sforzi, T., Buzzi, F., Morabito, G., Giardino, C., 2018. Mapping phytoplankton blooms in deep subalpine lakes from Sentinel-2A and Landsat-8. Hydrobiologia 824, 197–214. https://doi.org/10.1007/s10750-017-3462-2

Bricaud, A., Babin, M., Morel, A., Claustre, H., 1995. Variability in the chlorophyll-specific absorption coefficients of natural phytoplankton: Analysis and parameterization. J. Geophys. Res. 100, 332,13313-13321.

Bricker, S.B., Ferreira, J.G., Simas, T., 2003. An integrated methodology for assessment of estuarine trophic status. Ecol. Modell. 169, 39–60.

Buiteveld, H., Hakvoort, J.H.M., Donze, M., 1994. Optical properties of pure water, in: Ocean Optics XII. International Society for Optics and Photonics, pp. 174–183.

Campbell, G., Phinn, S.R., Dekker, A.G., Brando, V.E., 2011. Remote sensing of water

quality in an Australian tropical freshwater impoundment using matrix inversion and MERIS images. Remote Sens. Environ. 115, 2402–2414. https://doi.org/10.1016/j.rse.2011.05.003

Ciotti, A.M., Bricaud, A., 2006. Retrievals of a size parameter for phytoplankton and spectral light absorption by colored detrital matter from water-leaving radiances at SeaWiFS channels in a continental shelf region off Brazil. Limnol. Oceanogr. Methods 4, 237–253.

Clark, J.M., Schaeffer, B.A., Darling, J.A., Urquhart, E.A., Johnston, J.M., Ignatius, A.R., Myer, M.H., Loftin, K.A., Werdell, P.J., Stumpf, R.P., 2017. Satellite monitoring of cyanobacterial harmful algal bloom frequency in recreational waters and drinking water sources. Ecol. Indic. 80, 84–95. https://doi.org/10.1016/j.ecolind.2017.04.046

Concha, J.A., Schott, J.R., 2016. Retrieval of color producing agents in Case 2 waters using Landsat 8. Remote Sens. Environ. 185, 95–107. https://doi.org/10.1016/j.rse.2016.03.018

Dall'Olmo, G., Gitelson, A.A., 2005. Effect of bio-optical parameter variability on the remote estimation of chlorophyll-a concentration in turbid productive waters: experimental results. Appl. Opt. 44, 412–422.

Dall'Olmo, G., Gitelson, A.A., Rundquist, D.C., Leavitt, B., Barrow, T., Holz, J.C., 2005. Assessing the potential of SeaWiFS and MODIS for estimating chlorophyll concentration in turbid productive waters using red and near-infrared bands. Remote Sens. Environ. 96, 176–187. https://doi.org/10.1016/j.rse.2005.02.007

Darecki, M., Stramski, D., 2004. An evaluation of MODIS and SeaWiFS bio-optical

algorithms in the Baltic Sea. Remote Sens. Environ. 89, 326–350.

Dierssen, H.M., 2010. Perspectives on empirical approaches for ocean color remote sensing of chlorophyll in a changing climate. Proc. Natl. Acad. Sci. 107, 17073–17078. https://doi.org/10.1073/pnas.0913800107

DPIF, 1997. Algal Biodiversity in Tasmanian Farm Dams and Reservoirs. Department of Primary Industry and Fisheries, Hobart.

DPIPWE, 2013. Toxic Algal Bloom Update and Fishery Closures [WWW Document]. URL http://www.dpiw.tas.gov.au/inter.nsf/WebPages/SWIS-92A3LJ?open

ESA, 2018. SENTINEL-2 User Guide [WWW Document]. URL https://sentinel.esa.int/web/sentinel/user-guides/sentinel-2-msi (accessed 12.4.18).

Franz, B.A., Werdell, P.J., Meister, G., Kwiatkowska, E.J., Bailey, S.W., Ahmad, Z., McClain, C.R., 2006. MODIS land bands for ocean remote sensing applications, in: Proc. Ocean Optics XVIII, Montreal, Canada.

Garrison, T., 2007. Oceanography: an invitation to marine science. CengageBrain. com.

Gilerson, A., Gitelson, A., Zhou, J., Ioannou, I., Ahmed, S., 2009. Remote Estimation of Chlorophyll-a in coastal waters using red and near infrared spectral regions, in: Proceedings of the V International Conference “Current Problems in Optics of Natural Waters (ONW)”. St Petersburg, Russia, 8e11 September. p. 110e114.

Gilerson, A., Zhou, J., Hlaing, S., Ioannou, I., Gross, B., Moshary, F., Ahmed, S., 2008. Fluorescence Component in the Reflectance Spectra from Coastal Waters. II. Performance of retrieval algorithms. Opt. Express 16, 2446–2460.

Gilerson, A., Zhou, J., Hlaing, S., Ioannou, I., Schalles, J., Gross, B., Moshary, F., Ahmed, S., 2007. Fluorescence component in the reflectance spectra from coastal waters. Dependence on water composition. Opt. Express 15, 15702–15721. https://doi.org/10.1364/oe.15.015702

Gilerson, A.A., Gitelson, A.A., Zhou, J., Gurlin, D., Moses, W.J., Ioannou, I., Ahmed, S.A., 2010. Algorithms for remote estimation of chlorophyll-a in coastal and inland waters using red and near infrared bands. Opt. Express 18, 24109–24125. https://doi.org/10.1364/OE.18.024109

Gin, K.Y.H., Koh, S.T., Lin II, Chan, E.S., 2002. Application of spectral signatures and colour ratios to estimate chlorophyll in Singapore's coastal waters. Estuar. Coast. Shelf Sci. 55, 719–728. https://doi.org/10.1006/ecss.2001.0926

Gitelson, A.A., 1992. The peak near 700 nm on radiance spectra of algae and water: relationships of its magnitude and position with chlorophyll concentration. Int. J. Remote Sens. 13, 3367–3373. https://doi.org/10.1080/01431169208904125

Gitelson, A.A., Dall'Olmo, G., Moses, W., Rundquist, D.C., Barrow, T., Fisher, T.R., Gurlin, D., Holz, J., 2008. A simple semi-analytical model for remote estimation of chlorophyll-a in turbid waters: Validation. Remote Sens. Environ. 112, 3582–3593. https://doi.org/10.1016/j.rse.2008.04.015

Gitelson, A.A., Gao, B.C., Li, R.R., Berdnikov, S., Saprygin, V., 2011. Estimation of chlorophyll-a concentration in productive turbid waters using a Hyperspectral Imager for the Coastal Ocean-the Azov Sea case study. Environ. Res. Lett. 6. https://doi.org/10.1088/1748-9326/6/2/024023

Gitelson, A.A., Gurlin, D., Moses, W.J., Barrow, T., 2009. A bio-optical algorithm for

the remote estimation of the chlorophyll-a concentration in case 2 waters. Environ. Res. Lett. 4. https://doi.org/10.1088/1748-9326/4/4/045003

Gohin, F., Druon, J.N., Lampert, L., 2002. A five channel chlorophyll concentration algorithm applied to SeaWiFS data processed by SeaDAS in coastal waters. Int. J. Remote Sens. 23, 1639–1661.

Gons, H.J., 1999. Optical teledetection of chlorophyll a in turbid inland waters. Environ. Sci. Technol. 33, 1127–1132.

Gons, H.J., Auer, M.T., Effler, S.W., Ef, S.W., 2008. MERIS satellite chlorophyll mapping of oligotrophic and eutrophic waters in the Laurentian Great Lakes. Remote Sens. Environ. 112, 4098–4106. https://doi.org/http://dx.doi.org/10.1016/j.rse.2007.06.029

Gons, H.J., Rijkeboer, M., Ruddick, K.G., 2005. Effect of a waveband shift on chlorophyll retrieval from MERIS imagery of inland and coastal waters. J. Plankton Res. 27, 125–127. https://doi.org/10.1093/plankt/fbh151

Gons, H.J., Rijkeboer, M., Ruddick, K.G., 2002. A chlorophyll-retrieval algorithm for satellite imagery (Medium Resolution Imaging Spectrometer) of inland and coastal waters. J. Plankton Res. 24, 947–951.

Gordon, H.R., Brown, O.B., Evans, R.H., Brown, J.W., Smith, R.C., Baker, K.S., Clark, D.K., Herrine, S.K., Michael, B., Ma, W.L., Rossi, S., Dunn, S.R., Hyslop, T., 1988. A semianalytic radiance model of ocean color. J. Geophys. Res. Atmos. 93, 10909–10924. https://doi.org/10.1029/JD093iD09p10909

Gower, J., King, S., 2007. Validation of chlorophyll fluorescence derived from MERIS

on the west coast of Canada. Int. J. Remote Sens. 28, 625–635. https://doi.org/10.1080/01431160600821010

Gower, J.F.R.R., Doerffer, R., Borstad, G.A., 1999. Interpretation of the 685 nm peak in water-leaving radiance spectra in terms of fluorescence, absorption and scattering, and its observation by MERIS. Int. J. Remote Sens. 20, 1771–1786. https://doi.org/10.1080/014311699212470

Guo, Q., Wu, X., Bing, Q., Pan, Y., Wang, Z., Fu, Y., Wang, D., Liu, J., 2016. Study on retrieval of chlorophyll-a concentration based on Landsat OLI Imagery in the Haihe River, China. Sustain. 8. https://doi.org/10.3390/su8080758

Gurlin, D., Gitelson, A.A., Moses, W.J., 2011. Remote estimation of chl-a concentration in turbid productive waters - Return to a simple two-band NIR-red model? Remote Sens. Environ. 115, 3479–3490. https://doi.org/http://dx.doi.org/10.1016/j.rse.2011.08.011

Hoagland, P., Anderson, D.M., Kaoru, Y., White, A.W., 2002. The economic effects of harmful algal blooms in the United States: Estimates, assessment issues, and information needs. Estuaries 25, 819–837. https://doi.org/10.1007/BF02804908

Hydro Tasmania, 2014. Lake Trevallyn Algal Monitoring Program.

Ibelings, B.W., Backer, L.C., Kardinaal, W.E.A., Chorus, I., 2014. Current approaches to cyanotoxin risk assessment and risk management around the globe. Harmful Algae 40, 63–74. https://doi.org/10.1016/j.hal.2014.10.002

Kutser, T., 2009. Passive optical remote sensing of cyanobacteria and other intense phytoplankton blooms in coastal and inland waters. Int. J. Remote Sens. 30, 4401–

4425. https://doi.org/10.1080/01431160802562305

Kutser, T., 2004. Quantitative detection of chlorophyll in cyanobacterial blooms by satellite remote sensing. Limnol. Oceanogr. 49, 2179–2189. https://doi.org/10.4319/lo.2004.49.6.2179

Le, C., Li, Y., Zha, Y., Sun, D., Huang, C., Lu, H., 2009. A four-band semi-analytical model for estimating chlorophyll a in highly turbid lakes: the case of Taihu Lake, China. Remote Sens. Environ. 113, 1175–1182.

Leeuw, T., Boss, E., 2018. The HydroColor app: Above water measurements of remote sensing reflectance and turbidity using a smartphone camera. Sensors (Switzerland) 18. https://doi.org/10.3390/s18010256

Lim, J., Choi, M., 2015. Assessment of water quality based on Landsat 8 operational land imager associated with human activities in Korea. Environ. Monit. Assess. 187. https://doi.org/10.1007/s10661-015-4616-1

Masó, M., Garcés, E., 2006. Harmful microalgae blooms (HAB); problematic and conditions that induce them. Mar. Pollut. Bull. 53, 620–630. https://doi.org/http://dx.doi.org/10.1016/j.marpolbul.2006.08.006

Matthews, M.W., Odermatt, D., 2015. Improved algorithm for routine monitoring of cyanobacteria and eutrophication in inland and near-coastal waters. Remote Sens. Environ. 156, 374–382. https://doi.org/http://dx.doi.org/10.1016/j.rse.2014.10.010

Mishra, S., Mishra, D.R., 2012. Normalized difference chlorophyll index : A novel model for remote estimation of chlorophyll- a concentration in turbid productive waters. Remote Sens. Environ. 117, 394–406.

https://doi.org/10.1016/j.rse.2011.10.016

Mobley, C.D., Sundman, L.K., 2013. HydroLight 5.2—EcoLight 5.2 Users' Guide; Sequoia Scientific. Inc. Bellevue, WA, USA.

Morel, A., Prieur, L., 1977. Analysis of Variations in Ocean Color. Limnol. Oceanogr. 22, 709–722. https://doi.org/10.2307/2835253

Moses, W.J., Moses, W.J., Gitelson, A.A., Berdnikov, S., Povazhnyy, V., 2009. Satellite Estimation of Chlorophyll- a Concentration Using the Red and NIR Bands of MERIS The Azov Sea Case Study. Ieee Geosci. Remote Sens. Lett. 6. https://doi.org/http://dx.doi.org/10.1109/LGRS.2009.2026657

NASA, 2014. Components of MODIS [WWW Document]. URL http://modis.gsfc.nasa.gov/about/specifications.php (accessed 2.4.14).

Negri, A., Llewellyn, L., Doyle, J., Webster, N., Frampton, D., Blackburn, S., 2003. Paralytic shellfish toxins are restricted to few species among Australia's taxonomic diversity of cultured microalgae. J. Phycol. 39, 663–667. https://doi.org/10.1046/j.1529-8817.2003.02131.x

O'Reilly, J.E., Maritorena, S., Mitchell, B.G., Siegel, D.A., Carder, K.L., Garver, S.A., Kahru, M., McClain, C., 1998. Ocean color chlorophyll algorithms for SeaWiFS. J. Geophys. Res. Ocean. 103, 24937–24953.

O'Reilly, J.E., Maritorena, S., Siegel, D.A., O'Brien, M.C., Toole, D., Mitchell, B.G., Kahru, M., Chavez, F.P., Strutton, P., Cota, G.F., 2000. Ocean color chlorophyll a algorithms for SeaWiFS, OC2, and OC4: Version 4. SeaWiFS postlaunch calibration Valid. Anal. Part 3, 9–23.

Odermatt, D., Gitelson, A., Brando, V.E., Schaepman, M., 2012. Review of constituent retrieval in optically deep and complex waters from satellite imagery. Remote Sens. Environ. 118, 116–126. https://doi.org/10.1016/j.rse.2011.11.013

Palmer, S.C.J., Kutser, T., Hunter, P.D., 2015. Remote sensing of inland waters: Challenges, progress and future directions. Remote Sens. Environ. 157, 1–8. https://doi.org/10.1016/j.rse.2014.09.021

Sakuno, Y., Kunii, H., 2015. Chlorophyll-a estimation in Lake Shinji from Landsat-8 OLI data using Linear Combination Index (LCI) algorithm, in: International Geoscience and Remote Sensing Symposium (IGARSS). pp. 715–718. https://doi.org/10.1109/IGARSS.2015.7325864

Schiller, H., Doerffer, R., 1999. Neural network for emulation of an inverse model operational derivation of Case II water properties from MERIS data. Int. J. Remote Sens. 20, 1735–1746. https://doi.org/10.1080/014311699212443

Seppälä, J., Ylöstalo, P., Kaitala, S., Hällfors, S., Raateoja, M., Maunula, P., 2007. Ship-of-opportunity based phycocyanin fluorescence monitoring of the filamentous cyanobacteria bloom dynamics in the Baltic Sea. Estuar. Coast. Shelf Sci. 73, 489–500. https://doi.org/10.1016/j.ecss.2007.02.015

Shen, L., Xu, H., Guo, X., 2012. Satellite remote sensing of harmful algal blooms (HABs) and a potential synthesized framework. Sensors (Basel) 12, 7778–7803. https://doi.org/10.3390/s120607778

Skerratt, J.H., Bowman, J.P., Hallegraeff, G., James, S., Nichols, P.D., 2002. Algicidal bacteria associated with blooms of a toxic dinoflagellate in a temperate Australian estuary. Mar. Ecol. Prog. Ser. 244, 1–15. https://doi.org/10.3354/meps244001

Skirtun, M., Sahlqvist, P., Curtotti, R., Hobsbawn, P., 2012. Australian fisheries statistics 2011.

Song, K., Li, L., Tedesco, L.P., Li, S., Duan, H., Liu, D., Hall, B.E., Du, J., Li, Z., Shi, K., Zhao, Y., 2013. Remote estimation of chlorophyll-a in turbid inland waters: Three-band model versus GA-PLS model. Remote Sens. Environ. 136, 342–357. https://doi.org/10.1016/j.rse.2013.05.017

Stramski, D., Boss, E., Bogucki, D., Voss, K.J., 2004. The role of seawater constituents in light backscattering in the ocean. Prog. Oceanogr. 61, 27–56. https://doi.org/10.1016/j.pocean.2004.07.001

USGS, 2016. Landsat 8 (L8) Data Users Handbook, America.

Van Der Woerd, H.J., Pasterkamp, R., 2008. HYDROPT: A fast and flexible method to retrieve chlorophyll-a from multispectral satellite observations of optically complex coastal waters. Remote Sens. Environ. 112, 1795–1807. https://doi.org/10.1016/j.rse.2007.09.001

Verpoorter, C., Tranvik, L.J., Kutser, T., Seekell, D.A., 2014. A global inventory of lakes based on high-resolution satellite imagery 6396–6402. https://doi.org/10.1002/2014GL060641

World Health Organization, 1999. Toxic Cyanobacteria in Water: A guide to their public health consequences, monitoring and management, Retrieved March. https://doi.org/10.1046/j.1365-2427.2003.01107.x

Wynne, T.T., Stumpf, R.P., Tomlinson, M.C., Dyble, J., 2010. Characterizing a cyanobacterial bloom in western Lake Erie using satellite imagery and

meteorological data. Limnol. Oceanogr. 55, 2025–2036. https://doi.org/10.4319/lo.2010.55.5.2025

Wynne, T.T., Stumpf, R.P., Tomlinson, M.C., Warner, R.A., Tester, P.A., Dyble, J., Fahnenstiel, G.L., 2008. Relating spectral shape to cyanobacterial blooms in the Laurentian Great Lakes. Int. J. Remote Sens. 29, 3665–3672. https://doi.org/10.1080/01431160802007640

2 Evaluation of atmospheric correction and high-resolution processing on SeaDAS derived chlorophyll-a: An example from mid-latitude mesotrophic waters

This chapter was published in the peer review journal as:

Bramich, J. M., Bolch, C. J., & Fischer, A. M. (2018). Evaluation of atmospheric correction and high-resolution processing on SeaDAS-derived chlorophyll-a: an example from mid-latitude mesotrophic waters. *International Journal of Remote Sensing*, *39*(8), 2119-2138

Sections have been edited to accommodate inclusion in the thesis. The ‘as published’ version has been included as appendix A.

2.1 Abstract

In recent decades, great effort has gone into the development of chlorophyll-*a* (chl-a) retrieval algorithms for case 2 waters, where variations in the water leaving radiance signal are not well correlated with concentrations of chl-*a*. In this study we investigate the effectiveness of Moderate Resolution Imaging Spectroradiometer (MODIS) derived chl-*a* retrieval algorithms in the coastal waters around Tasmania, Australia. Algorithms were evaluated using matches between satellite imagery and *in-situ* water samples (number of samples, n = 16 to 65) derived from a 604-sample dataset collected over a nine-year period. Three aerosol correction models and three chl-*a* retrieval algorithms were evaluated using both standard and high-resolution processing procedures using the National Aeronautics and Space Administration's SeaDAS software package. Chl-*a* retrievals were evaluated in Bass Strait, where *in-situ* chl-*a* was less than 1 mg m^{-3} and retrievals were less affected by coloured dissolved organic matter (CDOM). Chlor_a, the default SeaDAS chl-*a* product, with the Management unit of the North Sea Mathematical models (MUMM) aerosol correction algorithm performed best (Root mean square error, RMSE = 0.09 mg m^{-3}; Mean absolute percentage error, MAPE = 34%; coefficient of determination, R^2 = 0.75). The fluorescence line height algorithm using Rayleigh corrected top of atmosphere reflectances (RMSE = 0.11 mg m^{-3}, MAPE = 41%, R^2 = 0.61) may provide an alternative in waters where full atmospheric correction is problematic and the 2-band red/near infrared algorithm failed to provide a meaningful estimate of chl-*a*. High-resolution processing of MODIS imagery improved spatial resolution but reduced chl-*a* retrieval accuracy, reducing the agreement between measured and predicted levels by between 12 and 25% depending on the retrieval algorithm. The SeaDAS default chlor_a product proved superior to the alternatives in mid-latitude mesotrophic coastal waters with low chl-*a* concentrations.

2.2 Introduction

Remote sensing of chlorophyll-*a* (chl-*a*) has numerous applications including climate modelling and harmful algal bloom detection, however the literature provides little evidence of a universally superior chl-*a* retrieval algorithm and numerous studies state the ineffectiveness of global ocean colour chl-*a* algorithms in complex waters (Dierssen, 2010; Gilerson et al., 2009; Gin et al., 2002; Gohin et al., 2002; Shang et al., 2014). Chl-*a* retrieval algorithms use observations of remote sensing reflectance, R_{rs} and estimate concentrations of water constituents based on either empirical relationships (O'Reilly et al., 2000, 1998), or in the case of semi-analytical models (Gilerson et al., 2010; Gitelson et al., 2008; Gons et al., 2002), the inherent optical properties (IOPs) of seawater constituents. To do this, the signal reaching the satellite sensor must be corrected for atmospheric effects. Early atmospheric correction algorithms relied on the 'black pixel assumption': that there will be zero water leaving radiance in the near infrared (NIR) part of the spectrum (Bailey et al., 2010). This assumption can be invalid for waters with high levels of particulate scattering and may result in negative remote sensing reflectances (Aurin et al., 2013). Alternatives to improve aerosol correction in waters where the dark pixel assumption is invalid include the National Aeronautical and Space Administration's (NASA) iterative NIR algorithm (Bailey et al., 2010), the use of short wave infra-red (SWIR) bands (Shi and Wang, 2009) and the Management unit of the North Sea Mathematical models (MUMM) atmospheric correction algorithms (Ruddick et al., 2006).

Empirical ocean colour chl-*a* retrieval algorithms such as the MODIS OC3 algorithm use reflectance ratios in the blue and green parts of the visible spectrum. These algorithms provide adequate results in case 1 waters where variations in the water

leaving radiance signal are mostly correlated with concentrations of chl-*a*. It is estimated that ninety-five percent of the world's oceans case 1 waters. However, in case 2 waters, factors such as turbidity and coloured dissolved organic matter (CDOM) affect the water leaving radiance signal (Morel and Prieur, 1977) and chl-*a* retrieval algorithms based on blue-green colour ratios have been shown to perform poorly (Gilerson et al., 2009; Gin et al., 2002; Gohin et al., 2002). Tasmanian coastal waters are optically complex. CDOM is the dominant light absorbing constituent and accounts 38-95% of absorption at 440 nm. Remaining absorption is due to particulate matter of which absorption due to phytoplankton varies widely from 3-91%. Mean chl-*a* levels are 0.69 ± 0.38 mg m^{-3} (Cherukuru et al., 2014) suggesting a mesotrophic classification (Antoine et al., 1996). Chl-*a* is less concentrated in central Bass Strait averaging approximately 0.2 mg m^{-3} (Gibbs et al., 1986) and while definitions vary (Antoine et al., 1996; Bricaud et al., 2004) it would seem sensible to classify this region as borderline mesotrophic/oligotrophic.

Spectral shape, or derivative, chl-*a* retrieval algorithms are an alternative to the OC3 algorithm that measure the height of a spectral peak against a linear baseline established at neighbouring wavelengths which, for even band spacing, approximates the second derivative of the spectra (Wynne et al., 2013). Gower et al. (1999) utilised chl-*a* fluorescence near 685 nm by measuring the peak at this wavelength to obtain fluorescence line height (FLH), providing a linear indicator of chl-*a* concentration. MODIS derived FLH is calculated using equation 2-1 where $R_{rs}(\lambda)$ is the remote sensing reflectance at wavelength λ nm (Gower and King, 2012):

$$\mathrm{FLH} = R_{rs}(678) - R_{rs}(667) - 0.1358(R_{rs}(748) - R_{rs}(667)) \qquad (2\text{-}1)$$

Spectral shape algorithms have an advantage in being effective from satellite imagery without full atmospheric correction (Gower and King, 2007) and have been applied to level 1 or Rayleigh corrected top of atmosphere reflectances (R_{rc}) in several applications including chl-*a* retrieval and harmful algal bloom detection and monitoring (Gower et al., 2008; Matthews and Odermatt, 2015; Ryan et al., 2008; Wynne et al., 2013).

NASA's SeaDAS software provides a default chl-*a* product, chlor_a, which uses a blended algorithm (NASA, 2017) that combines both ocean colour and spectral shape algorithms. The OC3 algorithm (O'Reilly et al., 2000) is used for chl-*a* > 0.2 mg m^{-3} and the colour index (CI) algorithm, a spectral shape algorithm that measures the distance of the green band from a linear baseline between neighbouring red and blue bands (Hu et al., 2012) is used for chl-*a* < 0.015 mg m^{-3}, in between values are blended (NASA, 2017).

Phytoplankton exhibit a reflectance peak near 700 nm (Gitelson, 1992) and many algorithms utilise this region of the spectrum (Dall'Olmo and Gitelson, 2005; Gilerson et al., 2010; Gitelson et al., 2009; Gons et al., 2008, 2002; Matthews et al., 2012; Matthews and Odermatt, 2015; Moses et al., 2012) which is less sensitive to the effects of absorption due to CDOM (Gilerson et al., 2010). While MODIS does not possess a band in this part of the spectrum a two band algorithm described in equation 2-2 has been derived, where *C* is the concentration of chl-*a*, and validated with some success (Gurlin et al., 2011; Moses et al., 2009) albeit in more productive waters than those described around Tasmania (Cherukuru et al., 2014; Gibbs et al., 1986). We will refer to this as the NR2 algorithm:

$$C \propto \mathrm{R}_{\mathrm{rs}}^{-1}(667)\mathrm{R}_{\mathrm{rs}}(748) \qquad (2\text{-}2)$$

The lack of a dominant global algorithm can be explained to some extent by the variation in the optical properties of the water bodies to which they have been applied. Phytoplankton specific absorption, to which many algorithms are sensitive, can vary according to algal type (Ahn et al., 1992), size (Ciotti and Bricaud, 2006) and concentration (Bricaud et al., 1995). Many successful demonstrations of red/NIR band ratio algorithms have occurred in highly eutrophic waters (Gitelson et al., 2009, 2008; Le et al., 2013; Moses et al., 2009). In addition to lacking the previously mentioned band near 700nm, the utility of MODIS based chl-*a* retrievals may also be affected by spatial resolution. Spatial resolution will determine, in part, the extent to which near coastal waters can be monitored. The bands designated for ocean colour applications have a spatial resolution of 1000 m/pixel, which compares poorly with 290 m/pixel and 90 m/pixel of the MERIS and hyperspectral imager for the coastal ocean (HICO) sensors respectively (Corson et al., 2008; ESA, 2014; NASA, 2014). All MODIS bands can be processed through interpolation to a resolution of 250 m/pixel (Franz et al., 2006) but there is little in the literature quantifying the effect this high-resolution mode has on the accuracy of chl-*a* retrievals. In this study we test a variety of atmospheric correction and chl-*a* retrieval processing chains and evaluate the effectiveness of the MODIS high-resolution processing mode.

2.3 Data and Methodology

2.3.1 In-situ data

Several third-party datasets containing *in-situ* chl-*a* measurements were used in this study (Table 2-1). Chl-*a* measurements were obtained using a shipborne Wetlabs combination fluorometer and turbidity sensor for the SOT08 dataset (IMOS, 2013a)

and via high performance liquid chromatography (HPLC) for the remaining datasets (CSIRO, 2013; IMOS, 2013b, 2013c, 2013d, 2013e, 2013f). Water samples spanned a decade from 2004 to 2014 and were taken from coastal waters surrounding the Australian state of Tasmania and in Bass Strait (Figure 2-1). Tasmania is centred at a latitude of approximately 42 degrees south (Figure 2-1) and is approximately three hundred and twenty kilometres across and three hundred and thirty kilometres from north to south. Absorption of light in the coastal water column in is dominated by CDOM, although highest in river discharge areas in the south-east and south-west (Cherukuru et al., 2014; Marzinelli et al., 2015) the effects can be observed many kilometres offshore in the southern ocean to the west (Clementson et al., 2001) and the western half of Bass Strait (Schroeder et al., 2008).

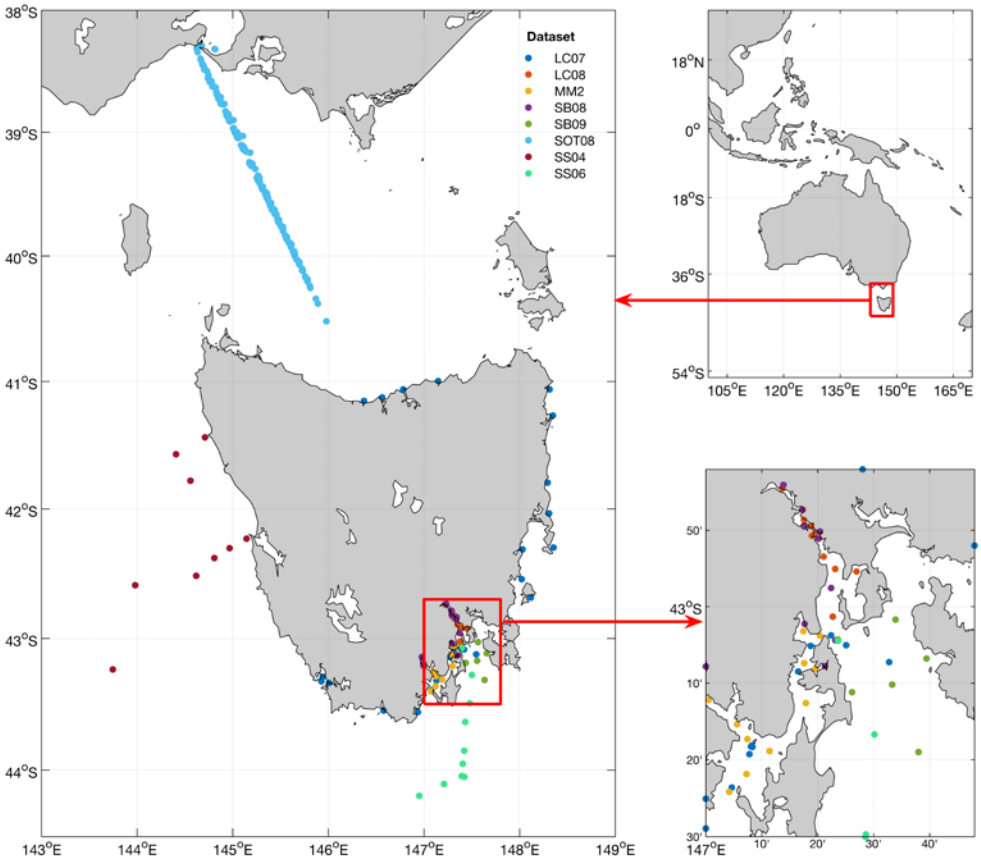

Figure 2-1: *In-situ* sample sites from eight research cruises conducted from July 2004 to January 2014. Storm Bay (inset, lower right) illustrates numerous nearshore sampling locations. For a full description of *in-situ* data sources see Table 2-1.

2.3.2 Image Analysis

Satellite imagery for the Aqua/MODIS sensor was obtained from the NASA ocean biology level one and two scene browser (NASA Goddard Space Flight Center, 2014). Level 1A imagery coinciding with *in-situ* sampling dates was downloaded. Images were processed to Level 2 using the SeaDAS 7.4 l2gen command and raw level 2 pixel values were used in further analysis. High-resolution processing was achieved by setting the l2gen resolution parameter to 250 (Franz et al., 2006), resulting in pixel sizes of approximately 250 metres compared to 1000 m for standard resolution processing. Several aerosol correction models were used for comparison: the default

iterative NIR, the short wave infrared (SWIR) (Wang and Shi, 2005) and the MUMM atmospheric correction method for turbid waters (Ruddick et al., 2000). In all cases, stray light masking was reduced to 3 x 3 pixels (Aurin et al., 2013) in order to reduce masking of pixels corresponding to near coastal sampling sites. SWIR atmospheric correction was implemented for all pixels as per Aurin et al. (2013) which involved setting the SWIR bands to 1240 nm and 2130 nm and modifying the cloud detection threshold to a more appropriate level for the 2130 nm band (0.018). Rayleigh corrected top of atmosphere reflectances (R_{rc}) were also retrieved for use with the fluorescence line height algorithm which does not require full atmospheric correction (Gower and King, 2012).

A match-up dataset was created by extracting 3 x 3 pixel box centred on each *in-situ* measurement location from same day satellite imagery within three hours of *in-situ* sampling. Spatial match-ups were identified as per Bailey and Werdell (2006). The match-up procedure (Figure 2-2) removed pixels of low quality, flagged pixels or those with poor sensor or solar geometry. Heterogeneity tests were then applied to satellite bands from 412 nm to 748 nm inclusive to limit the permitted spatial variability of pixels. Restricting the permitted coefficient of variation between pixels provides greater confidence in the assumption that *in-situ* point samples are a good representation of surrounding waters (Bailey and Werdell, 2006). Remote sensing reflectance for each satellite band was calculated using mean values of remaining valid pixels in each pixel box.

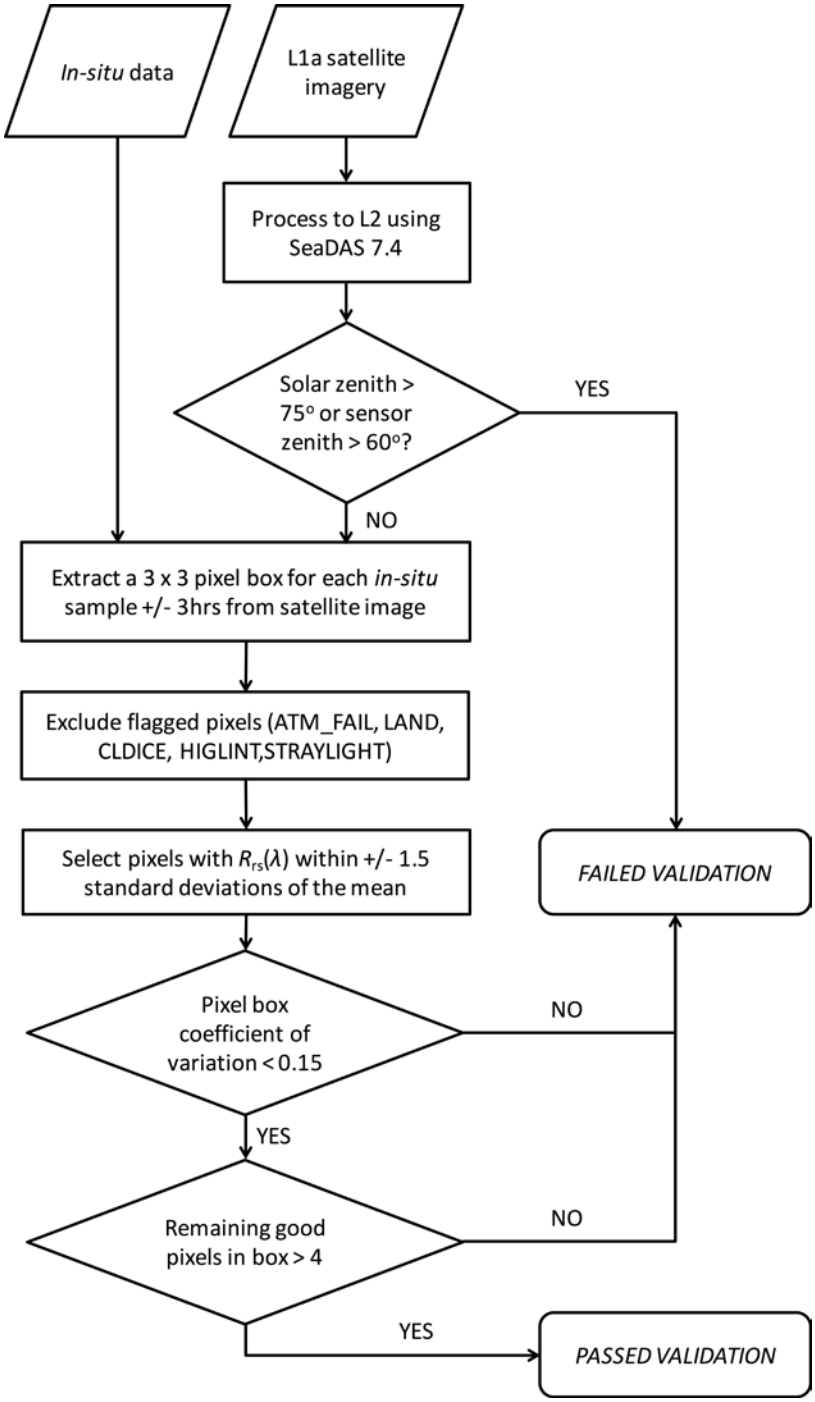

Figure 2-2: Satellite validation procedure adapted from Bailey and Werdell (2006)

Four chl-*a* retrieval algorithms were evaluated: the default SeaDAS chlor_a product, two implementations of FLH and the NR2 algorithm. The two FLH algorithms and the NR2 algorithm were calibrated against the *in-situ* dataset. For validation (Figure 2-2), mean values were taken from valid pixels in each pixel box. This means that the FLH

returned by SeaDAS was the mean FLH of valid pixels. In order to derive the peak height using the mean reflectances for valid pixels, a second variable, FLH2 was calculated using the standard MODIS FLH bands (Gower and King, 2012):

$$\text{FLH2} = R_{rc}(678) - R_{rc}(667) - 0.1358(R_{rc}(748) - R_{rc}(667)) \quad (2\text{-}3)$$

The predictive ability of each calibrated algorithm against external data was estimated using a 5-fold cross validation approach (Stone, 1974; Zhang, 1993). 5-fold cross validation makes best use of small datasets by allowing all data to be used independently for both calibration and validation. Four folds are used for model calibration and one for validation. This process is repeated until each fold has been used for validation (Arlot and Celisse, 2010; Zhang, 1993), hence predicted values are based on inputs independent of those used for model building. Cross validation was implemented in this study using the caret package in R (Kuhn, 2008). Predicted chl-*a* values for each fold were stored and error (E), bias (B), root mean square error (RMSE) and mean absolute percentage error (MAPE) were calculated as follows:

$$E = C_{\text{predicted}} - C_{\text{in-situ}} \quad (2\text{-}4)$$

$$B = \text{mean}(E) \quad (2\text{-}5)$$

$$\text{RMSE} = \text{sqrt}(\text{mean}(E^2)) \quad (2\text{-}6)$$

$$\text{MAPE} = \text{mean}(\text{abs}(E)/ C_{\text{in-situ}}) \times 100 \quad (2\text{-}7)$$

Where “sqrt” and “abs” are the mathematical square root and absolute value functions respectively. For algorithms requiring calibration, a final algorithm was calibrated using the entire sample and the coefficient of determination, R^2 was calculated. For the SeaDAS default chlor_a product, R^2 was calculated as the square of the linear

correlation coefficient, *r*, between observed and predicted chl-*a* concentrations. This process was conducted for the entire set of *in-situ* matchups and on a per dataset basis if sufficient data ($n \geq 10$) were available for analysis.

2.4 Results

2.4.1 Synthesis of in-situ data

In-situ chl-*a* concentrations ranged from 0.05 to 11.84 mg m^{-3}, however the majority of samples were at concentrations of less than 2 mg m^{-3} (Figure 2-3). Generally, mean chl-*a* concentrations greater than 1 mg m^{-3} were found in the south-east while northern and western waters had mean chl-*a* less than 0.5 mg m^{-3} (Table 2-1).

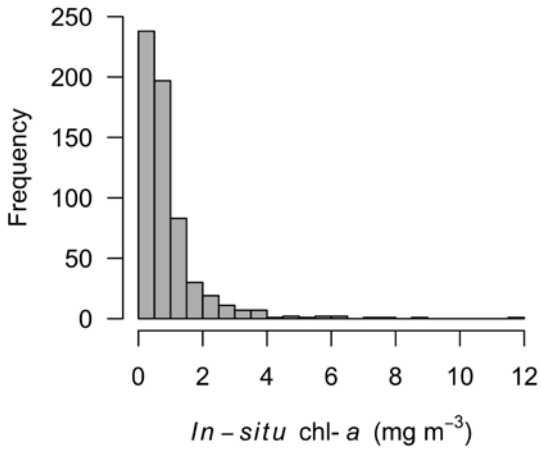

Figure 2-3: Distribution of *in-situ* chl-*a* concentrations from in situ samples

Table 2-1: Description of *in-situ* data sources (*n* = number of samples).

Dataset	Source	Data Period	Region	n	Chl-a (mg m-3) Minimum	Maximum	Mean
MM2	Aquafin CRC salmon project – monthly monitoring 2 (CSIRO, 2013)	September 2004 to October 2005	SE	125	0.19	6.28	1.33
SS04	Southern Surveyor 07/2004, HPLC Pigment and Ocean Colour Data (IMOS, 2013e)	July 2004	W	9	0.22	0.74	0.33
SS06	Southern Surveyor 03/2006 (IMOS, 2013b)	March 2006	S & SE	10	0.10	1.6	0.82
LC07	Tasmanian Coastal Waters, May 2007, HPLC Pigment and Ocean Colour Data (IMOS, 2013c)	May 2007	N, E, SE & SW	27	0.17	1.53	0.68
LC08	Tasmania, Derwent River, January 2008, HPLC pigment and Ocean Colour Data (IMOS, 2013f)	January 2008	SE	14	0.86	3.96	2.45
SB08	Storm Bay, Derwent and Huon River Estuaries, HPLC Pigment data (IMOS, 2013d)	November 2008 to December 2008	SE	12	0.74	11.52	4.56
SOT08	Spirit of Tasmania (IMOS, 2013a)	January 2009 to April 2009	N	170	0.00	1.24	0.42
SB09	Storm Bay (IMAS, pers. comm.)	November 2008 to January 2014	SE	237	0.14	5.47	0.91
	Collated dataset	**July 2004 to January 2014**		**604**	**0.05**	**11.84**	**0.94**

2.4.2 Satellite imagery

There were 356 *in-situ* samples that were within three hours of a corresponding MODIS image. The satellite validation procedure (Bailey and Werdell, 2006) further reduced the dataset to 202 matches between *in-situ* chl-*a* samples and satellite imagery.

Clouds were the dominant source of validation failure, causing more than sixty percent of pixel rejection although this figure was relatively consistent across processing methods (see Table 2-2). The main source of variation between processing methods was percentage of negative reflectances returned. R_{rc} processing returned less than one percent negative reflectances while of the aerosol correction algorithms, at standard

resolution, the MUMM algorithm was best performed returning one percent negative reflectances compared to the iterative NIR (2.7%) and SWIR (12%) algorithms. In all cases high resolution processing resulted in a higher percentage of negative reflectance values (Table 2-2).

Table 2-2: Percentage of pixels failing atmospheric correction (AC Fail), flagged as land, clouds or returning negative reflectances (total pixels extracted per image = 3204) and percentage valid pixels and matchups based on resolution and aerosol correction type.

		Invalid pixels by type (%)					
Resolution	Aerosol Correction	AC Fail	Land	Clouds	Negative R_{rs}	Valid pixels (%)	Match-ups
High	R_{rc} (none)	n/a	2.5	63.3	0.7	26.0	65
	MUMM	2.7	2.5	63.3	3.8	22.9	27
	Iterative NIR	3.1	2.5	63.3	11.9	14.8	2
	SWIR	0.9	2.5	68.7	15.3	7.8	1
Standard	R_{rc} (none)	n/a	7.0	61.7	0.1	20.7	52
	MUMM	4.5	7.0	61.7	1.0	19.7	32
	Iterative NIR	4.7	7.0	61.7	2.7	18.0	16
	SWIR	3.2	7.0	66.6	12.0	6.7	7

The final matchup dataset was heavily dominated by the SOT08 dataset for all processing methods (Table 2-3). The SOT08 dataset was the second largest dataset behind the SB09 dataset, but the sample points in Bass Strait were not at risk of being flagged as land or stray light. SOT08 data accounted for two-thirds of all high resolution R_{rc} matches with the SB09 dataset comprising 26%. For aerosol corrected standard resolution imagery, SOT08 data comprised 91% and 94% of matches for the MUMM and iterative NIR aerosol correction algorithms respectively.

Table 2-3: MODIS imagery matchups by dataset where total matchups for given processing parameters > 10.

		Number of matchups by dataset								
Resolution	**Aerosol Correction**	**MM2**	**SS04**	**SS06**	**LC07**	**LC08**	**SB08**	**SOT08**	**SB09**	**Total**
High	Rrc (none)	0	0	3	1	1	0	43	17	**65**
	MUMM	1	0	1	1	0	0	21	3	**27**
Standard	Rrc (none)	0	0	5	0	0	0	42	5	**52**
	MUMM AC	0	0	2	0	0	0	29	1	**32**
	Iterative NIR AC	0	0	1	0	0	0	15	0	**16**

2.4.3 Chlorophyll-a retrievals

The evaluation of chl-*a* retrievals for the different processing chains was confined to the SOT08 dataset which comprised such a high proportion of the total matchups (Table 2-3). Mean chl-*a* levels for the SOT08 dataset were 0.37 mg m^{-3} (Table 2-4) and approximately normally distributed (Figure 2-4).

Table 2-4: Description of post-validation *in-situ* data (*n* = number of samples).

		***In-situ* chl-*a* (mg m^{-3})**		
Dataset	***n***	**Minimum**	**Maximum**	**Mean**
LC07	2	0.86	0.86	0.86
LC08	1	1.13	1.13	1.13
MM2	1	1.13	1.13	1.13
SB09	27	0.18	3.05	0.86
SOT08	159	0.05	0.76	0.37
SS06	12	0.47	0.92	0.67
Collated	**202**	**0.05**	**3.05**	**0.47**

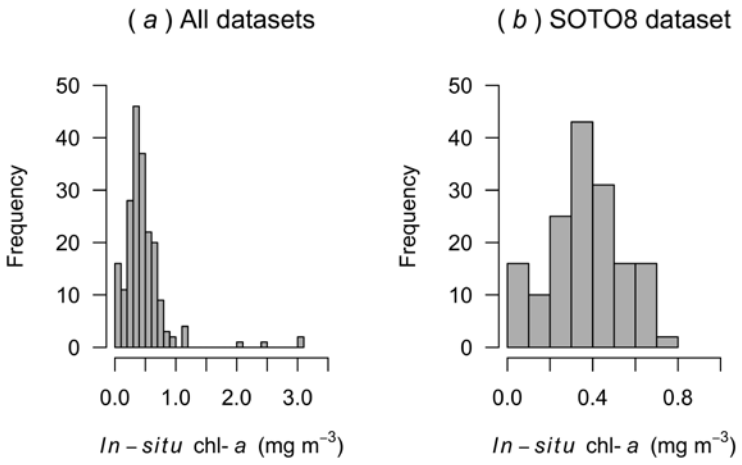

Figure 2-4: Post-validation *in-situ* chl-*a* distribution

The predicted accuracy of chl-*a* retrievals was similar for several processing chains. Better performing combinations were the MUMM/chlor_a (RMSE = 0.09 mg m^{-3}, MAPE = 34%, R^2 = 0.75), iterative NIR/FLH2 (RMSE = 0.09 mg m^{-3}, MAPE = 45%, R^2 = 0.69) and MUMM/FLH2 (RMSE = 0.10 mg m^{-3}, MAPE = 39%, R^2 = 0.65) at standard resolution and the MUMM/chlor_a (RMSE = 0.10 mg m^{-3}, MAPE = 39%, R^2 = 0.66) at high resolution while the NR2 band ratio was not statistically related to chl-*a* (Table 2-5).

Table 2-5: Bias (mg m^{-3}), RMSE (mg m^{-3}), MAPE and R^2 for chl-*a* retrieval processing chains against the SOT08 dataset (number of samples, $n > 10$). The chlor_a algorithm is a standard SeaDAS product so no regression was performed. In these instances, R^2 was obtained by squaring *r*, the linear correlation coefficient for the relationship between *in-situ* and predicted chl-*a*.

Resolution	AC type	Chl-*a* algorithm	*n*	Bias (mg m^{-3})	RMSE (mg m^{-3})	MAPE (%)	R^2
Standard	MUMM	chlor_a	29	0.03	0.09	34	0.75
Standard	Iterative NIR	FLH2	15	0.00	0.09	45	0.69
Standard	MUMM	FLH2	29	0.00	0.10	39	0.65
High	MUMM	chlor_a	21	0.02	0.10	39	0.66
Standard	Iterative NIR	chlor_a	15	-0.05	0.10	42	0.61
Standard	R_{rc}	FLH2	42	0.00	0.11	41	0.61
Standard	MUMM	FLH	29	0.00	0.11	42	0.56
Standard	Iterative NIR	FLH	15	0.00	0.11	52	0.58
High	R_{rc}	FLH2	43	0.01	0.14	58	0.46
High	MUMM	FLH2	21	0.00	0.15	50	0.49
High	MUMM	FLH	21	0.01	0.18	63	0.32

The simple linear regression used to calibrate the FLH and FLH2 algorithms resulted in negligible bias but for the chlor_a algorithm there was a positive bias when using MUMM atmospheric correction of 0.03 mg m^{-3} at standard resolution (Figure 2-5*a*) and 0.02 mg m^{-3} at high resolution. Use of iterative NIR aerosol correction at standard resolution resulted in a negative bias of 0.05 mg m^{-3} (Figure 2-5*c*) which suggests that the bias is caused by the choice of aerosol correction model.

The FLH2 algorithm, calculated using mean reflectances, outperformed FLH, calculated using the mean FLH from pixel matches, regardless of aerosol correction method (Table 2-5). Figure 2-5 shows plots of predicted versus measured chl-*a* for the better performing algorithms with any matches from the other datasets overlaid. From Figure 2-5*f* we can see that the FLH2 algorithm using R_{rc} reflectances may benefit from re-calibration between Bass Strait and southern waters. When recalibrated against the SS06 dataset performance improved dramatically (bias = -0.02 mg m^{-3}, RMSE = 0.10

mg m^{-3}, MAPE = 15%, R^2 = 0.87), although this recalibration is based on a very small amount of data (n = 5).

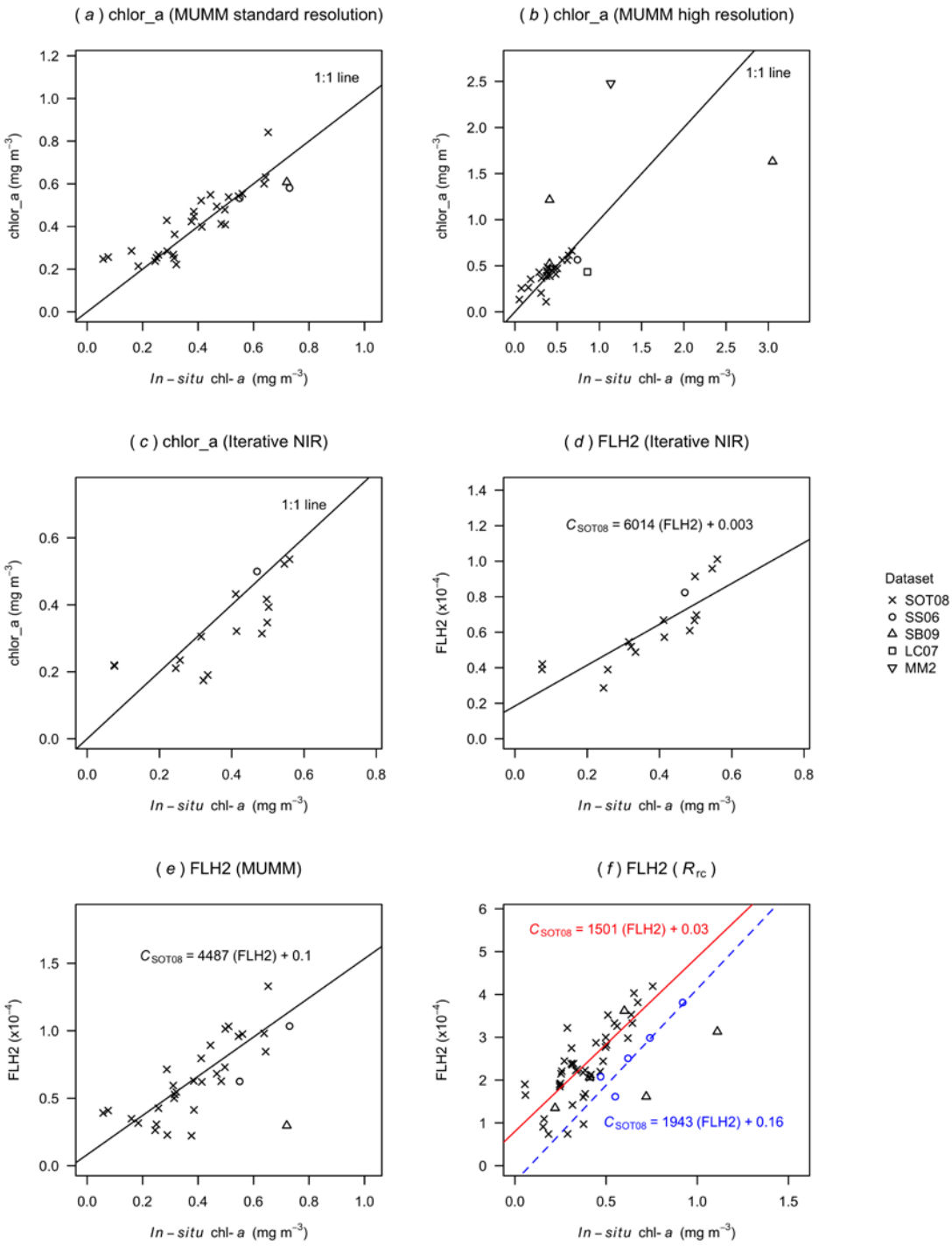

Figure 2-5: chlor_a and FLH2 retrieval algorithm performance versus *in-situ* chl-*a* for SOT08 dataset using MUMM aerosol correction at standard (*a*, *e*) and high (*b*) resolutions, standard resolution iterative NIR (*c*, *d*) and Rayleigh corrected reflectances (*f*).

2.4.4 MODIS high-resolution versus standard resolution

Processing of 1000 m/pixel bands to 250 m/pixel using the SeaDAS software results in an observable improvement in spatial resolution (Figure 2-6).

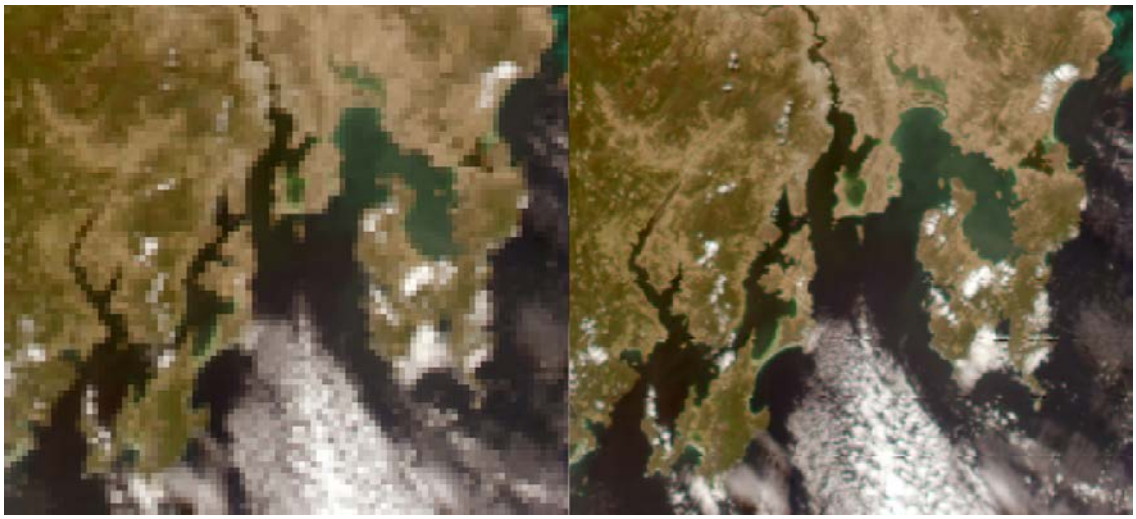

Figure 2-6: MODIS imagery of Storm Bay and surrounds in Tasmania at both 1000 m/pixel (left) and 250 m/pixel (right).

For R_{rc} reflectances and the MUMM and SWIR aerosol correction models, high-resolution processing returned 15-25% more valid pixels than corresponding standard resolution methods while for the iterative NIR aerosol correction model there was an 18% decrease in valid pixels. Only in the case of R_{rc} reflectances did high-resolution processing increase the number of *in-situ* matchups (Table 2-2). In all cases high-resolution processing led to an approximately 3% increase in the number of pixels flagged as cloud and increases of approximately 28% (SWIR), 340% (NIR) and 280% (MUMM) in the number of pixels with negative reflectance. (Table 2-2). The accuracy of chl-*a* retrievals was also reduced when using high-resolution mode (Table 2-6). For the FLH2 algorithm using R_{rc} reflectances R^2 fell from 0.45 to 0.17 and RMSE more than doubled from 0.16 to 0.38 mg m^{-3}. For MUMM corrected imagery, high-resolution processing caused a decline in R^2 for all algorithms except for FLH2 where R^2

increased marginally from 0.45 to 0.46 however RMSE increased from 0.15 to 0.52 mg m^{-3}. For the chlor_a product, R^2 decreased from 0.74 to 0.44 while RMSE increased from 0.09 to 0.43 mg m^{-3}, for the FLH algorithm R^2 decreased from 0.54 to 0.39 and RMSE increased from 0.11 to 0.12 and for the FLH2 algorithm R^2 decreased from 0.69 to 0.54 and RMSE increased from 0.09 to 0.12. High-resolution processing using iterative NIR or SWIR atmospheric correction did not yield enough *in-situ* matches for analysis.

Table 2-6: Comparison of chl-*a* retrieval accuracy between MODIS high and standard resolution processing for the SOT08 dataset.

		R^2			RMSE (mg m^{-3})		
AC Type	**Algorithm**	**Standard resolution**	**High resolution**	**Change (%)**	**Standard resolution**	**High resolution**	**Change (%)**
None (R_{rc})	FLH2	0.61	0.46	-25	0.11	0.14	+27
MUMM	chlor_a	0.75	0.66	-12	0.09	0.10	+10
	FLH	0.56	0.32	-43	0.11	0.18	+63
	FLH2	0.65	0.49	-25	0.10	0.15	+50

2.5 Discussion

2.5.1 High-resolution processing

High-resolution processing is of interest as the improved spatial resolution may improve remote sensing capability in near coastal areas (Figure 2-6). High resolution processing reduced the quantity of pixels flagged as land by almost two-thirds and, with the exception of iterative NIR aerosol correction, returned 15-25% more valid pixels than corresponding standard resolution methods (Table 2-2). These results appear purely a function of improved spatial resolution and did not necessarily result in an increase in *in-situ* matchups. High-resolution processing also reduced the accuracy of chl-*a* retrievals, both reducing the percentage of variation explained by each algorithm and, in most cases, increasing the error of each algorithm (Table 2-6). Chl-*a* retrieval

algorithms examined in this study use MODIS bands 8-15 which have a spatial resolution of 1000 m and a signal to noise ratio in the 750-1100 range. The first seven MODIS bands are primarily designed for land, cloud and aerosol detection: bands 1-2 in the red and NIR region and bands 3-7 in the blue/green and SWIR regions have spatial resolutions of 250 m and 500 m respectively with signal to noise ratios in the 70-275 range (NASA, 2014). MODIS standard 1 km resolution imagery can be processed to 250 m spatial resolution using the SeaDAS (l2gen). Radiances, path geometries and geolocation are interpolated to 250 m by setting the resolution parameter to 250 (Franz et al., 2006). The results seen here suggest that the high-resolution processing results in less accurate remote sensing reflectance values, possibly due to the much lower signal to noise ratio of the native high-resolution bands or the method of interpolation (NASA, 2014).

2.5.2 Effect of aerosol correction model

Evaluations of atmospheric correction algorithms generally involve comparing *in-situ* radiometric data with satellite derived reflectance. As the *in-situ* data used in this study did not include radiometry, the only insight into the effectiveness of atmospheric correction methods is to compare the accuracy of chl-*a* retrievals for differing atmospheric correction methods. While it is not possible to partition error between the atmospheric correction algorithm and the chl-*a* retrieval algorithm, we can make some informed evaluation of which methods of atmospheric correction are most useful in Tasmanian coastal waters.

The MUMM method of aerosol correction yielded the best performance in terms of reducing negative reflectance, increasing the total number of matchups (Table 2-2) and for the chlor_a product, was among the best performing chl-*a* retrieval algorithms

(Table 2-5). The SeaDAS default iterative NIR aerosol correction produced chl-*a* estimates with similar accuracy to the MUMM model (Table 2-5) however it resulted in fewer *in-situ* matchups due to producing a higher number of negative reflectances (Table 2-2). The MUMM aerosol correction algorithm assumes a constant ratio of reflectance between NIR bands (Ruddick et al., 2000) which seemed superior to the convergence based bio-optical model of the iterative NIR algorithm (Bailey et al., 2010). The assumption of zero water leaving radiance in the SWIR bands is theoretically more robust than using the NIR part of the spectrum (Shi and Wang, 2009) but this was not reflected in the results of this study. The SWIR aerosol correction model resulted in a five-fold increase in negative reflectances over the default algorithm (Table 2-2). While the basis for the SWIR algorithm may be sound, the NIR bands used by the other algorithms have much higher signal to noise ratios than SWIR bands 5 and 7 of the MODIS sensor (Aurin et al., 2013; NASA, 2014). The increased noise in the SWIR bands may explain the poor results observed.

The FLH2 algorithm was also applied to partially corrected top of atmosphere reflectances. This resulted in *in-situ* matches where aerosol correction had failed or resulted in negative reflectances and performance on the SOT08 dataset (n = 42, RMSE = 0.11 mg m^{-3}, MAPE = 41%, R^2 = 0.61,) was close to the results produced using MUMM (n = 29, RMSE = 0.10 mg m^{-3}, MAPE = 39%, R^2 = 0.65) and iterative NIR (n = 15, RMSE = 0.09 mg m^{-3}, MAPE = 45%, R^2 = 0.69) aerosol correction. Spectral shape algorithms such as fluorescence line height do not require complete atmospheric correction (Gower and King, 2012; Kudela et al., 2015; Lunetta et al., 2015) and whilst chl-*a* retrievals were less accurate than those of the best performing algorithms, use of partially corrected imagery, at standard resolution, resulted in 63% and 225% increases in the number of matchups compared to MUMM and iterative NIR aerosol corrections

respectively (Table 2-3). Spectral shape algorithms using partial atmospheric correction may be useful in waters where aerosol correction results in large numbers of negative reflectances or is otherwise problematic.

2.5.3 Chlorophyll-a retrieval algorithms

The failure of the NR2 chl-*a* retrieval algorithm is most likely a result of the low and relatively narrow range of chl-*a* values in the *in-situ* dataset. The NR2 algorithm is designed for productive waters with chl-*a* concentrations above 5 mg m^{-3} and performs most poorly at lower chl-*a* concentrations (Gitelson et al., 2009; Le et al., 2013; Moses et al., 2012), however *in-situ* chl-*a* concentrations in this study were up to two orders of magnitude less than those present in other studies. Many studies that show red/NIR algorithms to outperform traditional algorithms also utilise *in-situ* radiometry (Gitelson et al., 2008; Gurlin et al., 2011) or synthetic datasets (Gilerson et al., 2010). Moses et al. (2012) were able to obtain reasonably accurate estimates of chl-*a* concentration from satellite imagery but only after calibration with *in-situ* radiometric data. Le et al. (2013) found that when using MODIS imagery, the NR2 algorithm failed to be statistically related with chl-*a* but there was a significant correlation when using the same spectral bands from *in-situ* radiometry. Accurate atmospheric correction is essential when using this class of algorithms on satellite imagery to obtain quantitative estimates of chl-*a* concentration (Gitelson et al., 2011; Moses et al., 2009) and inadequate atmospheric correction would also contribute to the poor performance of this algorithm.

This study also examined two methods of deriving the fluorescence line height. The FLH variable as produced by the SeaDAS software, was the mean FLH of all valid pixels in the three-by-three pixel box obtained for each *in-situ* matchup given a minimum of five values. Recalculating the peak height using the mean reflectances

from the corresponding pixels, referred to in this report as the FLH2 variable, yielded improved results. Regardless of aerosol correction method or processing resolution, the FLH2 variable explained more variation in chl-*a* concentration with less error (Table 2-5). Using the mean value of reflectances surrounding the *in-situ* data point is in effect a basic form of data smoothing. The improved results suggest that image smoothing, which will reduce signal noise (Wang and Shi, 2012), may be beneficial to the fluorescence line height algorithm and is worthy of further investigation.

The SeaDAS chlor_a product produced the most accurate chl-*a* retrievals in this study. This may be due to a combination of closer to optimum chl-*a* concentrations and more favourable seawater properties around Tasmania's coasts, particularly in the north. The standard ocean colour algorithms (O'Reilly et al., 2000, 1998) comprise several versions dependent on the number and locations of appropriate blue and green spectral bands for a given sensor. The OC4v4 algorithm performs best for lower chl-*a* concentrations (Dierssen, 2010). The MODIS chlor_a product is further optimised for lower chl-*a* concentrations by progressively switching to the colour index algorithm (Hu et al., 2012) for chl-*a* < 0.2 mg m^{-3}. CDOM, which also absorbs light at blue wavelengths, can confound ocean colour algorithms that use blue and green wavelengths (Gilerson et al., 2009; Gin et al., 2002; Gohin et al., 2002). While CDOM is prevalent around Tasmanian coasts, it is lower in concentration and variability in the state's northern waters. The validation process resulted in samples predominantly from the SOT08 dataset, taken from Bass Strait, where these lower and more stable CDOM levels are found (Cherukuru et al., 2014; Schroeder et al., 2008) and more likely to covary with chl-*a* concentration. Global analysis of the distribution of coloured dissolved and detrital organic materials suggests that coasts of similar latitude to the study area may have comparable absorption due to CDOM and that local oceanic

processes rather than riverine discharges regulate this distribution (Siegel et al., 2002). This means the MUMM/chlor_a processing combination may be similarly effective forty degrees north or south of the equator, but due consideration should be given to local effects in near coastal areas.

Performance of the FLH2 algorithm against the SOT08 dataset was slightly inferior to the chlor_a algorithm, but was still able to explain 61% of the variation in chl-*a* with similar error margins (Table 2-5). The use of partially correct imagery allowed for increased matchups from the SB09 (n = 5) and SS06 (n = 5) datasets in the state's southeast where the MUMM model had yielded only a single match-up in each dataset and iterative NIR aerosol correction a single match in the SS06 dataset (Table 2-3). Examination of Figures 2-5c and 2-5d suggests that even within the spatial scale of Tasmania, a single fluorescence line height algorithm may not be optimal and that several locally calibrated algorithms could be preferable. FLH2 was strongly correlated with chl-*a* (R^2 = 0.87) for the SS06 dataset however these points were a poor fit for the regression model developed from the SOT08 dataset. This can be explained by the previously mentioned geographic variations in Tasmanian coastal waters. CDOM concentrations are typically higher in the south-east than the north (Cherukuru et al., 2014) and these variations, in addition to variations in minerals can cause decreases in photosynthetically available radiation and absorption of the fluorescence signal within the water column (Gilerson et al., 2008, 2007).

2.6 Conclusions

The results suggest that when using MODIS imagery the choice to take advantage of improved spatial resolution through high-resolution processing must be weighed against the resulting degradation in the accuracy of chl-*a* retrievals. The choice between

aerosol correction and chl-*a* retrieval algorithms is equivocal. The default chlor_a product (R^2 = 0.75, RMSE = 0.09 mg m^{-3}, MAPE = 34%) with MUMM aerosol correction performed best in the Bass Strait where retrievals appeared less affected by absorption in the blue region attributable to CDOM. However, the FLH algorithm using R_{rc} top of atmosphere reflectances may provide acceptable performance in waters where full atmospheric correction is problematic. The results also suggest that the FLH algorithm could benefit from recalibration between Tasmania's northern and south-eastern waters, which possess different characteristics with regards to CDOM (Cherukuru et al., 2014). The NR2 algorithm does not seem appropriate for use in Bass Strait or Tasmanian coastal waters as chl-*a* concentrations are well below its optimum range.

Due to the absence of *in-situ* radiometry in the datasets analysed, it was not possible to separate error due to algorithm performance from errors due to atmospheric correction. Subsequent investigations should include collection of *in-situ* radiometry. The study also highlighted several issues with the satellite platform in general. Clouds were the primary reason for the inability to match *in-situ* data followed by the near proximity of points of interest to land. A sensor with greater spatial resolution may reduce flagging of pixels as land or stray light but the presence of clouds remains a fundamental problem for satellite observations.

2.7 Acknowledgments

The authors wish to thank Lesley Clementson, CSIRO, for her assistance in the collation of *in-situ* data.

2.8 References

Ahn, Y.-H.H., Bricaud, A., Morel, A., 1992. Light backscattering efficiency and related properties of some phytoplankters. Deep Sea Res. Part A, Oceanogr. Res. Pap. 39, 1835–1855. https://doi.org/10.1016/0198-0149(92)90002-B

Antoine, D., André, J., Morel, A., 1996. Oceanic primary production: 2. Estimation at global scale from satellite (coastal zone color scanner) chlorophyll. Global Biogeochem. Cycles 10, 57–69.

Arlot, S., Celisse, A., 2010. A survey of cross-validation procedures for model selection 40–79. https://doi.org/10.1214/09-SS054

Aurin, D., Mannino, A., Franz, B., 2013. Spatially resolving ocean color and sediment dispersion in river plumes, coastal systems, and continental shelf waters. Remote Sens. Environ. 137, 212–225. https://doi.org/10.1016/j.rse.2013.06.018

Bailey, S.W., Franz, B.A., Werdell, P.J., 2010. Estimation of near-infrared water-leaving reflectance for satellite ocean color data processing. Opt. Express 18, 7521–7527.

Bailey, S.W., Werdell, P.J., 2006. A multi-sensor approach for the on-orbit validation of ocean color satellite data products. Remote Sens. Environ. 102, 12–23.

Bricaud, A., Babin, M., Morel, A., Claustre, H., 1995. Variability in the chlorophyll-specific absorption coefficients of natural phytoplankton: Analysis and parameterization. J. Geophys. Res. 100, 332,13313-13321.

Bricaud, A., Claustre, H., Ras, J., Oubelkheir, K., 2004. Natural variability of phytoplanktonic absorption in oceanic waters: Influence of the size structure of

algal populations. J. Geophys. Res. Ocean. 109.

Cherukuru, N., Brando, V.E., Schroeder, T., Clementson, L.A., Dekker, A.G., 2014. Influence of river discharge and ocean currents on coastal optical properties. Cont. Shelf Res. 84, 188–203. https://doi.org/http://dx.doi.org/10.1016/j.csr.2014.04.022

Ciotti, A.M., Bricaud, A., 2006. Retrievals of a size parameter for phytoplankton and spectral light absorption by colored detrital matter from water-leaving radiances at SeaWiFS channels in a continental shelf region off Brazil. Limnol. Oceanogr. Methods 4, 237–253.

Clementson, L.A., Parslow, J.S., Turnbull, A.R., McKenzie, D.C., Rathbone, C.E., 2001. Optical properties of waters in the Australasian sector of the Southern Ocean. J. Geophys. Res. Ocean. 106, 31611–31625. https://doi.org/10.1029/2000JC000359

Corson, M.R., Korwan, D.R., Lucke, R.L., Snyder, W.A., Davis, C.O., 2008. The hyperspectral imager for the coastal ocean (HICO) on the international space station, in: Geoscience and Remote Sensing Symposium, 2008. IGARSS 2008. IEEE International. IEEE, pp. IV-101-IV–104.

CSIRO, 2013. Aquafin CRC Salmon Project - Monthly Monitoring 2 - D'Entrecasteaux Channel and Huon Estuary - Sept 2004 - Oct 2005 [WWW Document]. URL http://www.marine.csiro.au/marq/edd_search.Browse_Citation?txtSession=8240

Dall'Olmo, G., Gitelson, A.A., 2005. Effect of bio-optical parameter variability on the remote estimation of chlorophyll-a concentration in turbid productive waters: experimental results. Appl. Opt. 44, 412–422.

Dierssen, H.M., 2010. Perspectives on empirical approaches for ocean color remote sensing of chlorophyll in a changing climate. Proc. Natl. Acad. Sci. 107, 17073–17078. https://doi.org/10.1073/pnas.0913800107

ESA, 2014. MERIS Frequently Asked Questions [WWW Document]. URL http://earth.esa.int/pub/ESA_DOC/ENVISAT/MERIS/VT-P017-DOC-005-E-01-01_meris.faq.1_1.pdf

Franz, B.A., Werdell, P.J., Meister, G., Kwiatkowska, E.J., Bailey, S.W., Ahmad, Z., McClain, C.R., 2006. MODIS land bands for ocean remote sensing applications, in: Proc. Ocean Optics XVIII, Montreal, Canada.

Gibbs, C.F., Tomczak, M., Longmore, A.R., Tomczak Jr, M., Longmore, A.R., 1986. The nutrient regime of Bass Strait. Mar. Freshw. Res. 37, 451–466. https://doi.org/https://doi.org/10.1071/MF9860451

Gilerson, A., Gitelson, A., Zhou, J., Ioannou, I., Ahmed, S., 2009. Remote Estimation of Chlorophyll-a in coastal waters using red and near infrared spectral regions, in: Proceedings of the V International Conference “Current Problems in Optics of Natural Waters (ONW)”. St Petersburg, Russia, 8e11 September. p. 110e114.

Gilerson, A., Zhou, J., Hlaing, S., Ioannou, I., Gross, B., Moshary, F., Ahmed, S., 2008. Fluorescence Component in the Reflectance Spectra from Coastal Waters. II. Performance of retrieval algorithms. Opt. Express 16, 2446–2460.

Gilerson, A., Zhou, J., Hlaing, S., Ioannou, I., Schalles, J., Gross, B., Moshary, F., Ahmed, S., 2007. Fluorescence component in the reflectance spectra from coastal waters. Dependence on water composition. Opt. Express 15, 15702–15721. https://doi.org/10.1364/oe.15.015702

Gilerson, A.A., Gitelson, A.A., Zhou, J., Gurlin, D., Moses, W.J., Ioannou, I., Ahmed, S.A., 2010. Algorithms for remote estimation of chlorophyll-a in coastal and inland waters using red and near infrared bands. Opt. Express 18, 24109–24125. https://doi.org/10.1364/OE.18.024109

Gin, K.Y.H., Koh, S.T., Lin II, Chan, E.S., 2002. Application of spectral signatures and colour ratios to estimate chlorophyll in Singapore's coastal waters. Estuar. Coast. Shelf Sci. 55, 719–728. https://doi.org/10.1006/ecss.2001.0926

Gitelson, A.A., 1992. The peak near 700 nm on radiance spectra of algae and water: relationships of its magnitude and position with chlorophyll concentration. Int. J. Remote Sens. 13, 3367–3373. https://doi.org/10.1080/01431169208904125

Gitelson, A.A., Dall'Olmo, G., Moses, W., Rundquist, D.C., Barrow, T., Fisher, T.R., Gurlin, D., Holz, J., 2008. A simple semi-analytical model for remote estimation of chlorophyll-a in turbid waters: Validation. Remote Sens. Environ. 112, 3582–3593. https://doi.org/10.1016/j.rse.2008.04.015

Gitelson, A.A., Gao, B.C., Li, R.R., Berdnikov, S., Saprygin, V., 2011. Estimation of chlorophyll-a concentration in productive turbid waters using a Hyperspectral Imager for the Coastal Ocean-the Azov Sea case study. Environ. Res. Lett. 6. https://doi.org/10.1088/1748-9326/6/2/024023

Gitelson, A.A., Gurlin, D., Moses, W.J., Barrow, T., 2009. A bio-optical algorithm for the remote estimation of the chlorophyll-a concentration in case 2 waters. Environ. Res. Lett. 4. https://doi.org/10.1088/1748-9326/4/4/045003

Gohin, F., Druon, J.N., Lampert, L., 2002. A five channel chlorophyll concentration algorithm applied to SeaWiFS data processed by SeaDAS in coastal waters. Int. J.

Remote Sens. 23, 1639–1661.

Gons, H.J., Auer, M.T., Effler, S.W., Ef, S.W., 2008. MERIS satellite chlorophyll mapping of oligotrophic and eutrophic waters in the Laurentian Great Lakes. Remote Sens. Environ. 112, 4098–4106. https://doi.org/http://dx.doi.org/10.1016/j.rse.2007.06.029

Gons, H.J., Rijkeboer, M., Ruddick, K.G., 2002. A chlorophyll-retrieval algorithm for satellite imagery (Medium Resolution Imaging Spectrometer) of inland and coastal waters. J. Plankton Res. 24, 947–951.

Gower, J., King, S., 2012. Use of satellite images of chlorophyll fluorescence to monitor the spring bloom in coastal waters. Int. J. Remote Sens. 33, 7469–7481. https://doi.org/10.1080/01431161.2012.685979

Gower, J., King, S., 2007. Validation of chlorophyll fluorescence derived from MERIS on the west coast of Canada. Int. J. Remote Sens. 28, 625–635. https://doi.org/10.1080/01431160600821010

Gower, J., King, S., Goncalves, P., 2008. Global monitoring of plankton blooms using MERIS MCI. Int. J. Remote Sens. 29, 6209–6216. https://doi.org/10.1080/01431160802178110

Gower, J.F.R.R., Doerffer, R., Borstad, G.A., 1999. Interpretation of the 685 nm peak in water-leaving radiance spectra in terms of fluorescence, absorption and scattering, and its observation by MERIS. Int. J. Remote Sens. 20, 1771–1786. https://doi.org/10.1080/014311699212470

Gurlin, D., Gitelson, A.A., Moses, W.J., 2011. Remote estimation of chl-a

concentration in turbid productive waters - Return to a simple two-band NIR-red model? Remote Sens. Environ. 115, 3479–3490. https://doi.org/http://dx.doi.org/10.1016/j.rse.2011.08.011

Hu, C.M., Lee, Z., Franz, B., 2012. Chlorophyll a algorithms for oligotrophic oceans: A novel approach based on three-band reflectance difference. J. Geophys. Res. 117. https://doi.org/10.1029/2011jc007395

IMOS, 2013a. IMOS - SOOP-Temperate Merchange Vessel (TMV) Sub-facility - Data collected on the Spirit of Tasmania I during transect between Melbourne and Devonport (delayed mode). [WWW Document]. URL https://catalogue-123.aodn.org.au/geonetwork/srv/eng/metadata.show?uuid=02640f4e-08d0-4f3a-956b-7f9b58966ccc (accessed 10.21.13).

IMOS, 2013b. Southern Surveyor Voyage SS 03/2006, Pigment and Ocean Colour Data [WWW Document]. URL http://www.marine.csiro.au/marq/edd_search.Browse_Citation?txtSession=14197 (accessed 10.21.13).

IMOS, 2013c. Tasmanian Coastal Waters, May 2007, HPLC Pigment and Ocean Colour Data [WWW Document]. URL http://www.marine.csiro.au/marq/edd_search.Browse_Citation?txtSession=14323 (accessed 10.21.13).

IMOS, 2013d. Storm Bay, Derwent and Huon River Estuaries, November 2008, HPLC Pigment data [WWW Document]. URL http://www.marine.csiro.au/marq/edd_search.Browse_Citation?txtSession=9017 (accessed 10.21.13).

IMOS, 2013e. Southern Surveyor Voyage SS 07/2004, HPLC Pigment and Ocean Colour Data [WWW Document]. URL http://www.marine.csiro.au/marq/edd_search.Browse_Citation?txtSession=14220 (accessed 10.21.13).

IMOS, 2013f. Tasmania, Derwent River, January 2008, HPLC Pigment and Ocean Colour Data [WWW Document]. URL http://www.marine.csiro.au/marq/edd_search.Browse_Citation?txtSession=14348 (accessed 10.21.13).

Kudela, R.M., Palacios, S.L., Austerberry, D.C., Accorsi, E.K., Guild, L.S., Torres-perez, J., 2015. Application of hyperspectral remote sensing to cyanobacterial blooms in inland waters. Remote Sens. Environ. 167, 196–205. https://doi.org/10.1016/j.rse.2015.01.025

Kuhn, M., 2008. Building Predictive Models in R Using the caret Package. J. Stat. Softw. 28, 1–26. https://doi.org/10.1053/j.sodo.2009.03.002

Le, C., Hu, C., Cannizzaro, J., English, D., Muller-Karger, F., Lee, Z., 2013. Evaluation of chlorophyll-a remote sensing algorithms for an optically complex estuary. Remote Sens. Environ. 129, 75–89. https://doi.org/http://dx.doi.org/10.1016/j.rse.2012.11.001

Lunetta, R.S., Schaeffer, B.A., Stumpf, R.P., Keith, D., Jacobs, S.A., Murphy, M.S., 2015. Evaluation of cyanobacteria cell count detection derived from MERIS imagery across the eastern USA. Remote Sens. Environ. 157, 24–34. https://doi.org/http://dx.doi.org/10.1016/j.rse.2014.06.008

Marzinelli, E.M., Williams, S.B., Babcock, R.C., Barrett, N.S., Johnson, C.R., Jordan,

A., Kendrick, G.A., Pizarro, O.R., Smale, D.A., Steinberg, P.D., 2015. Large-Scale Geographic Variation in Distribution and Abundance of Australian Deep-Water Kelp Forests. PLoS One 10, e0118390. https://doi.org/10.1371/journal.pone.0118390

Matthews, M.W., Bernard, S., Robertson, L., 2012. An algorithm for detecting trophic status (chlorophyll-a), cyanobacterial-dominance, surface scums and floating vegetation in inland and coastal waters. Remote Sens. Environ. 124, 637–652. https://doi.org/10.1016/j.rse.2012.05.032

Matthews, M.W., Odermatt, D., 2015. Improved algorithm for routine monitoring of cyanobacteria and eutrophication in inland and near-coastal waters. Remote Sens. Environ. 156, 374–382. https://doi.org/http://dx.doi.org/10.1016/j.rse.2014.10.010

Morel, A., Prieur, L., 1977. Analysis of variations in ocean color 1. Limnol. Oceanogr. 22, 709–722.

Moses, W.J., Gitelson, A.A., Berdnikov, S., Povazhnyy, V., 2009. Estimation of chlorophyll-a concentration in case II waters using MODIS and MERIS data—successes and challenges. Environ. Res. Lett. 4, 45005. https://doi.org/10.1088/1748-9326/4/4/045005

Moses, W.J., Gitelson, A.A., Berdnikov, S., Saprygin, V., Povazhnyi, V., 2012. Operational MERIS-based NIR-red algorithms for estimating chlorophyll-a concentrations in coastal waters - The Azov Sea case study. Remote Sens. Environ. 121, 118–124. https://doi.org/10.1016/j.rse.2012.01.024

NASA, 2017. Chlorophyll a (chlor_a) [WWW Document]. URL https://oceancolor.gsfc.nasa.gov/atbd/chlor_a/ (accessed 7.1.17).

NASA, 2014. Components of MODIS [WWW Document]. URL http://modis.gsfc.nasa.gov/about/specifications.php (accessed 2.4.14).

NASA Goddard Space Flight Center, 2014. Moderate-resolution Imaging Spectroradiometer (MODIS) Aqua Ocean Color Data [WWW Document]. https://doi.org/doi: 10.5067/AQUA/MODIS_OC.2014.0.

O'Reilly, J.E., Maritorena, S., Mitchell, B.G., Siegel, D.A., Carder, K.L., Garver, S.A., Kahru, M., McClain, C., 1998. Ocean color chlorophyll algorithms for SeaWiFS. J. Geophys. Res. Ocean. 103, 24937–24953.

O'Reilly, J.E., Maritorena, S., Siegel, D.A., O'Brien, M.C., Toole, D., Mitchell, B.G., Kahru, M., Chavez, F.P., Strutton, P., Cota, G.F., 2000. Ocean color chlorophyll a algorithms for SeaWiFS, OC2, and OC4: Version 4. SeaWiFS postlaunch calibration Valid. Anal. Part 3, 9–23.

Ruddick, K.G., De Cauwer, V., Park, Y.-J., Moore, G., 2006. Seaborne measurements of near infrared water-leaving reflectance: The similarity spectrum for turbid waters. Limnol. Oceanogr. 51, 1167–1179. https://doi.org/10.4319/lo.2006.51.2.1167

Ruddick, K.G., Ovidio, F., Rijkeboer, M., 2000. Atmospheric correction of SeaWiFS imagery for turbid coastal and inland waters. Appl. Opt. 39, 897–912.

Ryan, J.P., Gower, J.F.R., King, S.A., Bissett, W.P., Fischer, A.M., Kudela, R.M., Kolber, Z., Mazzillo, F., Rienecker, E. V, Chavez, F.P., 2008. A coastal ocean extreme bloom incubator. Geophys. Res. Lett. 35.

Schroeder, T., Brando, V.E., Cherukuru, N., Clementson, L., Blondeau-Patissier, D.,

Dekker, A.G., Schaale, M., Fischer, J., 2008. Remote sensing of apparent and inherent optical properties of Tasmanian coastal waters: application to MODIS data, in: Proceedings of The XIX Ocean Optics Conference, Barga, Italy.

Shang, S.L., Dong, Q., Hu, C.M., Lin, G., Li, Y.H., Shang, S.P., 2014. On the consistency of MODIS chlorophyll a products in the northern South China Sea. Biogeosciences 11, 269–280.

Shi, W., Wang, M., 2009. An assessment of the black ocean pixel assumption for MODIS SWIR bands. Remote Sens. Environ. 113, 1587–1597.

Siegel, D.A., Maritorena, S., Nelson, N.B., Hansell, D.A., Lorenzi-Kayser, M., 2002. Global distribution and dynamics of colored dissolved and detrital organic materials. J. Geophys. Res. Ocean. 107, 14–21. https://doi.org/10.1029/2001JC000965

Stone, M., 1974. Cross-validatory choice and assessment of statistical predictions. J. R. Stat. Soc. Ser. B 111–147.

Wang, M.H., Shi, W., 2012. Sensor Noise Effects of the SWIR Bands on MODIS-Derived Ocean Color Products. Ieee Trans. Geosci. Remote Sens. 50, 3280–3292. https://doi.org/10.1109/tgrs.2012.2183376

Wang, M.H., Shi, W., 2005. Estimation of ocean contribution at the MODIS near-infrared wavelengths along the east coast of the US: Two case studies. Geophys. Res. Lett. 32. https://doi.org/10.1029/2005gl022917

Wynne, T.T., Stumpf, R.P., Briggs, T.O., 2013. Comparing MODIS and MERIS spectral shapes for cyanobacterial bloom detection. Int. J. Remote Sens. 34, 6668–

6678. https://doi.org/10.1080/01431161.2013.804228

Zhang, P., 1993. Model selection via multifold cross validation. Ann. Stat. 299–313.

3 Partial Least Squares derived chlorophyll-a retrieval from Landsat 8 OLI imagery

3.1 Abstract

The Landsat 8 operational land imager (OLI) has a spatial resolution of 30 metres, which provides the potential to extend capabilities for remote sensing of chlorophyll-a (chl-a) to lakes and near coastal waters where it was not previously possible. However, OLI band positioning is not ideal for many existing chl-a retrieval algorithms. We propose a partial least squares regression (PLSR) derived algorithm to help overcome these limitations. PLSR is well established in laboratory spectral analysis but relatively untried in remotely sensed chl-a retrievals from satellite imagery. The PLSR algorithm was calibrated and validated against *in-situ* data (number of samples, n = 30) from Lake Trevallyn in Tasmania, Australia. The algorithm was developed against a calibration subset of the data (n = 20) and able to provide chl-a estimates strongly correlated with *in-situ* values from the withheld validation dataset (n = 10, normalised root mean squared error of prediction = 21.6%; coefficient of determination = 0.67; Nash-Sutcliffe efficiency = 0.53; bias = -0.03 μg/L). These results demonstrate the suitability of PLSR algorithms and Landsat 8 OLI imagery to complement the capability of *in-situ* instrumentation for local water quality monitoring applications.

3.2 Introduction

Harmful Algal Blooms (HABs) present risks to human and ecosystem health (Anderson et al., 2012; Ibelings et al., 2014; World Health Organization, 1999). HAB events are on the increase globally (Anderson et al., 2012; Paerl and Otten, 2013) and are of a growing concern to water managers, who in some cases have legally binding targets with regards to toxin levels and/or cell biovolumes (Ibelings et al., 2014). HAB events occur in practically every coastal region of the world (Anderson et al., 2012) and cyanobacteria related HAB events are expanding geographically and threating the

ecology of some of the world's most important freshwater resources (Paerl et al., 2011). The economic impacts associated with detection and monitoring and effects to recreation and tourism amount to billions of dollars globally (Hoagland et al., 2002; Sanseverino et al., 2016). Satellite remote sensing is one tool that can assist in the detection and monitoring of algal blooms (Anderson et al., 2017; Kutser, 2009; Palmer et al., 2015), however many inland water bodies are too small to be monitored using satellite sensors designed for ocean colour monitoring (Clark et al., 2017; Palmer et al., 2015). The Landsat 8 operational land imager (OLI), operated by National Aeronautics and Space Administration's (NASA) and the United States Geographical Survey (USGS), offers the potential to improve remote sensing capabilities in smaller lakes and near coastal areas due to its 30 m spatial resolution in the visible and near infrared (NIR) bands (USGS, 2016). This represents a great improvement over platforms designed for ocean colour monitoring such as NASA's Moderate Resolution Imaging Spectroradiometer (MODIS) and the European Space Agency's (ESA) Sentinel 3 ocean and land colour instrument (OLCI) sensor which have native spatial resolutions of approximately 1000 m and 300 m, respectively (ESA, 2018; NASA, 2014). In addition to improved spatial resolution, improved signal to noise ratio (SNR) and 12-bit digitisation give Landsat OLI the spectral and radiometric capability for retrieval of in-water constituents (Franz et al., 2015). However, for chlorophyll-a (chl-a) retrievals in complex waters, the OLI band positioning is considered less than ideal (Beck et al., 2016; Olmanson et al., 2016; Palmer et al., 2015). Retrievals in complex waters can be confounded by coloured dissolved organic matter (CDOM), which like chl-a, absorbs light in the blue part of the spectrum (Morel and Prieur, 1977). Chl-a algorithms that utilise the red and NIR part of the spectrum are less affected by CDOM (Gitelson et al., 2008) but the OLI NIR band is too far from either the chl-a absorption peak in the red

(Beck et al., 2016) or the reflectance peak near 700 nm (Gitelson, 1992) to make use of such algorithms. Spectral shape algorithms such as fluorescence line height (Gower et al., 1999) and maximum chlorophyll index (Gower et al., 2008) utilise chl-a fluorescence near 685 nm to estimate the chl-a concentration, but again OLI lacks a band positioned between the red and NIR to identify this peak. In order to mitigate the less than ideal band positioning of OLI, we propose a partial least squares regression (PLSR) derived algorithm for chl-a retrievals.

The mathematical basis for PLSR, which is a derivative of principal component analysis, is well described in literature (Abdi, 2010; Mevik and Wehrens, 2007; Wold et al., 2001). PLSR reprojects the input matrix into latent variable space. Latent variables are linear combinations of the original input variables and are chosen to have maximum covariation with the response variables. PLSR has two main advantages over ordinary least squares regression: it is not confounded in cases with more predictor variables than samples and it is not adversely affected by collinearities of predictor variables (Geladi and Kowalski, 1986; Mevik and Wehrens, 2007; Wold et al., 1984). These properties make PLSR suited to spectral data analysis and PLSR based models are currently well established in laboratory based spectroscopy (Norgaard et al., 2000; Westad and Martens, 2000; Wold et al., 2001). There is also a growing body of literature evaluating PLSR derived model performance from remotely sensed data in both terrestrial (Chi et al., 2018; Dou et al., n.d.; Ewald et al., 2018; Samamad et al., 2018; Zhang et al., 2018) and marine and freshwater (Acar-denizli et al., 2018; Ali and Ortiz, 2016; Blix and Eltoft, 2018; Cao et al., 2018) applications. PLSR has been used to estimate chl-a from aerially obtained hyperspectral data in Lake Erie (Ali and Ortiz, 2016) and Long Bay, South Carolina (Ryan and Ali, 2016) showed good agreement, R^2 = 0.84 and R^2 = 0.80 respectively, with *in-situ* values, and outperformed sixteen

different band ratio algorithms utilising both blue/green and red/NIR spectral regions. Song et al. (2013) used a combination of genetic algorithms and PLSR to build chl-a retrieval algorithms from hyperspectral data. Genetic algorithms were used for input determination from spectral bands, ratios and first derivatives, in most cases preferred inputs were in the red-edge not covered by the Landsat 8 OLI. Blix and Eltoft (2018) found that PLSR based algorithms outperformed the ocean colour algorithms when individual satellite bands and the band ratios used by traditional ocean colour algorithms (O'Reilly et al., 2000, 1998) were used as PLSR inputs to estimate oceanic chl-a concentrations from MERIS, MODIS and Sea-viewing Wide Field-of-View Sensor (SeaWiFS) imagery.

In this study, the intention is not to provide a detailed comparison of Landsat 8 OLI chl-a retrieval algorithms. The non-ideal band positioning of OLI (Beck et al., 2016) means that many existing and better performing algorithms for the OLI sensor use modelling tools such as artificial neural networks (Amanollahi et al., 2017; Guo et al., 2016), non-linear random sample consensus (Kim et al., 2016) or spectral matching against locally calibrated lookup tables (Concha and Schott, 2016). These require recalibration to apply to new study areas and some algorithms are developed for waters far more productive than those examined in this study (Guo et al., 2016; Ha et al., 2017). Here, the aim is to investigate the potential of PLSR derived algorithms to utilise the improved spatial resolution of Landsat 8 OLI for remote chl-a retrievals in inland waters by evaluating both individual bands and band ratios as inputs to PLSR models.

3.3 Data and Methodology

3.3.1 In-situ data

In-situ data was collected from a monitoring buoy located in Lake Trevallyn in Tasmania, Australia (Figure 3-1). Lake Trevallyn is a 12.3 million cubic metre run of river hydro-electric storage reservoir located on the lower South Esk River and is managed by Hydro Tasmania. It has a catchment of approximately 9,500 square kilometres and is used for a variety of water-based recreational activities. It is also an important source of drinking water for the city of Launceston. The lake has experienced several blooms of the potentially toxic *Anabaena circinalis* since January, 2007 (Hydro Tasmania, 2014).

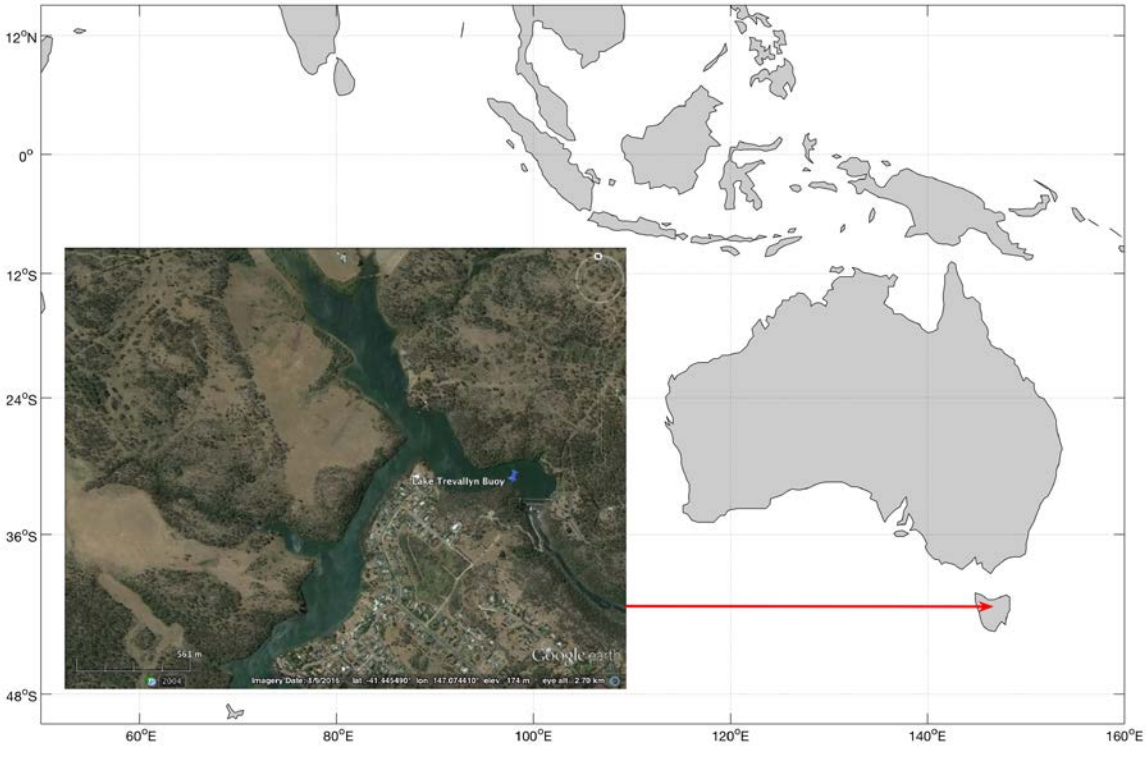

Figure 3-1: Location of *in-situ* monitoring buoy in Lake Trevallyn, Tasmania, Australia

The Lake Trevallyn buoy, managed by Natural Resource Management (NRM) North, was equipped with a Hydrolab DS5X sonde and Turner Designs fluorometric probe. The instrument was deployed at a depth of approximately half a metre and configured to transmit *in-situ* chl-a readings to a central database every fifteen minutes. The probe was equipped with a rotating brush that cleaned the sensor prior to every reading. The whole instrument was extracted, cleaned and calibrated every six weeks throughout deployment, which commenced in late 2013. A two-point calibration was used that utilised reference samples of distilled water and a water sample of known chl-a concentration from the deployment site that had been laboratory analysed at Analytical Services Tasmania (pers. comm.). The *in-situ* dataset used in this study spans the period November 2013 to the end of November 2016, however as the buoy was removed from the lake in periods of predicted high flow, typically from June to October, there is little data from the wetter months.

3.3.2 Satellite Imagery

Level 1 satellite imagery was download from the Landsat OLI/TIRS Collection 1 archive using the Earth Explorer tool (https://earthexplorer.usgs.gov/). Images were downloaded for each date corresponding with the *in-situ* monitoring period, only products of tier 1 quality (USGS, 2019) were used.

Imagery was atmospherically corrected using the Acolite software to both Rayleigh corrected reflectances and fully corrected reflectances, the latter using the dark spectrum aerosol correction method (Vanhellemont and Ruddick, 2018). The pixel extraction feature of SeaDAS 7.5.1 was used to extract pixels corresponding to the *in-situ* monitoring and pixels flagged as cloud were removed. All extracted pixels were within 15 minutes of the corresponding *in-situ* sample time.

3.3.3 Algorithm Development

The Lake Trevallyn *in-situ* dataset was divided into two random stratified data partitions meaning that both datasets had similar ranges of chl-a concentrations. Two thirds of *in-situ* samples were used for algorithm calibration and the remaining third was withheld for validation. PLSR models were built using individual satellite bands and band ratios as inputs. All inputs were scaled and centred. PLSR was performed using repeated (20 times) ten-fold cross validation. Cross validation allows for independent use of all data while ensuring that models are assessed on data that were not used for model building (Arlot and Celisse, 2010; Zhang, 1993). The optimal number of components were chosen for each model by minimising the root mean squared error of cross validation (RMSECV) (Mevik and Cederkvist, 2004). Models were tuned using backward variable elimination: input variables were ranked by each input's variable importance in the projection (VIP) scores, the least important variable was removed and the model was rebuilt (Mehmood et al., 2012).

The performance of the resulting group of models was evaluated against the validation dataset. Models were ranked based on minimal root mean squared error of prediction (RMSEP), which was also normalised (NRMSEP) using the range of *in-situ* chl-a values. Model fit was indicated using the coefficient of determination, R^2, the bias and Nash-Sutcliffe efficiency (NSE). Bias is the mean difference between measured and predicted values and gives an indication of persistent over or under-estimation. NSE ranges from minus infinity to one: negative values indicate that using the mean value of the observed data would have been a better predictor than the model (Krause et al., 2005).

R-studio was used for algorithm development and data analysis. Data partitioning was performed using the createDataPartition function of the caret package (Kuhn, 2008) and PLSR models were built using the pls package (Mevik and Wehrens, 2007). Model tuning was performed using the VIP function in the plsVarSel package (Mehmood et al., 2012). NSE was calculated using the HydroGOF package (Zambrano-Bigiarini, 2017).

3.4 Results

3.4.1 In-situ data and satellite imagery

Thirty-two of sixty-two images matching the *in-situ* data collection were removed due to reflectance values greater than 0.0215 in the 1609 nm SWIR band indicating cloud. This resulted in a matchup dataset of just 30 samples. Atmospheric correction was not successful on more than one third of the remaining images, with eleven of thirty image matches containing negative reflectances. The majority of these were in the blue bands. As removing these images would have reduced an already small dataset, modelling was performed using the Rayleigh corrected reflectances.

The partitioning of Lake Trevallyn *in-situ* data resulted in calibration and validation datasets with similar ranges of chl-a concentrations (Table 3-1): median values were 1.82 mg m^{-3} and 1.72 mg m^{-3}, respectively and *in-situ* chl-a ranged from 0.07 to 15.81 mg m^{-3} for calibration data and 0.34 to 7.10 mg m^{-3} for validation data.

Table 3-1: Five number summaries of *in-situ* chl-a concentrations for each dataset (n = number of valid satellite matches).

		In-situ chl-a (mg m^{-3})				
Dataset	**n**	**Minimum**	**1st Quartile**	**Median**	**3rd Quartile**	**Maximum**
Calibration	20	0.07	1.46	1.73	3.82	15.81
Validation	10	0.51	1.30	1.70	2.35	11.29

3.4.2 Selection of PLSR Model

The best performing model (NRMSEP = 21.6%, bias = -0.03 mg m^{-3}, R^2 = 0.67, NSE = 0.53) consisted of seven band ratio inputs and contained one component. However, there was very little difference in the performance of the leading models (Table 3-2). The next three models, all single component models, with eight, six and nine inputs respectively had NRMSEP of less than 23%, $R^2 > 0.6$ and NSE > 0.48. Models using band inputs instead of ratios performed poorly, the best such model had an NSE of 0.02 indicating that it was barely better than using the mean *in-situ* chl-a concentration as a predictor.

Band ratios seemed more effective than individual bands as inputs. When comparing models with the same number of inputs those that used band ratios consistently performed better than those using individual bands. For models with four to seven inputs, those using band ratios had RMSEP < 24% and NSE > 0.46. Models using band inputs had RMSEP > 30% and NSE < 0.02 (Table 3-2)

.

Table 3-2: Performance of PLSR models sorted by input type and ranked according to minimal RMSEP.

Input type	Number of Inputs	Number of Components	RMSEP (mg m^{-3})	NRMSEP (%)	Bias (mg m^{-3})	R^2	NSE
Ratios	7	1	2.33	21.6	-0.03	0.67	0.53
	8	1	2.40	22.2	-0.02	0.65	0.50
	6	1	2.41	22.3	-0.08	0.62	0.50
	9	1	2.45	22.8	0.02	0.62	0.48
	4	1	2.49	23.1	-0.30	0.52	0.46
	10	1	2.51	23.3	-0.01	0.55	0.46
	5	1	2.51	23.3	-0.19	0.52	0.46
	17	1	2.73	25.3	0.03	0.40	0.36
	18	1	2.77	25.7	0.01	0.37	0.34
	20	1	2.78	25.8	0.00	0.37	0.33
	21	1	2.79	25.9	0.00	0.37	0.33
	19	1	2.80	26.0	-0.01	0.35	0.32
	3	1	3.00	27.8	-0.42	0.25	0.23
	2	2	3.39	31.5	-0.74	0.07	0.01
	13	7	4.42	41.0	-1.65	0.00	-0.69
	14	7	4.52	41.9	-1.51	0.01	-0.76
	15	7	4.81	44.7	-1.34	0.03	-1.00
	16	7	5.01	46.5	-1.26	0.04	-1.17
	12	10	6.80	63.1	-1.10	0.11	-2.99
	11	10	6.85	63.5	-1.20	0.11	-3.05
Bands	7	2	3.38	31.3	-0.83	0.22	0.02
	5	1	3.40	31.5	-1.03	0.16	0.00
	6	1	3.40	31.5	-1.02	0.16	0.00
	4	1	3.41	31.6	-1.03	0.16	0.00
	3	1	3.53	32.8	-1.12	0.16	-0.08
	2	1	3.54	32.9	-1.06	0.19	-0.08

The model with the smallest number of inputs that still had reasonable performance was the four-input model (NRMSEP = 23.1%, bias = -0.30 mg m^{-3}, R^2 = 0.52, NSE = 0.46). When comparing the VIP rating of band ratio inputs in better performing model the order of input importance was the same. The most important inputs were the ratio of the short wave infrared (SWIR) bands, band numbers 6 and 7. Next was the ratio of NIR band 5 to the shorter SWIR band 6 followed by the ratios of red band 4 to SWIR band 6 and the blue band 2 to green band 3 (Table 3-3).

Table 3-3: VIP rankings for 7 input and 4 input models. OLI band centres are B1=443 nm, B2=480 nm, B3=560 nm, B4=655 nm, B5=865 nm, B6=1610 nm and B7=2200 nm.

7 input model		4 input model	
Band ratio	**Variable importance**	**Band ratio**	**Variable Importance**
B6/B7	1.55	B6/B7	1.32
B5/B6	1.25	B5/B6	1.06
B4/B6	0.96	B4/B6	0.82
B2/B3	0.79	B2/B3	0.67
B1/B6	0.75		
B2/B4	0.73		
B1/B3	0.65		

The best performing model showed a tendency to overestimate chl-a for concentrations less than 5 mg m^{-3} and underestimate at higher concentrations (Figure 3-2).

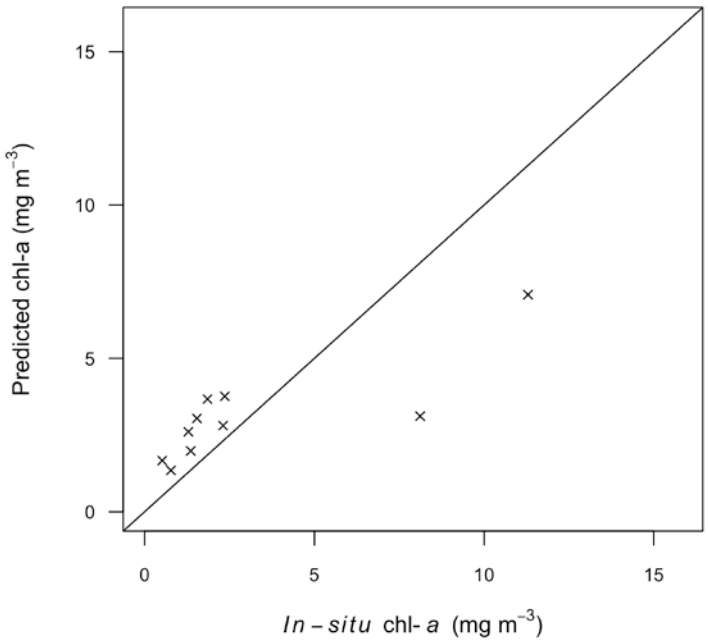

Figure 3-2: Validation plot of predicted versus in-situ chl-a for the 7-input model.

3.5 Discussion

Aerosol correction performed poorly resulting in negative reflectances, mostly in the blue bands, for 11 of 30 images. This adds to the growing body of literature that

suggests for the retrieval of water quality parameters from Landsat imagery there is little benefit to full atmospheric correction (Kallio et al., 2008; Kutser, 2012; Olmanson et al., 2008; Tebbs et al., 2013).

The best performing model (NRMSEP = 21.6%, bias = -0.03 mg m^{-3}, R^2 = 0.67, NSE = 0.53) was a single component model using seven band ratio inputs. That a single component resulted in the smallest predictive error means that the final model is effectively a multiple linear regression of the input band ratios. The tendency of this model to overestimate chl-a at lower concentrations and underestimate for chl-a above 5 mg m^{-3} limits its usefulness, but it still may assist in detecting large changes in biomass. It is also possible this issue is an artefact of the validation dataset, where only two in-situ samples had chl-a greater than 5 mg m^{-3}.

VIP scores can be used to give an indication of the importance of individual inputs to the overall model. Inputs with VIP > 1 are often considered to indicate highly influential inputs while those with VIP < 0.8 might be considered unimportant, however the true location of these thresholds is dependent on the nature of the dataset (Chong and Jun, 2005; Gosselin et al., 2010). When examining the VIP scores for the band ratio inputs the ratio of B6 (1610 nm) with B7 (2200 nm), B5 (865 nm) and B4 (655 nm), respectively, had the highest VIP scores in both the seven and four input models (Table 3-3). It was expected that better results would be achieved using band ratios inputs than with individual band inputs. Band ratios can supress variations in illumination (Beck et al., 2016) and mitigate atmospheric effects by normalising useful signals to atmospheric conditions at the time of image capture (Kutser, 2012).

It was not expected that the ratios of bands 6 (1610 nm) to 7 (2200 nm) would appear so important in modelling. These bands are in the SWIR region and are strongly

absorbed by water and unlikely to be correlated with chl-a. However, bands in the SWIR region are utilised by atmospheric correction algorithms (Shi and Wang, 2009; Wang and Shi, 2005) and as this study used Rayleigh corrected top of atmosphere reflectances, any model would need to allow for atmospheric effects on the signal. Based on VIP scores, the next most important for ratios for both the 7-input and 4-input modes were the ratios of band 5 (865 nm) to band 6 (1610 nm) and band 4 (655 nm) to band 6 (1610 nm) (Table 3-3). If we consider SWIR band 6 as a normalising band (Kutser, 2012) then both the red band at 655 nm and NIR band at 865 nm could be representative of turbidity (Dogliotti et al., 2015; Nechad et al., 2010). The ratio of blue band 2 (480 nm) to green band 3 (560 nm) utilised by oceanic chl-a retrieval algorithms (O'Reilly et al., 2000, 1998) had VIP scores less than 0.8 which suggests marginal importance to the model (Chong and Jun, 2005; Gosselin et al., 2010). This is not surprising as the blue to green ratio alone can be confounded by CDOM and particulates (Chapter 1). It is likely given that inputs representative of turbidity were ranked more highly than the blue to green ratio that this model may be dependent on the extent to which chl-a covaries with turbidity and would need local recalibration before implementation elsewhere.

To date, there are few published attempts to use PLSR regression for satellite based chl-a retrievals over water. Comparison with existing algorithms is problematic as the commonly cited R^2, in isolation, has limits as a measurement of model accuracy and published measures of prediction error vary (Krause et al., 2005). The performance of the PLSR algorithm presented here is comparable to that of recently published chl-a retrieval algorithms for the OLI sensor, of which the better performing generally have $R^2 > 0.5$ for localised datasets ranging from 10 to 44 samples (Amanollahi et al., 2017;

Beck et al., 2016; Concha and Schott, 2016; Guo et al., 2016; Ha et al., 2017; Kim et al., 2016; Lim and Choi, 2015; Masocha et al., 2017).

The development of such models is important. Purpose built ocean colour sensors such as OLCI are expected to be capable of more accurate estimation of chl-a concentrations. However, OLCI has a 300m spatial resolution that is only capable of resolving 5.6% of lakes in the continental United States of at least one hectare in area (Clark et al., 2017). Improvements in spatial resolutions are need for smaller inland reservoirs which are common sources of potable water (Beck et al., 2016) and for monitoring algal blooms where chl-a concentrations can vary several orders of magnitude within an OLCI pixel (Kutser, 2004). This suggests that, for many inland waters, algorithms that can make use of the limited spectral capability but improved spatial resolution of sensors such as the Landsat 8 OLI or the newer Sentinel 2 multi spectral imager (MSI) would be of great value in extending the spatial coverage of monitoring networks.

3.6 Conclusions

The results of this study suggest that PLSR algorithms can be used to derive estimates of chl-a concentration from Landsat 8 OLI imagery of sufficient accuracy (NRMSEP = 21.6%, bias = -0.03 mg m^{-3}, R^2 = 0.67, NSE = 0.53) for certain applications. The methods presented here do not require full atmospheric correction of satellite imagery and would seem most suitable to extend the spatial monitoring capability of water managers with some existing *in-situ* monitoring regime in place. Such a configuration would also permit the ongoing validation and, if necessary, recalibration of the algorithm.

3.7 Acknowledgments

This project received funding by Sense-T. The authors would like to thank Michael Attard and Toni Furlong from NRM North for access to *in-situ* chlorophyll-a data and instrumentation details.

The Landsat 8 OLI/TIRS collection 1, level 1 data products were retrieved from the online Earth Explorer, courtesy of the NASA Land Processes Distributed Active Archive Center (LP DAAC), USGS/Earth Resources Observation and Science (EROS) Center, Sioux Falls, South Dakota, https://earthexplorer.usgs.gov/.

3.8 References

Abdi, H., 2010. Partial least squares regression and projection on latent structure regression. Wiley Interdiscip. Rev. Comput. … 2, 97–106. https://doi.org/10.1002/wics.051

Acar-denizli, N., Dedicado, P., Basarir, G., Caballero, I., 2018. Functional regression on remote sensing data in oceanography. Environ. Ecol. Stat. 277–304. https://doi.org/10.1007/s10651-018-0405-7

Ali, K.A., Ortiz, J.D., 2016. Multivariate approach for chlorophyll-a and suspended matter retrievals in Case II type waters using hyperspectral data. Hydrol. Sci. J. 61, 200–213. https://doi.org/10.1080/02626667.2014.964242

Amanollahi, J., Kaboodvandpour, S., Majidi, H., 2017. Evaluating the accuracy of ANN and LR models to estimate the water quality in Zarivar International Wetland, Iran. Nat. Hazards 85, 1511–1527. https://doi.org/10.1007/s11069-016-2641-1

Anderson, D.M., Boerlage, S.F.E., Dixon, M.B., 2017. Harmful Algal Blooms (HABs) and Desalination : A Guide to Impacts, Monitoring , and Management.

Anderson, D.M., Cembella, A.D., Hallegraeff, G.M., 2012. Progress in Understanding Harmful Algal Blooms: Paradigm Shifts and New Technologies for Research, Monitoring, and Management. Ann. Rev. Mar. Sci. 4, 143–176. https://doi.org/doi:10.1146/annurev-marine-120308-081121

Arlot, S., Celisse, A., 2010. A survey of cross-validation procedures for model selection 40–79. https://doi.org/10.1214/09-SS054

Beck, R., Zhan, S., Liu, H., Tong, S., Yang, B., Xu, M., Ye, Z., Huang, Y., Shu, S., Wu, Q., Wang, S., Berling, K., Murray, A., Emery, E., Reif, M., Harwood, J., Young, J., Nietch, C., Macke, D., Martin, M., Stillings, G., Stump, R., Su, H., 2016. Comparison of satellite reflectance algorithms for estimating chlorophyll-a in a temperate reservoir using coincident hyperspectral aircraft imagery and dense coincident surface observations. Remote Sens. Environ. 178, 15–30. https://doi.org/10.1016/j.rse.2016.03.002

Blix, K., Eltoft, T., 2018. Evaluation of Feature Ranking and Regression Methods for Oceanic Chlorophyll-a Estimation. IEEE J. Sel. Top. Appl. Earth Obs. Remote Sens. 11, 1403–1418. https://doi.org/10.1109/JSTARS.2018.2810704

Cao, Y., Ye, Y., Zhao, H., Jiang, Y., Wang, H., Shang, Y., Wang, J., 2018. Remote sensing of water quality based on HJ-1A HSI imagery with modified discrete binary particle swarm optimization-partial least squares (MDBPSO-PLS) in inland waters: A case in Weishan Lake. Ecol. Inform. 44, 21–32. https://doi.org/10.1016/j.ecoinf.2018.01.004

Chi, Y., Shi, H., Zheng, W., Sun, J., 2018. Simulating spatial distribution of coastal soil carbon content using a comprehensive land surface factor system based on remote sensing. Sci. Total Environ. 628–629, 384–399. https://doi.org/10.1016/j.scitotenv.2018.02.052

Chong, I.G., Jun, C.H., 2005. Performance of some variable selection methods when multicollinearity is present. Chemom. Intell. Lab. Syst. 78, 103–112. https://doi.org/10.1016/j.chemolab.2004.12.011

Clark, J.M., Schaeffer, B.A., Darling, J.A., Urquhart, E.A., Johnston, J.M., Ignatius,

A.R., Myer, M.H., Loftin, K.A., Werdell, P.J., Stumpf, R.P., 2017. Satellite monitoring of cyanobacterial harmful algal bloom frequency in recreational waters and drinking water sources. Ecol. Indic. 80, 84–95. https://doi.org/10.1016/j.ecolind.2017.04.046

Concha, J.A., Schott, J.R., 2016. Retrieval of color producing agents in Case 2 waters using Landsat 8. Remote Sens. Environ. 185, 95–107. https://doi.org/10.1016/j.rse.2016.03.018

Dogliotti, A.I., Ruddick, K.G., Nechad, B., Doxaran, D., Knaeps, E., 2015. A single algorithm to retrieve turbidity from remotely-sensed data in all coastal and estuarine waters. Remote Sens. Environ. 156, 157–168. https://doi.org/10.1016/j.rse.2014.09.020

Dou, Z., Cui, L., Li, J., Zhu, Y., Gao, C., Pan, X., n.d. Hyperspectral Estimation of the Chlorophyll Content in Short-Term and Long-Term Restorations of Mangrove in Quanzhou Bay Estuary , China. https://doi.org/10.3390/su10041127

ESA, 2018. User Guides - Sentinel 3 OLCI [WWW Document]. URL https://sentinel.esa.int/web/sentinel/user-guides/sentinel-3-olci (accessed 9.14.18).

Ewald, M., Aerts, R., Lenoir, J., Fassnacht, F.E., Nicolas, M., Skowronek, S., Piat, J., Honnay, O., Garzón-López, C.X., Feilhauer, H., Van De Kerchove, R., Somers, B., Hattab, T., Rocchini, D., Schmidtlein, S., 2018. LiDAR derived forest structure data improves predictions of canopy N and P concentrations from imaging spectroscopy. Remote Sens. Environ. 211, 13–25. https://doi.org/10.1016/j.rse.2018.03.038

Franz, B.A., Bailey, S.W., Kuring, N., Werdell, P.J., 2015. Ocean color measurements

with the Operational Land Imager on Landsat-8: implementation and evaluation in SeaDAS. J. Appl. Remote Sens. 9, 096070. https://doi.org/10.1117/1.JRS.9.096070

Geladi, P., Kowalski, B.R., 1986. Partial least-squares regression: a tutorial. Anal. Chim. Acta 185, 1–17. https://doi.org/10.1016/0003-2670(86)80028-9

Gitelson, A.A., 1992. The peak near 700 nm on radiance spectra of algae and water: relationships of its magnitude and position with chlorophyll concentration. Int. J. Remote Sens. 13, 3367–3373. https://doi.org/10.1080/01431169208904125

Gitelson, A.A., Dall'Olmo, G., Moses, W., Rundquist, D.C., Barrow, T., Fisher, T.R., Gurlin, D., Holz, J., 2008. A simple semi-analytical model for remote estimation of chlorophyll-a in turbid waters: Validation. Remote Sens. Environ. 112, 3582–3593. https://doi.org/10.1016/j.rse.2008.04.015

Gosselin, R., Rodrigue, D., Duchesne, C., 2010. A Bootstrap-VIP approach for selecting wavelength intervals in spectral imaging applications. Chemom. Intell. Lab. Syst. 100, 12–21. https://doi.org/10.1016/j.chemolab.2009.09.005

Gower, J., King, S., Goncalves, P., 2008. Global monitoring of plankton blooms using MERIS MCI. Int. J. Remote Sens. 29, 6209–6216. https://doi.org/10.1080/01431160802178110

Gower, J.F.R.R., Doerffer, R., Borstad, G.A., 1999. Interpretation of the 685 nm peak in water-leaving radiance spectra in terms of fluorescence, absorption and scattering, and its observation by MERIS. Int. J. Remote Sens. 20, 1771–1786. https://doi.org/10.1080/014311699212470

Guo, Q., Wu, X., Bing, Q., Pan, Y., Wang, Z., Fu, Y., Wang, D., Liu, J., 2016. Study on retrieval of chlorophyll-a concentration based on Landsat OLI Imagery in the Haihe River, China. Sustain. 8. https://doi.org/10.3390/su8080758

Ha, N.T.T., Koike, K., Nhuan, M.T., Canh, B.D., Thao, N.T.P., Parsons, M., 2017. Landsat 8/OLI Two bands ratio algorithm for chlorophyll-a concentration mapping in hypertrophic waters: An application to west lake in Hanoi (Vietnam). IEEE J. Sel. Top. Appl. Earth Obs. Remote Sens. 10, 4919–4929. https://doi.org/10.1109/JSTARS.2017.2739184

Hoagland, P., Anderson, D.M., Kaoru, Y., White, A.W., 2002. The economic effects of harmful algal blooms in the United States: Estimates, assessment issues, and information needs. Estuaries 25, 819–837. https://doi.org/10.1007/BF02804908

Hydro Tasmania, 2014. Lake Trevallyn Algal Monitoring Program.

Ibelings, B.W., Backer, L.C., Kardinaal, W.E.A., Chorus, I., 2014. Current approaches to cyanotoxin risk assessment and risk management around the globe. Harmful Algae 40, 63–74. https://doi.org/10.1016/j.hal.2014.10.002

Kallio, K., Attila, J., Härmä, P., Koponen, S., Pulliainen, J., Hyytiäinen, U.-M., Pyhälahti, T., 2008. Landsat ETM+ images in the estimation of seasonal lake water quality in boreal river basins. Environ. Manage. 42, 511–522.

Kim, H.H., Ko, B.C., Nam, J.Y., 2016. Predicting chlorophyll-a using Landsat 8 OLI sensor data and the non-linear RANSAC method – a case study of Nakdong River, South Korea. Int. J. Remote Sens. 37, 3255–3271. https://doi.org/10.1080/01431161.2016.1196839

Krause, P., Boyle, D.P., Bäse, F., 2005. Comparison of different efficiency criteria for hydrological model assessment. Adv. Geosci. 5, 89–97. https://doi.org/10.5194/adgeo-5-89-2005

Kuhn, M., 2008. Building Predictive Models in R Using the caret Package. J. Stat. Softw. 28, 1–26. https://doi.org/10.1053/j.sodo.2009.03.002

Kutser, T., 2012. The possibility of using the Landsat image archive for monitoring long time trends in coloured dissolved organic matter concentration in lake waters. Remote Sens. Environ. 123, 334–338. https://doi.org/10.1016/j.rse.2012.04.004

Kutser, T., 2009. Passive optical remote sensing of cyanobacteria and other intense phytoplankton blooms in coastal and inland waters. Int. J. Remote Sens. 30, 4401–4425. https://doi.org/10.1080/01431160802562305

Kutser, T., 2004. Quantitative detection of chlorophyll in cyanobacterial blooms by satellite remote sensing. Limnol. Oceanogr. 49, 2179–2189. https://doi.org/10.4319/lo.2004.49.6.2179

Lim, J., Choi, M., 2015. Assessment of water quality based on Landsat 8 operational land imager associated with human activities in Korea. Environ. Monit. Assess. 187. https://doi.org/10.1007/s10661-015-4616-1

Masocha, M., Dube, T., Nhiwatiwa, T., Choruma, D., 2017. Testing utility of Landsat 8 for remote assessment of water quality in two subtropical African reservoirs with contrasting trophic states. Geocarto Int. https://doi.org/10.1080/10106049.2017.1289561

Mehmood, T., Liland, K.H., Snipen, L., Sæbø, S., 2012. A review of variable selection

methods in Partial Least Squares Regression. Chemom. Intell. Lab. Syst. 118, 62–69. https://doi.org/10.1016/j.chemolab.2012.07.010

Mevik, B.-H., Wehrens, R., 2007. The pls Package: Principle Component and Partial Least Squares Regression in R. J. Stat. Softw. 18, 1–24. https://doi.org/10.1002/wics.10

Mevik, B.H., Cederkvist, H.R., 2004. Mean squared error of prediction(MSEP) estimates for principal component regression(PCR) and partial least squares regression(PLSR). J. Chemom. 18, 422–429. https://doi.org/10.1002/cem.887

Morel, A., Prieur, L., 1977. Analysis of Variations in Ocean Color. Limnol. Oceanogr. 22, 709–722. https://doi.org/10.2307/2835253

NASA, 2014. Components of MODIS [WWW Document]. URL http://modis.gsfc.nasa.gov/about/specifications.php (accessed 2.4.14).

Nechad, B., Ruddick, K.G., Park, Y., 2010. Calibration and validation of a generic multisensor algorithm for mapping of total suspended matter in turbid waters. Remote Sens. Environ. 114, 854–866. https://doi.org/10.1016/j.rse.2009.11.022

Norgaard, L., Wagner, J., Nielsen, J.P., Munc, L., Engelsen, S.B., 2000. nterval Partial Least-Squares Regression (iPLS): A Comparative Chemometric Study with an Example from Near-Infrared Spectroscopy 54, 413–419.

O'Reilly, J.E., Maritorena, S., Mitchell, B.G., Siegel, D.A., Carder, K.L., Garver, S.A., Kahru, M., McClain, C., 1998. Ocean color chlorophyll algorithms for SeaWiFS. J. Geophys. Res. Ocean. 103, 24937–24953.

O'Reilly, J.E., Maritorena, S., Siegel, D.A., O'Brien, M.C., Toole, D., Mitchell, B.G.,

Kahru, M., Chavez, F.P., Strutton, P., Cota, G.F., 2000. Ocean color chlorophyll a algorithms for SeaWiFS, OC2, and OC4: Version 4. SeaWiFS postlaunch calibration Valid. Anal. Part 3, 9–23.

Olmanson, L.G., Bauer, M.E., Brezonik, P.L., 2008. Remote Sensing of Environment A 20-year Landsat water clarity census of Minnesota ' s 10 , 000 lakes. Remote Sens. Environ. 112, 4086–4097. https://doi.org/10.1016/j.rse.2007.12.013

Olmanson, L.G.L.G., Brezonik, P.L.P.L., Finlay, J.C., Bauer, M.E.M.E., 2016. Comparison of Landsat 8 and Landsat 7 for regional measurements of CDOM and water clarity in lakes. Remote Sens. Environ. 185, 119–128. https://doi.org/10.1016/j.rse.2016.01.007

Paerl, H.W., Hall, N.S., Calandrino, E.S., 2011. Controlling harmful cyanobacterial blooms in a world experiencing anthropogenic and climatic-induced change. Sci. Total Environ. 409, 1739–1745. https://doi.org/10.1016/j.scitotenv.2011.02.001

Paerl, H.W., Otten, T.G., 2013. Harmful Cyanobacterial Blooms: Causes, Consequences, and Controls. Microb. Ecol. 65, 995–1010. https://doi.org/10.1007/s00248-012-0159-y

Palmer, S.C.J., Kutser, T., Hunter, P.D., 2015. Remote sensing of inland waters: Challenges, progress and future directions. Remote Sens. Environ. 157, 1–8. https://doi.org/10.1016/j.rse.2014.09.021

Ryan, K., Ali, K., 2016. Application of a partial least-squares regression model to retrieve chlorophyll-a. Ocean Sci. J. 51, 209–221.

Samamad, N.T.I., Ribeiro, L.P.D., de Almeida Lopes, M.M., Puschmann, R., de

Oliveira Silva, E., 2018. Near infrared spectroscopy, a suitable tool for fast phenotyping – The case of cashew genetic improvement. Sci. Hortic. (Amsterdam). 238, 363–368. https://doi.org/10.1016/j.scienta.2018.05.007

Sanseverino, I., Conduto, D., Pozzoli, L., Dobricic, S., Lettieri, T., 2016. Algal bloom and its economic impact. https://doi.org/10.2788/660478

Shi, W., Wang, M., 2009. An assessment of the black ocean pixel assumption for MODIS SWIR bands. Remote Sens. Environ. 113, 1587–1597.

Song, K., Li, L., Tedesco, L.P., Li, S., Duan, H., Liu, D., Hall, B.E., Du, J., Li, Z., Shi, K., Zhao, Y., 2013. Remote estimation of chlorophyll-a in turbid inland waters: Three-band model versus GA-PLS model. Remote Sens. Environ. 136, 342–357. https://doi.org/10.1016/j.rse.2013.05.017

Tebbs, E.J., Remedios, J.J., Harper, D.M., 2013. Remote sensing of chlorophyll-a as a measure of cyanobacterial biomass in Lake Bogoria, a hypertrophic, saline–alkaline, flamingo lake, using Landsat ETM +. Remote Sens. Environ. 135, 92–106. https://doi.org/http://dx.doi.org/10.1016/j.rse.2013.03.024

USGS, 2019. What are Landat Collection 1 Tiers? [WWW Document].

USGS, 2016. Landsat 8 (L8) Data Users Handbook, America.

Vanhellemont, Q., Ruddick, K., 2018. Atmospheric correction of metre-scale optical satellite data for inland and coastal water applications. Remote Sens. Environ. 216, 586–597. https://doi.org/10.1016/j.rse.2018.07.015

Wang, M.H., Shi, W., 2005. Estimation of ocean contribution at the MODIS near-infrared wavelengths along the east coast of the US: Two case studies. Geophys.

Res. Lett. 32. https://doi.org/10.1029/2005gl022917

Westad, F., Martens, H., 2000. Variable selection in near infrared spectroscopy based on significance testing in partial least squares regression. J. Near Infrared Spectrosc. 8, 117–124. https://doi.org/10.1255/jnirs.271

Wold, S., Ruhe, A., Wold, H., Dunn, III, W.J., 1984. The Collinearity Problem in Linear Regression. The Partial Least Squares (PLS) Approach to Generalized Inverses. SIAM J. Sci. Stat. Comput. 5, 735–743. https://doi.org/10.1137/0905052

Wold, S., Sjöström, M., Eriksson, L., 2001. PLS-regression: A basic tool of chemometrics. Chemom. Intell. Lab. Syst. 58, 109–130. https://doi.org/10.1016/S0169-7439(01)00155-1

World Health Organization, 1999. Toxic Cyanobacteria in Water: A guide to their public health consequences, monitoring and management, Retrieved March. https://doi.org/10.1046/j.1365-2427.2003.01107.x

Zambrano-Bigiarini, M., 2017. Goodness-of-fit Functions for Comparison of Simulated and Observed [WWW Document]. URL https://cran.r-project.org/web/packages/hydroGOF/hydroGOF.pdf (accessed 9.1.18).

Zhang, C., Liu, J., Shang, J., Cai, H., 2018. Capability of crop water content for revealing variability of winter wheat grain yield and soil moisture under limited irrigation. Sci. Total Environ. 631–632, 677–687. https://doi.org/10.1016/j.scitotenv.2018.03.004

Zhang, P., 1993. Model selection via multifold cross validation. Ann. Stat. 299–313.

4 Improved Sentinel 2 chlorophyll-a retrievals using dynamic chlorophyll-a specific absorption coefficient: A Lake Erie case study

4.1 Abstract

The Sentinel 2 platform offers greatly improved spatial resolution over other satellite platforms designed for water based chl-a retrievals and includes a “red-edge” band at 704 nm not present on the Landsat 8 operational land imager. Results of this study indicate an improved semi-analytical model for chlorophyll-a (chl-a) retrievals by replacing a fixed chl-a specific absorption coefficient (*a**) with a variable model. This method was applied to three Sentinel 2 images taken over the Lake Erie western basin correlating with an in-situ dataset of 24 samples where chl-a ranged from 1.89 mg m^{-3} to 70.20 mg m^{-3}. The variable *a** model produced chl-a retrievals with normalised root mean squared error of prediction (NRMSEP) = 7.5%, bias = -0.47 mg m^{-3}, coefficient of determination (R^2) = 0.91 and Nash-Sutcliffe efficiency (NSE) = 0.90). This represented a 23% reduction in NRMSEP, an 85% reduction in bias and an increase in NSE of 7% over the default algorithm using a fixed *a** value. Creation of chl-a retrieval algorithms that consider the variability in *a** should result in algorithms that perform better against a wide range of chl-a concentrations and are less likely to require local recalibration. Obtaining accurate chl-a retrievals from a satellite platform with the spatial resolution of Sentinel 2 will allow satellite monitoring of many more inland waters than previously possible.

4.2 Introduction

Cyanobacteria blooms are potentially toxic and present hazards to both human and animal health (World Health Organization, 1999) and there is evidence to suggest their frequency is increasing globally (Anderson et al., 2017, 2012). Water managers in many countries are responsible for monitoring cell biovolumes and/or toxin levels to ensure they remain within safe levels (Ibelings et al., 2014). Remote sensing of

chlorophyll-a (chl-a) is used as a proxy for algal biomass on a variety of satellite platforms and can be a powerful tool in the detection and monitoring of algal blooms (Shen et al., 2012). HABs are spatially and temporally heterogenous and monitoring is required over large coasts and a vast number of lakes (Kutser, 2009). Satellite platforms designed for ocean colour monitoring such as the moderate resolution imaging spectrometer (MODIS), visible infrared imaging radiometer suite (VIIRS) and Sentinel 3's ocean and land colour instrument (OLCI) have spatial resolutions of approximately 1000, 740 and 300 metres respectively (ESA, 2018a; NASA, 2014). However, even OLCI's 300m spatial resolution is only able to resolve approximately 5% of lakes in North America (Clark et al., 2017) and the spatial resolution of existing marine remote sensing platform is considered a challenge to adequate remote sensing of inland waters (Palmer et al., 2015).

The European Space Agency's (ESA) Sentinel 2 platform offers bands with native spatial resolutions of 10, 20 and 60 m (Table 4-1). Additionally, Sentinel 2's five-day revisit time offers improved temporal coverage to the Landsat 8 operational land imager (OLI) which operates on a sixteen day cycle (USGS, 2016). The presence of a "red-edge" band centred near the 705 nm wavelength also suggests the MSI instrument may be suitable to wider range of chl-a retrieval algorithms than the Landsat 8 OLI (Beck et al., 2016) as this spectral region is less affected by coloured dissolved organic matter (CDOM) (Gitelson et al., 2008).

Several studies have already investigated the capabilities of the MSI sensor to estimate chl-a. Toming et al. (2016) found a strong relationship between the height of the 705 nm peak above neighbouring bands and chl-a ($R^2 = 0.83$) using 23 samples from nine Estonian lakes. Chen et al. (2017) found an empirical algorithm using the ratio of the

705 nm band to the 664 nm band performed poorly against 41 samples from Lake Huron, but performance improved when multiple band ratios were used as in puts to a neural network algorithm (R^2 = 0.95, NRMSE = 10.4%) and Ha et al. (Ha et al., 2017) found the best predictor (R^2 = 0.68) of chl-a based on 30 samples from a Vietnamese lake to be an exponential model using the ratio of green (560 nm) to red (665 nm). These studies have all fit algorithms to local water bodies, and it is likely they will need to be recalibrated for use elsewhere.

The three-band algorithm of Gons (1999; Gons et al., 2008, 2005, 2002) has, possibly, the potential for greater generalisability due to its semi-analytic design. The algorithm derives the concentration of chl-a (C) from the following relationship:

$$C = \frac{R(a_w(\lambda_2) + b_b) - a_w(\lambda_1) - {b_b}^p}{a^*(\lambda_1)} \qquad (4\text{-}1)$$

where R is the ratio of water surface reflectance (ρ_w) at wavelengths λ_1 and λ_2, $a^*(\lambda_1)$ and $a_w(\lambda)$ are the wavelength dependant chl-a specific absorption coefficient and absorption due to water respectively, b_b is the backscattering coefficient and p is an empirically derived constant. This algorithm, which will subsequently referred to as G99, is particularly interesting as it has been successfully validated without recalibration in fresh and estuarine waters in Europe, North America and China using surface radiometry (Gons, 1999; Gons et al., 2002). G99 has also been calibrated for use with the ESA's medium resolution imaging spectrometer (MERIS) using λ_1 = 664 nm, λ_2 = 708 and λ_3 = 778, which are quite close to Sentinel 2 MSI's bands 4, 5 and 7, respectively (Table 4-1). After substituting absorption due to water at each wavelength from Buiteveld et al. (1994), equation 4-1 simplifies to (Gons et al., 2005):

$$C = \frac{R(0.70 + b_b) - 0.40 - {b_b}^{1.05}}{a^*(664)} \qquad (4\text{-}2)$$

and the backscattering coefficient is calculated using NIR band, λ_3 = 778 nm:

$$b_b = \frac{1.61\ \rho_w(778)}{0.082 - 0.6\ \rho_w(778)} \qquad (4\text{-}3)$$

$a^*(\lambda_1)$ has been shown to vary widely depending on the size, type and concentration of phytoplankton (Bricaud et al., 1995; Sathyendranath et al., 1987) and variation in $a^*(672)$ explained almost all residuals in the initial description of the algorithm (Gons, 1999). In subsequent validations where algorithm performance has been poor, it has been primarily attributed to an unsuitable choice of $a^*(\lambda_1)$ (Dall'Olmo and Gitelson, 2005; Gurlin et al., 2011). However, $a^*(\lambda_1)$ generally takes a fixed value in published implementations of the algorithm.

The primary purpose of this study is to investigate the effect of variable modelling of $a^*(\lambda_1)$ on algorithm performance with a view to broadening the generalisability of the algorithm. Whilst it is not possible to make an *a priori* determination of some sources of variation in $a^*(\lambda_1)$, the inverse relationship between a^* and chl-a concentration, C, can be expressed in the following form (Bricaud et al., 1995):

$$a^*(\lambda) = A\ C^{-B} \qquad (4\text{-}4)$$

where A and B are wavelength dependent constants. Suitable values for A and B will be determined and $a^*(665)$ will be recalibrated using an initial estimate of C derived using the G99 default of $a^*(665) = 0.015$ and equation 4-4 above. The effect of this process on chl-a retrieval accuracy will be quantified.

Full atmospheric correction is required to derive $\rho_w(\lambda)$ from satellite imagery. The Acolite software package applies a new dark spectrum atmospheric correction algorithm (Vanhellemont and Ruddick, 2018) and given the spectral similarity of

Sentinel 2 MSI bands 4, 5 and 7 (Table 4-1) also implements the MERIS calibrated G99 as per equations 4-2 and 4-3 above, with $a^*_{MSI}(665) \approx a^*(664)_{MERIS} = 0.015$.

However, as the Acolite software also implements two additional red-edge chl-a retrieval algorithms their performance will also be evaluated for comparison. The first is a three band model (Moses et al., 2012, 2009) shown in equation 4-5, which will be referred to as M09:

$$C = 232.29\,\{[R_{rs}^{-1}(\lambda_1) - R_{rs}^{-1}(\lambda_2)]\,R_{rs}(\lambda_3)\} + 23.174 \qquad (4\text{-}5)$$

where $R_{rs}(\lambda_1)$, $R_{rs}(\lambda_2)$ and $R_{rs}(\lambda_3)$ are the remote sensing reflectances at MSI bands 4, 5 and 7 respectively. The second, derived from the normalised difference chlorophyll index (NDCI) (Mishra and Mishra, 2012), is shown in equations 4-6 and 4-7 and will be subsequently referred to as NDCI:

$$x = \frac{R_{rs}(\lambda_2) - R_{rs}(\lambda_1)}{R_{rs}(\lambda_2) + R_{rs}(\lambda_1)} \qquad (4\text{-}6)$$

$$C = 14.039 + 86.115\,x + 194.325\,x^2 \qquad (4\text{-}7)$$

where λ_1 and λ_2 are MSI bands 4 at 665 nm and 5 at 704 nm respectively.

4.3 Data and Methodology

4.3.1 In-situ data

In-situ data from the western basin of Lake Erie (Figure 3-1), which is prone to blooms dominated by *Microcystis aeruginosa* (Vincent et al., 2004; Wynne et al., 2010), was provided through the Great Lakes Environmental Research laboratory (GLERL) weekly monitoring programme. The programme runs from April to October each year

and data from 2017 and 2018 were used in this study. Water samples were collected on a weekly basis from depths of 0.75m +/- 0.25 m and were laboratory analysed for turbidity, absorption due to CDOM at 400 nm^{-1} and chlorophyll-a (pers. comm.).

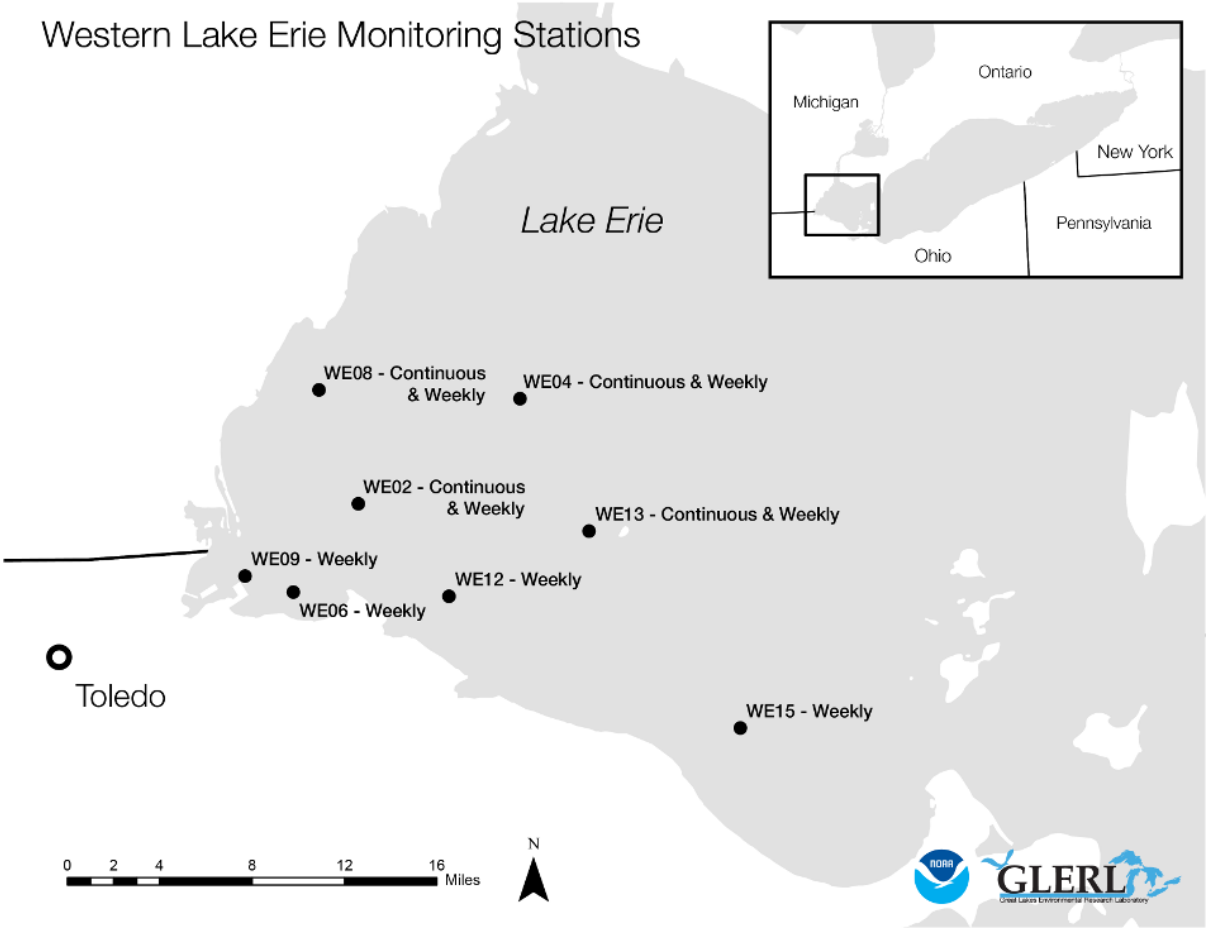

Figure 4-1: Map showing location of weekly *in-situ* sampling sites. Source: Great Lakes Environmental Research Laboratory (https://www.glerl.noaa.gov/res/HABs_and_Hypoxia/WLEMicrocystin2017.html).

4.3.2 Satellite Imagery

The Sentinel 2 constellation consists of two satellites: Sentinel 2A, launched in June 2015, and Sentinel 2B, launched in March 2017. Each satellite is equipped with a

multi-spectral imager (MSI) and has a revisit time of 10 days, their orbits are offset to give the constellation a revisit time of 5 days. The MSI spectral bands (Table 4-1) have native spatial resolutions of 10, 20 and 60 metres (ESA, 2018b).

Table 4-1: Spectral band configuration for the MSI instrument on board each Sentinel 2 satellite (ESA, 2018b)**.**

Spatial Resolution (m)	Band number	Sentinel 2A		Sentinel 2B	
		Central wavelength (nm)	Bandwidth (nm)	Central wavelength (nm)	Bandwidth (nm)
10	2	492.4	98	492.1	98
	3	559.8	45	559.0	46
	4	664.6	38	664.9	39
	8	832.8	145	832.9	133
20	5	704.1	19	703.8	20
	6	740.5	18	739.1	18
	7	782.8	28	779.7	28
	8a	864.7	33	864.0	32
	11	1613.7	143	1610.4	141
	12	2202.4	242	2185.7	238
60	1	442.7	27	442.2	45
	9	945.1	26	943.2	27
	10	1373.5	75	1376.9	76

Level 1C Sentinel 2 satellite imagery that corresponded to *in-situ* sampling locations was downloaded from the ESA open data access hub (https://scihub.copernicus.eu/). Imagery was spatially subset to the area of interest and atmospherically corrected to a level 2 product using the Acolite software package (Vanhellemont and Ruddick, 2016). Remote sensing reflectance for each band was returned in addition to chl-a estimates from the G99, M09 and NDCI algorithms. For the G99 and M09 algorithms, a second retrieval was made using λ_3 = 740 nm (band 6), these modified algorithms will be referred to as G99_740 and M09_740 respectively.

Level-2 pixel values corresponding to in-situ sampling locations and within twelve hours of the recorded sample collection time were extracted using the pixel extraction feature of NASA's SeaDAS 7.5.1 software tool.

4.3.3 Algorithm validation and tuning

To evaluate the effect of a variable model for $a^*(\lambda_1)$, three models of the relationship between a^* and C (equation 4-2) were compared: two from the literature and a localised model optimised to the *in-situ* data. The first model was the result of linear interpolation for λ_1 = 664.75 nm, the mid-point between the band centres for band 4 on the two Sentinel 2 satellites, against the table published in Bricaud et al. (1995), which gives:

$$a^*_{Bricaud}(664.75) = 0.015\, C^{-0.1333} \qquad (4\text{-}8)$$

Equation 4-8 is based on oceanic studies. Several alternate parametrisations of equation 4-4 from inland waters are available. These include values derived from three Estonian lakes (Paavel et al., 2016), fifteen Polish lakes (Ficek et al., 2012) and a single highly eutrophic Japanese lake (Yoshimura et al., 2012). However, as Gilerson et al. (2010) collected data from multiple field trips in Nebraska lakes, Chesapeake Bay and Long Island Sound that included a mixture of salt and freshwater and a range of chl-a concentrations from 2 mg m^{-3} to more than 240 mg m^{-3} it was felt that their relationship (Equation 4-9) would provide the greatest potential for generalisability.

$$a^*_{Gilerson}(665) = 0.022\, C^{-0.1675} \qquad (4\text{-}9)$$

Finally, a localised model was created. During bloom periods in Lake Erie, *M. aeruginosa* is the dominant species (Wynne et al., 2010). Wojtasiewicz and Stoń-Egiert

(2016) published a value of $a^*(675)$ for *M. aeruginosa* of 0.022 which was converted to $a^*(665)$ using equation 4-10 (Gilerson et al., 2010):

$$a^*(665) = 0.412\ a^*(675)^{0.8373} \quad (4\text{-}10)$$

This resulted in equation 4-11:

$$a^*_{localised}(665) = 0.017\ C^{-B} \quad (4\text{-}11)$$

where the value of *B* would be determined by optimising to the *in-situ* data.

Algorithm performance was evaluated using the root mean squared error of prediction (RMSEP), which was also normalised using the range of in-situ chl-a values into percentage RMSEP (NRMSEP), and bias, which was the mean difference between predicted and observed chl-a values. Model fit was reported using both the standard coefficient of determination (R^2) and the Nash-Sutcliffe model efficiency (NSE), which ranges from one to minus infinity, where negative values suggest that the model is inferior to using the mean value of the observed data as a predictor (Krause et al., 2005).

4.4 Results

4.4.1 Description of in-situ data

The sampling dates for the GLERL weekly monitoring programme for 2017 and 2018 coincided with three Sentinel 2 images where sampling stations were not obscured by cloud. This resulted in 24 *in-situ* water sample matches from October 2nd, 2017 and July 9th and August 13th, 2018. *In-situ* chl-a values ranged from 1.89 mg m^{-3} to 70.20 mg m^{-3} with mean and median values of 21.54 mg m^{-3} and 18.59 mg m^{-3} respectively.

4.4.2 Default algorithm performance

The most accurate chl-a retrievals using default parameters were obtained using the G99 algorithm with 9.8% NRMSEP compared to 14.6% and 21.7% for the M09 and NDCI algorithms respectively. The -3.30 mg m^{-3} bias produced by the G99 algorithm was less than half the bias of the M09 and NDCI algorithms, -7.13 mg m^{-3} and the -9.28 mg m^{-3} respectively (Table 4-2).

For the G99 and M09 algorithms, moving λ_3 from 780 nm to 740 nm had minimal impact on performance. The M09 algorithm was more affected with RMSEP and bias increasing by approximately five percent compared to the G99 algorithm where RMSEP increased by less than one percent and bias increased by less than 3 percent.

Table 4-2: Performance of Acolite red-edge retrieval algorithms using default parameters.

Algorithm	RMSEP (mg m^{-3})	NRMSEP (%)	Bias (mg m^{-3})	R^2	NSE
G99	6.67	9.80	-3.30	0.92	0.84
G99_740	6.70	9.80	-3.39	0.92	0.84
M09	9.97	14.60	-7.13	0.86	0.64
M09_740	10.43	15.30	-7.52	0.86	0.60
NDCI	14.79	21.70	-9.28	0.89	0.20

All algorithms showed a negative bias (Table 4-2), however the G99 algorithm only begins to noticeably underestimate chl-a for in-situ chl-a concentrations of approximately 20 mg m^{-3} and above (Figure 4-2a) whereas the M09 algorithm consistently underestimates chl-a concentration across the entire range (Figure 4-2c). The NDCI algorithm appears to generalise poorly to this study area, whilst the relationship between the predicted and in-situ values is quite linear with $R^2 = 0.89$ (Table 4-2) both the gradient and intercept appear to be poorly calibrated (Figure 4-2e).

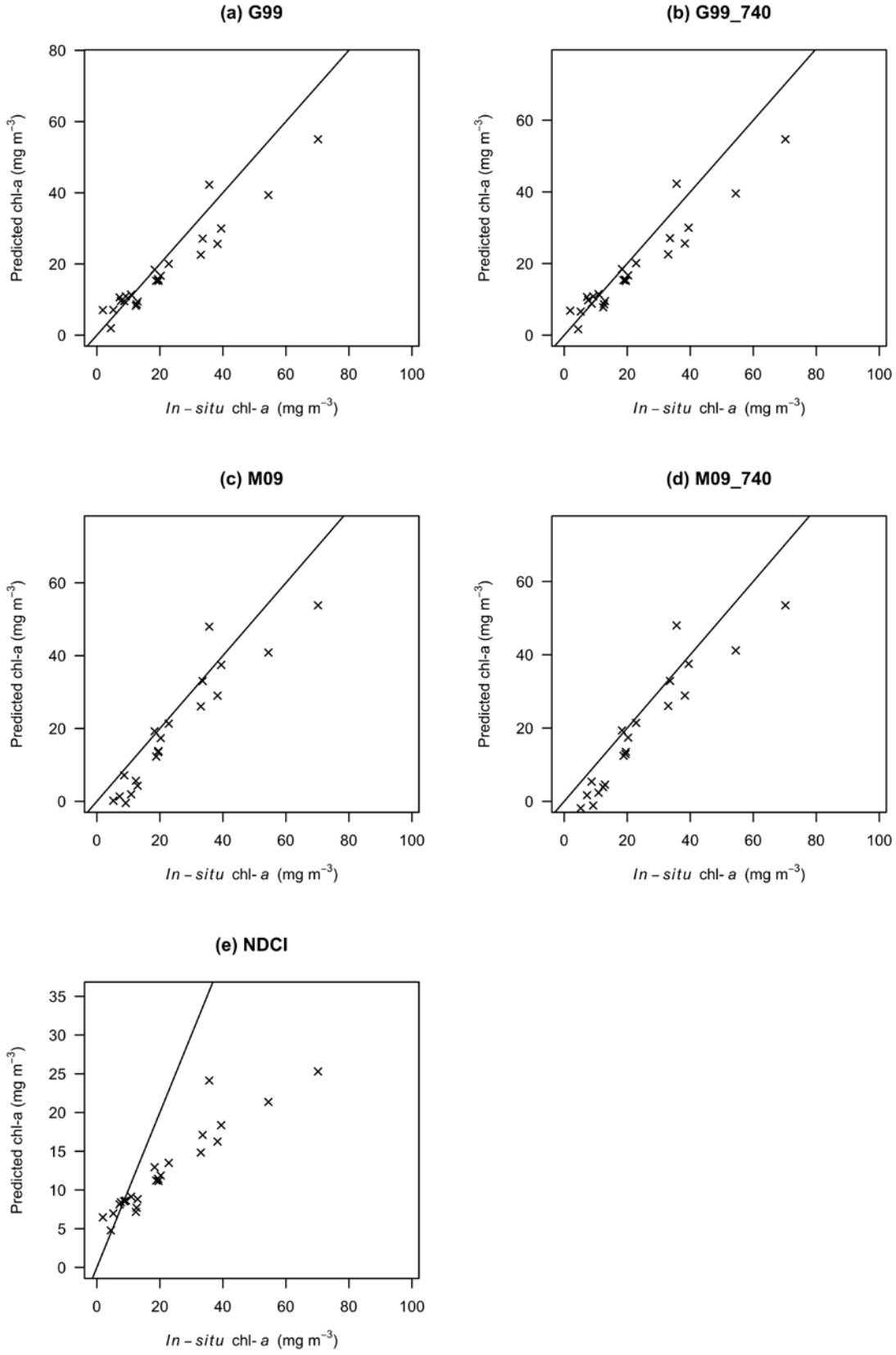

Figure 4-2: Validation plots showing predicted versus in-situ chl-a for the G99 (a), G99_740 (b), M09 (c), M09_740 (d) and NDCI (e) algorithms. The straight line in each plot is the 1:1 line.

4.4.3 Dynamic modelling of chl-a specific absorption coefficient

The optimum index *B* for the $a^*_{localised}$ model (equation 4-11) was 0.089. This was determined by increasing *B* from 0.01 to 0.25 in 0.001 increments and choosing the value for minimal RMSEP, which also resulted in an almost zero bias.

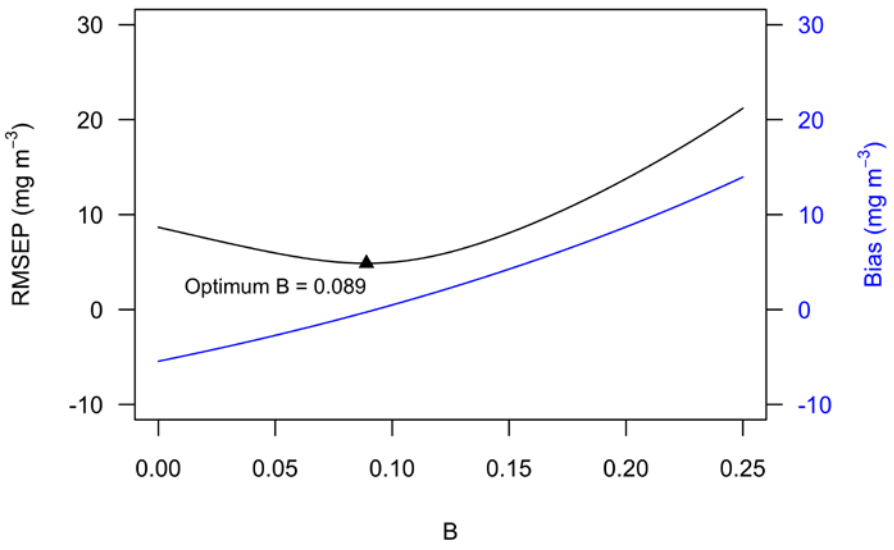

Figure 4-3: Determination of optimal index B for localised model of a*(665). Minimal RMSEP was for B = 0.089.

When compared to the fixed *a** value used by the default G99 algorithm, all variable models take a noticeably smaller value of *a** once chl-a concentration exceeds 20 mg m^{-3}. The $a^*_{Bricaud}$ model and the localised model have similar starting values, at 0.020 and 0.021 for C = 0.1 mg m^{-3}, but the latter model decays more slowly and for higher chl-a concentrations is closer to that of the $a^*_{Gilerson}$ model which is 0.032 for *C* = 0.1 mg m^{-3} but has a more rapid rate of decay with increasing chl-a concentration (Figure 4-4).

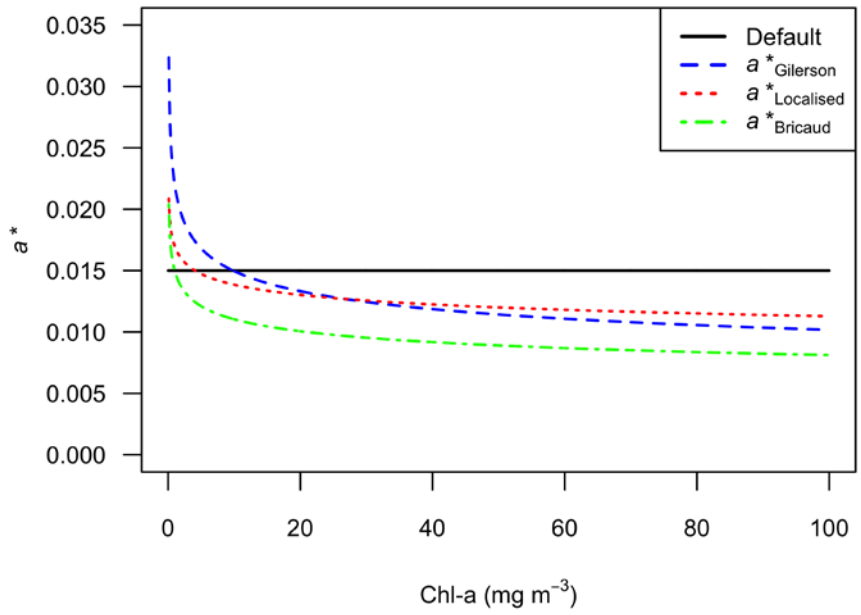

Figure 4-4: Relationship between a* and chl-a concentration for each of the tested models.

The effect of the variable a^* modelling on chl-a retrievals was noticeable, both the $a^*_{Gilerson}$ and $a^*_{localised}$ models did a good job in correcting the negative bias for $C > 20$ mg m^{-3} without visibly affecting the fit at lower chl-a concentrations (Figure 4-5), which resulted in reductions in RMSEP of 23% and 27% respectively. In both cases, bias was reduced by more than 85% and the NSE of the models improved by more than 7% (Table 4-3).

Table 4-3: Performance of G99 algorithm using different models for $a^*(665)$.

a^* model	RMSEP (mg m^{-3})	NRMSEP (%)	Bias (mg m^{-3})	R^2	NSE
Default (a^* = 0.015)	6.67	9.80	-3.30	0.92	0.84
$a^*_{localised}$	4.87	7.10	-0.27	0.91	0.91
$a^*_{Gilerson}$	5.13	7.50	-0.47	0.91	0.90
$a^*_{Bricaud}$	9.90	14.50	6.19	0.91	0.64

The $a^*_{Bricaud}$ model resulted in degraded performance. The lower $a^*(665)$ values produced by this model throughout almost the entire range of chl-a concentrations overcompensated for the negative bias of the default G99 algorithm and the tendency to underestimate for higher chl-a concentrations. This resulted in a visible overestimation of *C* for almost the entire data range (Figure 4-5).

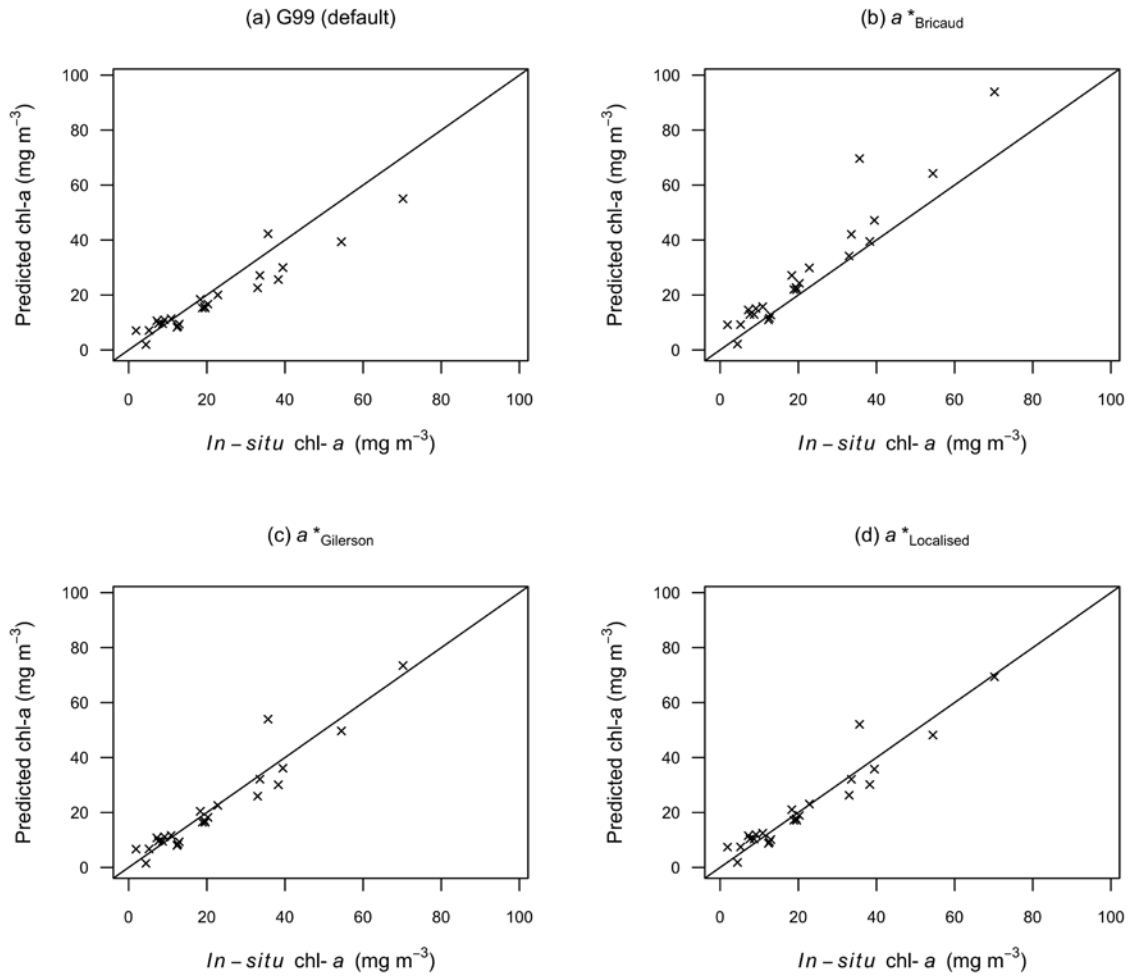

Figure 4-5: Validation plots comparing default G99 algorithm (a) with different models of *a versus chl-a concentration (b, c, d). The straight line on each plot is the 1:1 line.**

4.5 Discussion

The purpose of this study was to investigate the effect of dynamic recalibration of the chl-a specific absorption coefficient, a^*, on the accuracy of chl-a retrievals produced by the G99 algorithm and to validate the performance of the other red-edge chl-a retrieval algorithms included with the Acolite software package using the Sentinel 2 MSI sensor.

The G99 algorithm was the best performing of those compared without optimisation NRMSEP = 9.8%, bias = -3.30 mg m^{-3}, NSE = 0.84), however the default algorithm showed increasing underestimation with increasing chl-a (Figure 4-2a). This pattern is unsurprising as the mathematical arrangement of the G99 algorithm is such that the numerator, estimated absorption due to chl-a, is divided by a fixed value for $a^*(\lambda_1)$ to yield chl-a concentration, C, (equations 4-1 and 4-2). The default algorithm fails consider the inverse relationship between $a^*(\lambda_1)$ and C (Bricaud et al., 1995; Gilerson et al., 2010; Sathyendranath et al., 1987). A similar pattern was seen in the original MERIS validation of G99 where lower values of C were overpredicted but higher values were more accurately estimated (Gons et al., 2002). In this case in the initial parametrisation of the model $a^*(\lambda_1)$ was determined by choosing the value for optimal fit to the calibration data (Gons et al., 2002). This likely resulted in a choice of $a^*(\lambda_1)$ appropriate for moderate to high chl-a concentrations, but too small for lower concentrations. Subsequent recalibrations of the algorithm (Gons et al., 2008, 2005; Gurlin et al., 2011) have followed a similar approach: use of the calibration dataset to determine a fixed $a^*(\lambda_1)$ that provides the optimal fit to the data which may further explain why the G99 algorithm has been shown to be inaccurate for lower chl-a concentrations (Gons et al., 2008) or to generally underestimate (Gurlin et al., 2011).

A localised model of $a^*(665)$ was compared to two derived from literature. Given the dominance of *M. aeruginosa* in Lake Erie bloom periods (Vincent et al., 2004; Wynne et al., 2010) and that the extent to which $a^*(\lambda)$ varies with C can depend on algal type (Augusti and Phlips, 1992; Bricaud et al., 1995), $a^*_{localised}$ was optimised to local data to see if regional calibration of the $a^*(665)$ model was beneficial. Unfortunately, given the small number of *in-situ* matches with satellite imagery (N = 24), it did not make sense to further split the data into calibration and validation datasets. As the $a^*_{localised}$ model was optimised to the entire dataset there is a likelihood of overfitting. Given the performance of $a^*_{localised}$ (NRMSEP = 7.10%, bias = -0.27 mg m^{-3}, NSE = 0.91) was only marginally better than for $a^*_{Gilerson}$ (NRMSEP = 7.50%, bias = -0.47 mg m^{-3}, NSE = 0.90), it would seem sensible to consider $a^*_{Gilerson}$ the most appropriate model. $a^*_{Gilerson}$ was derived from field samples from Nebraska lakes, Chesapeake Bay and Long Island Sound where C ranged from almost 2 mg m^{-3} to in excess of 240 mg m^{-3} (Gilerson et al., 2010). Whilst more extensive validation against a larger range of water types and locations is necessary, the improved performance of the G99 algorithm when combined with $a^*_{Gilerson}$, both of which were calibrated externally and independently, suggests this combination may be suitable for a broader range of water types. The third model $a^*_{Bricaud}$ produced a more rapid decay of $a^*(665)$ resulting in an overestimation. The poor performance of this model is not surprising given it was developed based on samples collected from oceanic cruises where $0.03 < C < 24.5$ mg m^{-3} (Bricaud et al., 1995). It should be noted that the relationship between chl-a specific absorption coefficient and chl-a concentration varies both spatially and temporally on both local and regional levels (Paavel et al., 2016; Yoshimura et al., 2012), therefore a localised relationship for $a^*(665)$ may yield optimal results. However where these parameters are not known use of $a^*_{Gilerson}$ may improve default algorithm performance.

It should be noted that $a^*_{Gilerson}$ was previously used to form an advanced version of the M09 algorithm and a related two band algorithm with similar objectives to those of this study (Gilerson et al., 2010). Similarly, the G99 algorithm can be reformulated by substitution of $a^*_{Gilerson}$ (equation 4-9) into the initial algorithm (equation 4-2) yielding:

$$C = \left\{\frac{R(0.70 + b_b) - 0.40 - {b_b}^{1.05}}{0.022}\right\}^{1.201} \quad (4\text{-}12)$$

where b_b remains as described in equation 4-3. Alternatively, the default algorithm output can simply be multiplied by the fixed $a^*(665) = 0.015$ and divided by the dynamically revised values of $a^*(665)$.

With regards to the other chl-a retrieval algorithms, all three red-edge algorithms included with the Acolite software showed good linearity with the in-situ chl-a concentrations, $0.86 < R^2 < 0.92$, suggesting any could be recalibrated for the Lake Erie western basin. However, only the G99 and M09 algorithms, with NRMSEP of 9.8% and 14.6% respectively, may be useful without recalibration. It should also be noted that the best model basis for the three band input to M09 index is not clear, as both linear (Gitelson et al., 2008; Moses et al., 2009) and quadratic (Gitelson et al., 2009; Mishra and Mishra, 2012) fits have been suggested in different studies. As the G99 and M09 algorithms require accurate atmospheric correction (Gons et al., 2002; Moses et al., 2009) it could be reasonably inferred from the results that the new dark spectrum aerosol correction algorithm used by the Acolite software (Vanhellemont and Ruddick, 2018) produces acceptable results, at least in the red and NIR region of the spectrum used by these algorithms.

The significance of this research is two-fold. Further increasing the generalisability of an chl-a retrieval algorithm that has already been applied on multiple continents (Gons, 1999; Gons et al., 2002) without recalibration could enhance the accuracy of chl-a

remote sensing on a number of platforms. This would lead to improved ability to detect and monitor high biomass algal blooms (Anderson et al., 2017). Finally, validation on a platform with the spatial resolution of Sentinel 2 will extend monitoring capabilities to tens of millions more of the world's estimated 117 million lakes (Verpoorter et al., 2014).

4.6 Conclusions

Sentinel 2 MSI imagery and Acolite dark spectrum aerosol correction combined for accurate chl-a retrievals in the Lake Erie western basin. The G99 algorithm (Gons et al., 2002) was the best performing of those included in the Acolite package. Performance of the default G99 algorithm was improved by including a variable model for $a^*(665)$ to reflect the inverse relationship between $a^*(665)$ and chl-a concentration (Bricaud et al., 1995; Sathyendranath et al., 1987). RMSEP was reduced by 23%, bias by 85% and NSE increased from 0.84 to 0.90 for the preferred model, a^*_{Gilerson} (Gilerson et al., 2010).

Neither the G99 algorithm or a^*_{Gilerson} model were recalibrated to the local data, suggesting that this combination may generalise to a wider range of water bodies. However, given the small sample size and single location in this study, further validation is still necessary.

4.7 Acknowledgments

The authors would like to thank Tom Johengen, Cooperative Institute for Great Lakes Research, for provision of *in*-situ data and the European Space agency for their open access to satellite imagery.

4.8 References

Anderson, D.M., Boerlage, S.F.E., Dixon, M.B., 2017. Harmful Algal Blooms (HABs) and Desalination : A Guide to Impacts, Monitoring , and Management.

Anderson, D.M., Cembella, A.D., Hallegraeff, G.M., 2012. Progress in Understanding Harmful Algal Blooms: Paradigm Shifts and New Technologies for Research, Monitoring, and Management. Ann. Rev. Mar. Sci. 4, 143–176. https://doi.org/doi:10.1146/annurev-marine-120308-081121

Augusti, S., Phlips, E.J., 1992. Light absorption by cyanobacteria : Implications of the colonial growth form. Limnol. Oceanogr. 37, 434–441.

Beck, R., Zhan, S., Liu, H., Tong, S., Yang, B., Xu, M., Ye, Z., Huang, Y., Shu, S., Wu, Q., Wang, S., Berling, K., Murray, A., Emery, E., Reif, M., Harwood, J., Young, J., Nietch, C., Macke, D., Martin, M., Stillings, G., Stump, R., Su, H., 2016. Comparison of satellite reflectance algorithms for estimating chlorophyll-a in a temperate reservoir using coincident hyperspectral aircraft imagery and dense coincident surface observations. Remote Sens. Environ. 178, 15–30. https://doi.org/10.1016/j.rse.2016.03.002

Bricaud, A., Babin, M., Morel, A., Claustre, H., 1995. Variability in the chlorophyll-specific absorption coefficients of natural phytoplankton: Analysis and parameterization. J. Geophys. Res. 100, 332,13313-13321.

Buiteveld, H., Hakvoort, J.H.M., Donze, M., 1994. Optical properties of pure water, in: Ocean Optics XII. International Society for Optics and Photonics, pp. 174–183.

Chen, J., Zhu, W., Tian, Y.Q., Yu, Q., Zheng, Y., Huang, L., 2017. Remote estimation of colored dissolved organic matter and chlorophyll-a in Lake Huron using Sentinel-2 measurements. J. Appl. Remote Sens. 11, 36007.

Clark, J.M., Schaeffer, B.A., Darling, J.A., Urquhart, E.A., Johnston, J.M., Ignatius, A.R., Myer, M.H., Loftin, K.A., Werdell, P.J., Stumpf, R.P., 2017. Satellite monitoring of cyanobacterial harmful algal bloom frequency in recreational waters and drinking water sources. Ecol. Indic. 80, 84–95. https://doi.org/10.1016/j.ecolind.2017.04.046

Dall'Olmo, G., Gitelson, A.A., 2005. Effect of bio-optical parameter variability on the remote estimation of chlorophyll-a concentration in turbid productive waters: experimental results. Appl. Opt. 44, 412–422.

ESA, 2018a. User Guides - Sentinel 3 OLCI [WWW Document]. URL https://sentinel.esa.int/web/sentinel/user-guides/sentinel-3-olci (accessed 9.14.18).

ESA, 2018b. SENTINEL-2 User Guide [WWW Document]. URL https://sentinel.esa.int/web/sentinel/user-guides/sentinel-2-msi (accessed 12.4.18).

Ficek, D., Meler, J., Zapadka, T., Stoń-Egiert, J., 2012. Modelling the light absorption coefficients of phytoplankton in Pomeranian lakes (Northern Poland). Фундаментальная и прикладная гидрофизика 5, 54–63.

Gilerson, A.A., Gitelson, A.A., Zhou, J., Gurlin, D., Moses, W.J., Ioannou, I., Ahmed, S.A., 2010. Algorithms for remote estimation of chlorophyll-a in coastal and inland waters using red and near infrared bands. Opt. Express 18, 24109–24125. https://doi.org/10.1364/OE.18.024109

Gitelson, A.A., Dall'Olmo, G., Moses, W., Rundquist, D.C., Barrow, T., Fisher, T.R., Gurlin, D., Holz, J., 2008. A simple semi-analytical model for remote estimation of chlorophyll-a in turbid waters: Validation. Remote Sens. Environ. 112, 3582–3593. https://doi.org/10.1016/j.rse.2008.04.015

Gitelson, A.A., Gurlin, D., Moses, W.J., Barrow, T., 2009. A bio-optical algorithm for the remote estimation of the chlorophyll-a concentration in case 2 waters. Environ. Res. Lett. 4. https://doi.org/10.1088/1748-9326/4/4/045003

Gons, H.J., 1999. Optical teledetection of chlorophyll a in turbid inland waters. Environ. Sci. Technol. 33, 1127–1132.

Gons, H.J., Auer, M.T., Effler, S.W., Ef, S.W., 2008. MERIS satellite chlorophyll mapping of oligotrophic and eutrophic waters in the Laurentian Great Lakes. Remote Sens. Environ. 112, 4098–4106. https://doi.org/http://dx.doi.org/10.1016/j.rse.2007.06.029

Gons, H.J., Rijkeboer, M., Ruddick, K.G., 2005. Effect of a waveband shift on

chlorophyll retrieval from MERIS imagery of inland and coastal waters. J. Plankton Res. 27, 125–127. https://doi.org/10.1093/plankt/fbh151

Gons, H.J., Rijkeboer, M., Ruddick, K.G., 2002. A chlorophyll-retrieval algorithm for satellite imagery (Medium Resolution Imaging Spectrometer) of inland and coastal waters. J. Plankton Res. 24, 947–951.

Gurlin, D., Gitelson, A.A., Moses, W.J., 2011. Remote estimation of chl-a concentration in turbid productive waters - Return to a simple two-band NIR-red model? Remote Sens. Environ. 115, 3479–3490. https://doi.org/http://dx.doi.org/10.1016/j.rse.2011.08.011

Ha, N.T.T., Thao, N.T.P., Koike, K., Nhuan, M.T., 2017. Selecting the best band ratio to estimate chlorophyll-a concentration in a tropical freshwater lake using sentinel 2A images from a case study of Lake Ba Be (Northern Vietnam). ISPRS Int. J. Geo-Information 6. https://doi.org/10.3390/ijgi6090290

Ibelings, B.W., Backer, L.C., Kardinaal, W.E.A., Chorus, I., 2014. Current approaches to cyanotoxin risk assessment and risk management around the globe. Harmful Algae 40, 63–74. https://doi.org/10.1016/j.hal.2014.10.002

Krause, P., Boyle, D.P., Bäse, F., 2005. Comparison of different efficiency criteria for hydrological model assessment. Adv. Geosci. 5, 89–97. https://doi.org/10.5194/adgeo-5-89-2005

Kutser, T., 2009. Passive optical remote sensing of cyanobacteria and other intense phytoplankton blooms in coastal and inland waters. Int. J. Remote Sens. 30, 4401–4425. https://doi.org/10.1080/01431160802562305

Mishra, S., Mishra, D.R., 2012. Normalized difference chlorophyll index : A novel model for remote estimation of chlorophyll- a concentration in turbid productive waters. Remote Sens. Environ. 117, 394–406. https://doi.org/10.1016/j.rse.2011.10.016

Moses, W.J., Gitelson, A.A., Berdnikov, S., Saprygin, V., Povazhnyi, V., 2012. Operational MERIS-based NIR-red algorithms for estimating chlorophyll-a concentrations in coastal waters - The Azov Sea case study. Remote Sens.

Environ. 121, 118–124. https://doi.org/10.1016/j.rse.2012.01.024

Moses, W.J., Moses, W.J., Gitelson, A.A., Berdnikov, S., Povazhnyy, V., 2009. Satellite Estimation of Chlorophyll- a Concentration Using the Red and NIR Bands of MERIS The Azov Sea Case Study. Ieee Geosci. Remote Sens. Lett. 6. https://doi.org/http://dx.doi.org/10.1109/LGRS.2009.2026657

NASA, 2014. Components of MODIS [WWW Document]. URL http://modis.gsfc.nasa.gov/about/specifications.php (accessed 2.4.14).

Paavel, B., Kangro, K., Arst, H., Reinart, A., Kutser, T., Nõges, T., 2016. Parameterization of chlorophyll-specific phytoplankton absorption coefficients for productive lake waters. J. Limnol. 75, 423–438. https://doi.org/10.4081/jlimnol.2016.1426

Palmer, S.C.J., Kutser, T., Hunter, P.D., 2015. Remote sensing of inland waters: Challenges, progress and future directions. Remote Sens. Environ. 157, 1–8. https://doi.org/10.1016/j.rse.2014.09.021

Sathyendranath, S., Lazzara, L., Prieur, L., 1987. Variations in the spectral values of specific absorption of phytoplankton 32.

Shen, L., Xu, H., Guo, X., 2012. Satellite remote sensing of harmful algal blooms (HABs) and a potential synthesized framework. Sensors (Basel) 12, 7778–7803. https://doi.org/10.3390/s120607778

Toming, K., Kutser, T., Laas, A., Sepp, M., Paavel, B., Nõges, T., 2016. First Experiences in Mapping Lake Water Quality Parameters with Sentinel-2 MSI Imagery. Remote Sens. 8, 1–14. https://doi.org/10.3390/rs8080640

USGS, 2016. Landsat 8 (L8) Data Users Handbook, America.

Vanhellemont, Q., Ruddick, K., 2018. Atmospheric correction of metre-scale optical satellite data for inland and coastal water applications. Remote Sens. Environ. 216, 586–597. https://doi.org/10.1016/j.rse.2018.07.015

Vanhellemont, Q., Ruddick, K., 2016. ACOLITE FOR SENTINEL-2 : AQUATIC APPLICATIONS OF MSI IMAGERY 9–13.

Verpoorter, C., Tranvik, L.J., Kutser, T., Seekell, D.A., 2014. A global inventory of lakes based on high-resolution satellite imagery 6396–6402. https://doi.org/10.1002/2014GL060641

Vincent, R.K., Qin, X., McKay, R.M.L., Miner, J., Czajkowski, K., Savino, J., Bridgeman, T., 2004. Phycocyanin detection from LANDSAT TM data for mapping cyanobacterial blooms in Lake Erie. Remote Sens. Environ. 89, 381–392.

Wojtasiewicz, B., Stoń-Egiert, J., 2016. Bio-optical characterization of selected cyanobacteria strains present in marine and freshwater ecosystems. J. Appl. Phycol. 28, 2299–2314. https://doi.org/10.1007/s10811-015-0774-3

World Health Organization, 1999. Toxic Cyanobacteria in Water: A guide to their public health consequences, monitoring and management, Retrieved March. https://doi.org/10.1046/j.1365-2427.2003.01107.x

Wynne, T.T., Stumpf, R.P., Tomlinson, M.C., Dyble, J., 2010. Characterizing a cyanobacterial bloom in western Lake Erie using satellite imagery and meteorological data. Limnol. Oceanogr. 55, 2025–2036. https://doi.org/10.4319/lo.2010.55.5.2025

Yoshimura, K., Zaitsu, N., Sekimura, Y., Matsushita, B., Fukushima, T., Imai, A., 2012. Parameterization of chlorophyll a-specific absorption coefficients and effects of their variations in a highly eutrophic lake: A case study at Lake Kasumigaura, Japan. Hydrobiologia 691, 157–169. https://doi.org/10.1007/s10750-012-1066-4

5 A chlorophyll-a retrieval algorithm for the HydroColor app

5.1 Abstract

The HydroColor app allows rapid measurements of water colour to be obtained by technical staff or citizen scientists using the digital camera on a mobile device. The app estimates remote sensing reflectance (R_{rs}) in the red, green and blue bands and derives turbidity and suspended particulate matter. Chl-a retrieval algorithms were developed using band ratio inputs indicative of optically active water constituents and partial least squares regression. The models were evaluated against a dataset of 49 HydroColor image sequences along with *in-situ* chl-a and turbidity measurements collected over a one-year period. The chl-a algorithm using the ratio of R_{rs}(blue)/ R_{rs}(green) was unable to meaningfully predict *in-situ* chl-a (coefficient of determination, R^2 = 0.11; bias = 0.21 mg m^{-3}; Nash-Sutcliffe efficiency = -0.02). Adding inputs representing absorption due to CDOM and turbidity produced models able to detect relative changes of *in-situ* chl-a (R^2 = 0.56 to 0.60; bias = 0.11 to 0.15 mg m^{-3}; NSE = 0.39 to 0.46). While these results are considered encouraging, further development is recommended against an *in-situ* dataset with greater variability in water quality parameters. Improvement in such algorithms will allow rapid water quality monitoring from relatively inexpensive and readily available devices.

5.2 Introduction

Harmful algal blooms (HABs) are a global phenomenon of increasing concern to water management and environment agencies (Anderson et al., 2017, 2012; Falconer, 2001; Ibelings et al., 2014; Klemas, 2012; World Health Organization, 1999). Remote sensing of chlorophyll-a (chl-a) as an indicator of algal biomass or concentration can be an important tool in the detection and monitoring such blooms (Anderson et al., 2017; Kutser, 2009). Algorithms that estimate chl-a concentration have been implemented on

a variety of satellite platforms, however satellite platforms have several shortcomings: spatial resolution can be inadequate for the monitoring of smaller water bodies (Clark et al., 2017; Palmer et al., 2015), clouds can prevent coverage in the order of half the time (Bailey and Werdell, 2006; Bramich et al., 2018; Bresciani et al., 2018) and many chl-a retrieval algorithms are dependent on accurate atmospheric correction (Dall'Olmo et al., 2005; Gons et al., 2008; Mishra and Mishra, 2012; O'Reilly et al., 2000). The use of digital cameras in remote chl-a retrievals could mitigate many of these shortcomings: use by hand or at low altitude could greatly reduce the impact of clouds and the atmosphere, and allow rapid detection of potentially dangerous blooms in small water bodies (Kutser, 2009).

Most digital cameras capture relatively broad red, green and blue bands for each pixel (Berra et al., 2015; Goddijn-Murphy et al., 2009; Leeuw and Boss, 2018; Matasaru, 2014). Given the spectral limitations of these devices the most appropriate class of chl-a retrieval algorithm appears to be the OCx algorithms that use the ratio of blue to green remote sensing reflectance (R_{rs}) but these can be confounded by CDOM and turbidity (Chapter 1). Algorithms designed to avoid these limitations typically require one or more bands in the NIR (Dall'Olmo and Gitelson, 2005; Gilerson et al., 2010; Gons, 1999; Gower et al., 2005, 1999; Mishra and Mishra, 2012; Moses et al., 2012) which makes them unsuitable for use with a typical digital camera.

The HydroColor app (Leeuw, 2014; Leeuw and Boss, 2018), available for iOS and Android devices, provides mobile devices with remote sensing capabilities using the in-built camera. The user uses the device camera to take images of the water surface, the sky and a grey 18% reflectance card. The HydroColor app derives remote sensing reflectance in the red, green and blue bands from the radiance signal captured by the

camera as per Mobley (1999). Solar geometry is derived from the device's GPS and HydroColor uses the device's gyrometer and compass to guide the user to optimal camera direction and elevation for image capture. HydroColor also derives turbidity, suspended particulate matter and the backscattering coefficient in the red band (Leeuw and Boss, 2018). An empirical chl-a retrieval algorithm was tested early in the project. This modified blue/green ratio was not included in the final version of the app (Leeuw, 2014). The algorithm was of the following form:

$$x = \frac{R_{rs}(blue) - R_{rs}(red)}{R_{rs}(green) - R_{rs}(red)} \quad (5\text{-}13)$$

$$C = 3.09\, e^{-0.6x} \quad (5\text{-}14)$$

where C is the concentration of chl-a.

The aim of this study is to develop an operational chl-a retrieval algorithm for use with HydroColor app using the ratio of the blue to green bands. As previously described, it is necessary to determine the extent to which CDOM and turbidity affect the water leaving reflectance signal. The HydroColor turbidity retrieval algorithm has been shown to demonstrate good agreement with *in-situ* data (Leeuw and Boss, 2018):

$$T = \frac{22.57\, R_{rs}(red)}{0.044 - R_{rs}(red)} \quad (5\text{-}15)$$

where T is turbidity in nephelometric turbidity units (NTU).

Absorption due to CDOM, a_{cdom}, has been remotely derived using either a linear relationship with the ratio of red to blue bands (Goddijn-Murphy et al., 2009; Koponen et al., 2007) or the ratio of red to green bands, which takes the following form (Kutser et al., 2005):

$$a_{cdom}(420) = 5.13 \left\{\frac{R_{rs}(red)}{R_{rs}(green)}\right\}^{2.67} \quad (5\text{-}16)$$

Partial least squares regression (PLSR), described in chapter 3, will be used to determine the relationship between inputs. As it is not clear which is the better indicator of a_{cdom}, the ratios of red to blue and red to green bands will both be tested in addition to the non-linear model described in equation 5-16. Similarly, both the HydroColor turbidity algorithm (equation 5-15) and R_{rs}(red) will be compared as indicators of turbidity.

5.3 Data and Methodology

5.3.1 Field data

In-situ data was collected from Lake Trevallyn (Chapter 3) and Craigbourne Dam in Tasmania, Australia (Figure 5-1). Craigbourne Dam is a 12.5 million cubic metre irrigation reservoir and flood mitigation facility in the state's southeast (Tasmanian Irrigation, 2019). Both the toxic *Microcystis aeruginosa* and potentially toxic *A. circinalis* have been detected in Craigbourne dam with the latter in bloom proportions (DPIF, 1997).

Sampling was conducted in Lake Trevallyn, approximately quarterly, from January 2018 to January 2019 to produce a dataset representative of seasonal variations. Sampling at Craigbourne Dam was limited to a single visit in October 2018 as sampling on other visits was cancelled due to high winds.

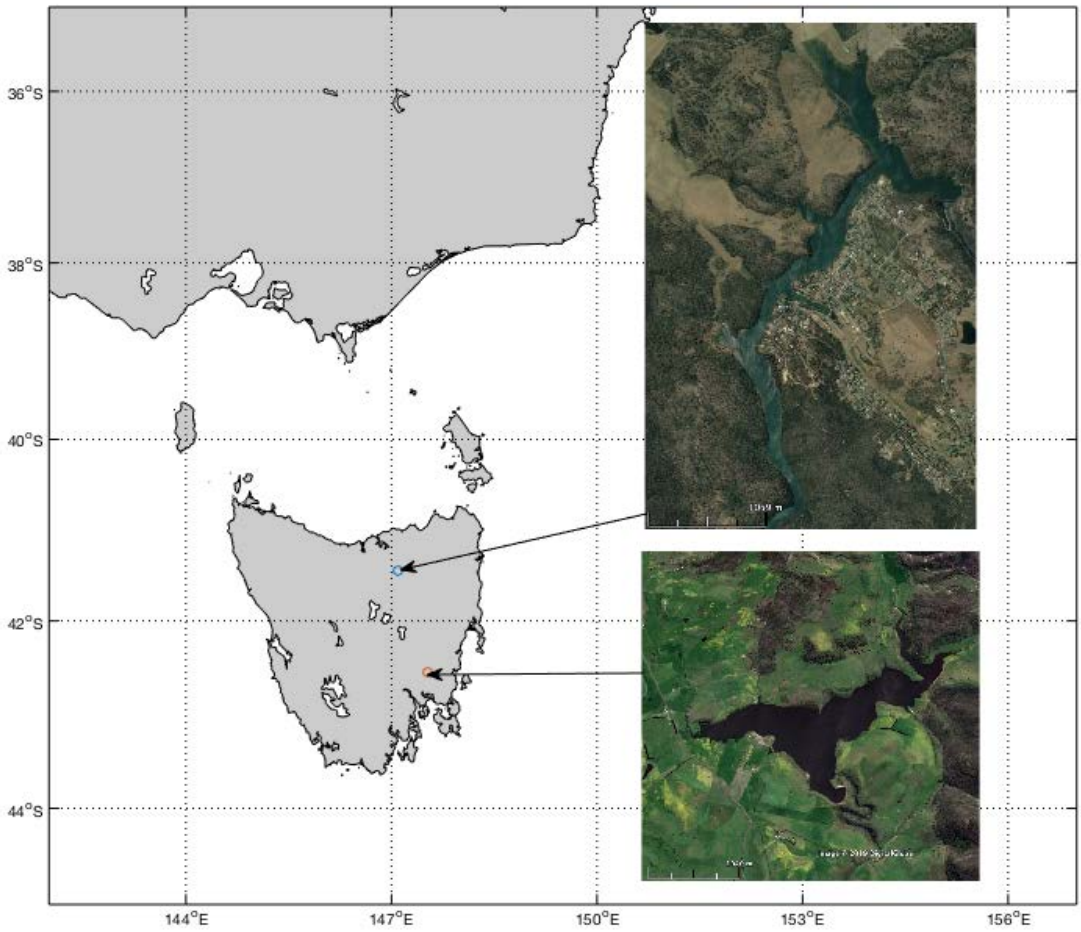

Figure 5-1: Lake Trevallyn and Craigbourne Dam in Tasmania, Australia

In-situ chl-a and turbidity were measured using a YSI EXO2 sonde equipped with the combination EXO chlorophyll and blue green algae (CBGA) and EXO turbidity probes. The sonde was regularly recalibrated using two-point calibrations between distilled water and rhodamine, for the CBGA probe, or polymer turbidity standard for the turbidity probe.

In the field, the sonde was configured to sample at one second intervals and the clock was synchronised with an iPhone 5s that was installed with the HydroColor app. At each sampling location the sonde probes were immersed to a depth of approximately 0.3 to 0.5 m and allowed to stabilise for approximately one minute. The sequence of grey card, sky and water images required by the HydroColor app were collected.

Images were later checked for quality by examining the highlighted pixel area in the HydroColor user interface: sample sets with shadow over the water pixels or cloud over the sky pixels were removed from the dataset, as were those where the sun zenith angle was not between 15 degrees and 60 degrees (Leeuw and Boss, 2018). The in-situ data streams for chl-a and turbidity were smoothed using a five-point smoothing filter and matched to the samples in the HydroColor library by date and time.

5.3.2 Algorithm Development

The field data was partitioned into random stratified partitions. Approximately two-thirds were used for calibration and the remainder for validation. Several PLSR models were developed using the calibration dataset following the methods described in chapter 3. Different possible indicators of CDOM and turbidity were compared. In all cases, inputs were scaled and centred, and the optimum number of components was chosen based on lowest root mean squared error of prediction (RMSEP) after ten-fold cross validation. Models were then compared to each other using the validation dataset.

Several measures of model performance were calculated. RMSEP was normalised using the range of in-situ chl-a values (NRMSEP). Model fit was indicated using the coefficient of determination, R^2, and bias, the mean difference between measured and predicted values. Nash-Sutcliffe efficiency (NSE) was also calculated. NSE ranges from minus infinity to one: negative values indicate that using the mean value of the observed data would have been a better predictor than the model (Krause et al., 2005).

R-studio was used for algorithm development and data analysis. Data partitioning was performed using the createDataPartition function of the caret package (Kuhn, 2008) and

PLSR models were built using the pls package (Mevik and Wehrens, 2007). NSE was calculated using the HydroGOF package.

5.4 Results

Examination of the entire in-situ dataset from Lake Trevallyn and Craigbourne Dam shows a poor correlation between chl-a and turbidity with Pearson's co-efficient of correlation, r = 0.13. This correlation remains poor (r = -0.32) if the four samples with relatively high turbidity taken from Lake Trevallyn on July 12th, 2018 (mid-winter) are excluded (Figure 5-2).

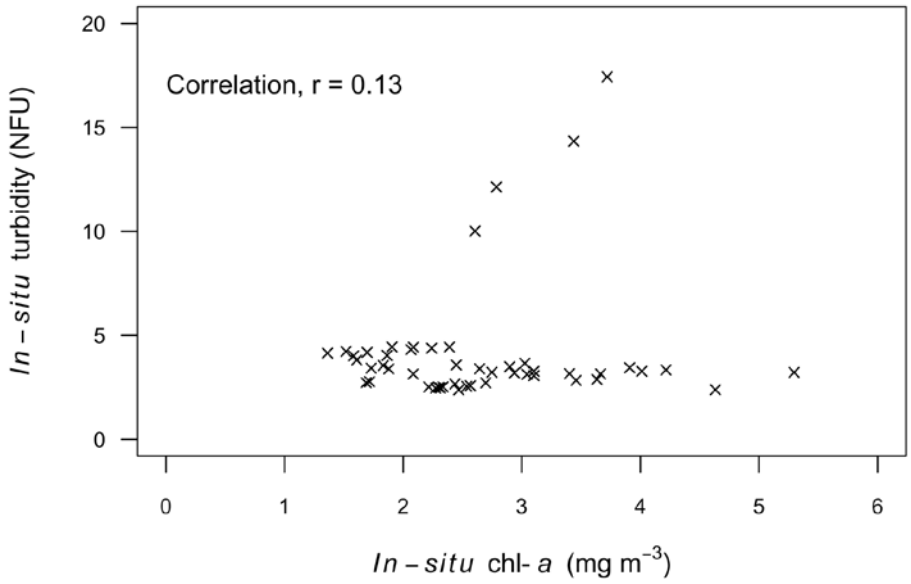

Figure 5-2: Relationship between *in-situ* chl-a and in-situ turbidity.

After partitioning, the calibration dataset contained 33 samples ranging from 1.36 to 5.30 mg m^{-3} and a median of 2.47 mg m^{-3} and the validation dataset contained 16 samples with chl-a ranging from 1.36 to 3.66 mg m^{-3} and a median of 2.54 mg m^{-3} (Table 5-1).

Table 5-1: Range of *in-situ* chl-a values for the calibration and validation datasets

		In-situ chl-a (mg m^{-3})				
Dataset	**n**	**Minimum**	**1st Quartile**	**Median**	**3rd Quartile**	**Maximum**
Calibration	33	1.52	2.08	2.47	3.40	5.30
Validation	16	1.36	2.00	2.54	2.96	3.66

The HydroColor turbidity algorithm was moderately correlated with *in-situ* turbidity, r = 0.68 (Figure 5-3a). The HydroColor algorithm however, offered little advantage over remote sensing reflectance to in the red channel, R_{rs}(red) as an indicator of turbidity with r = 0.66 (Figure 5-3b). The HydroColor algorithm is not perfectly correlated with R_{rs}(red) as the turbidity values stored in the app are rounded to the nearest whole NTU and R_{rs} values are rounded to the nearest $0.001sr^{-1}$. The theoretical relationship between the HydroColor algorithm and R_{rs}(red) is shown in Figure 5-3d.

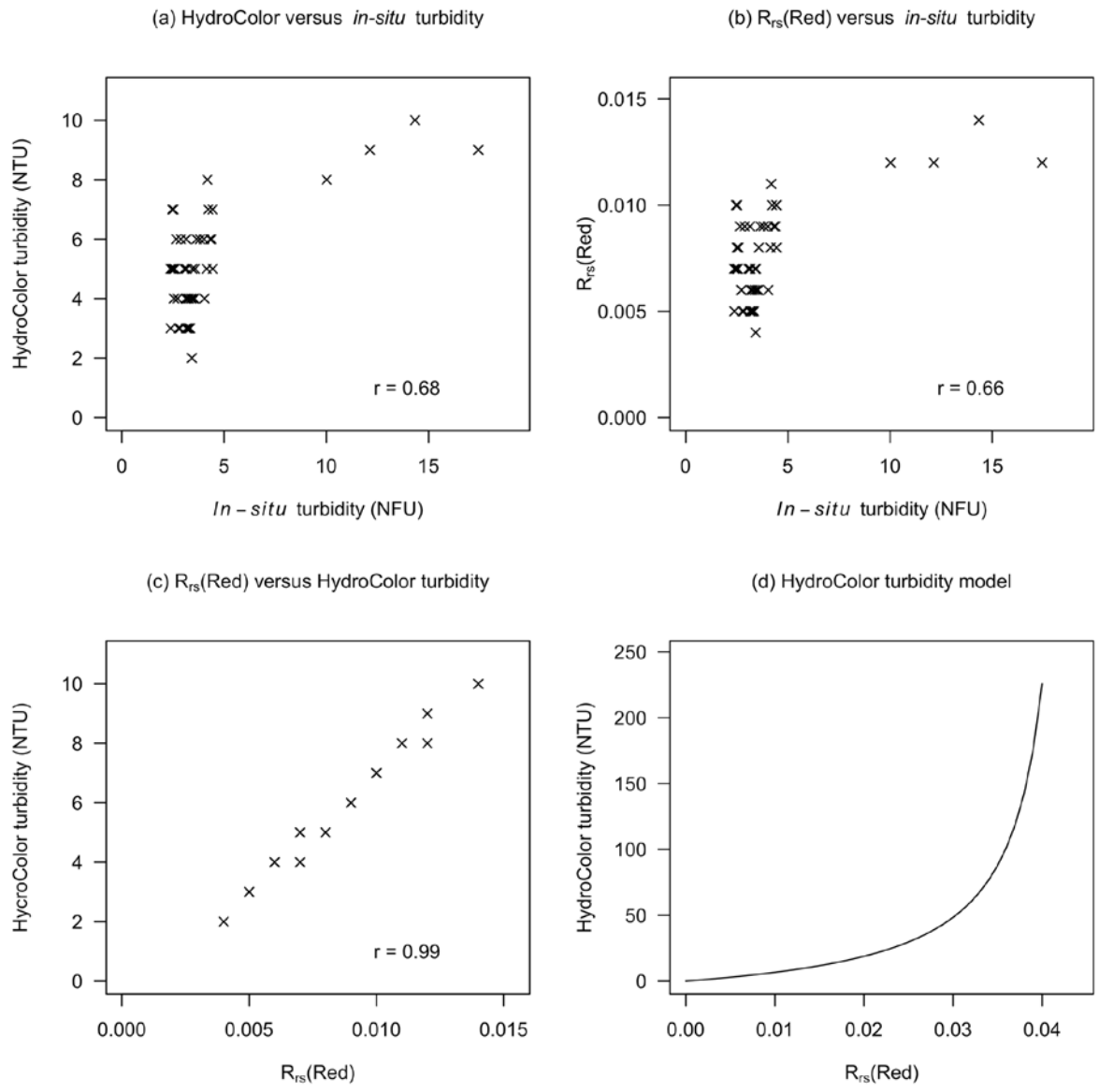

Figure 5-3: Performance of HydroColor turbidity algorithm versus *in-situ* turbidity (a), the relationship between R_{rs}(red) and *in-situ* turbidity (b), the relationship between HydroColor turbidity and R_{rs}(red) (c) and the HydroColor algorithm relationship with R_{rs}(red). Figures (a) to (c) are based on the entire *in-situ* dataset (N = 49).

Three different indicators of a_{cdom} and two indicators of turbidity were evaluated. Additionally, a control model was built using a single input: the ratio of blue to green remote sensing reflectance. The best performing model against the validation dataset used equation 5-16 (Kutser et al., 2005) to represent a_{cdom} and R_{rs}(red) to represent turbidity (NRMSEP = 21.6%, bias = 0.11 mg m^{-3}, NSE = 0.46). However, all

algorithms, which included inputs for a_{cdom} and turbidity, were similar in performance with NRMSEP ranging from 21.6% to 23% and NSE ranging from 0.39 to 0.46. This was in contrast to the model with only the blue to green ratio that had a NSE of -0.02 suggesting that it had worse predictive power than using the mean value of observed chl-a (Table 5-2).

Table 5-2: Performance of PLSR models against the validation dataset (N = 16). All models used the ratio R_{rs}(blue)/R_{rs}(green) as an indication of chl-a with different inputs evaluated for a_{cdom} and turbidity.

CDOM input	Turbidity input	RMSEP (mg m^{-3})	NRMSEP (%)	Bias (mg m^{-3})	R^2	NSE
Kutser et al. 2005	Red	0.50	21.6	0.11	0.56	0.46
Red/Green	Red	0.50	21.9	0.13	0.58	0.45
Kutser et al. 2005	HydroColor turbidity	0.51	22.2	0.12	0.58	0.44
Red/Blue	Red	0.51	22.3	0.14	0.58	0.43
Red/Green	HydroColor turbidity	0.52	22.5	0.14	0.60	0.42
Red/Blue	HydroColor turbidity	0.53	23.0	0.15	0.60	0.39
None	None	0.68	29.8	0.21	0.11	-0.02

The similarity in performance of models with the different inputs for a_{cdom} and turbidity is also apparent in the validation plots (Figure 5-4 b-g) where in all cases the lower *in-situ* chl-a values were overestimated, while the higher values were underestimated. The model using only the ratio of R_{rs}(blue) to R_{rs}(green) as an input, showed a similar trend, but predicted almost no variability in chl-a relative to the other models.

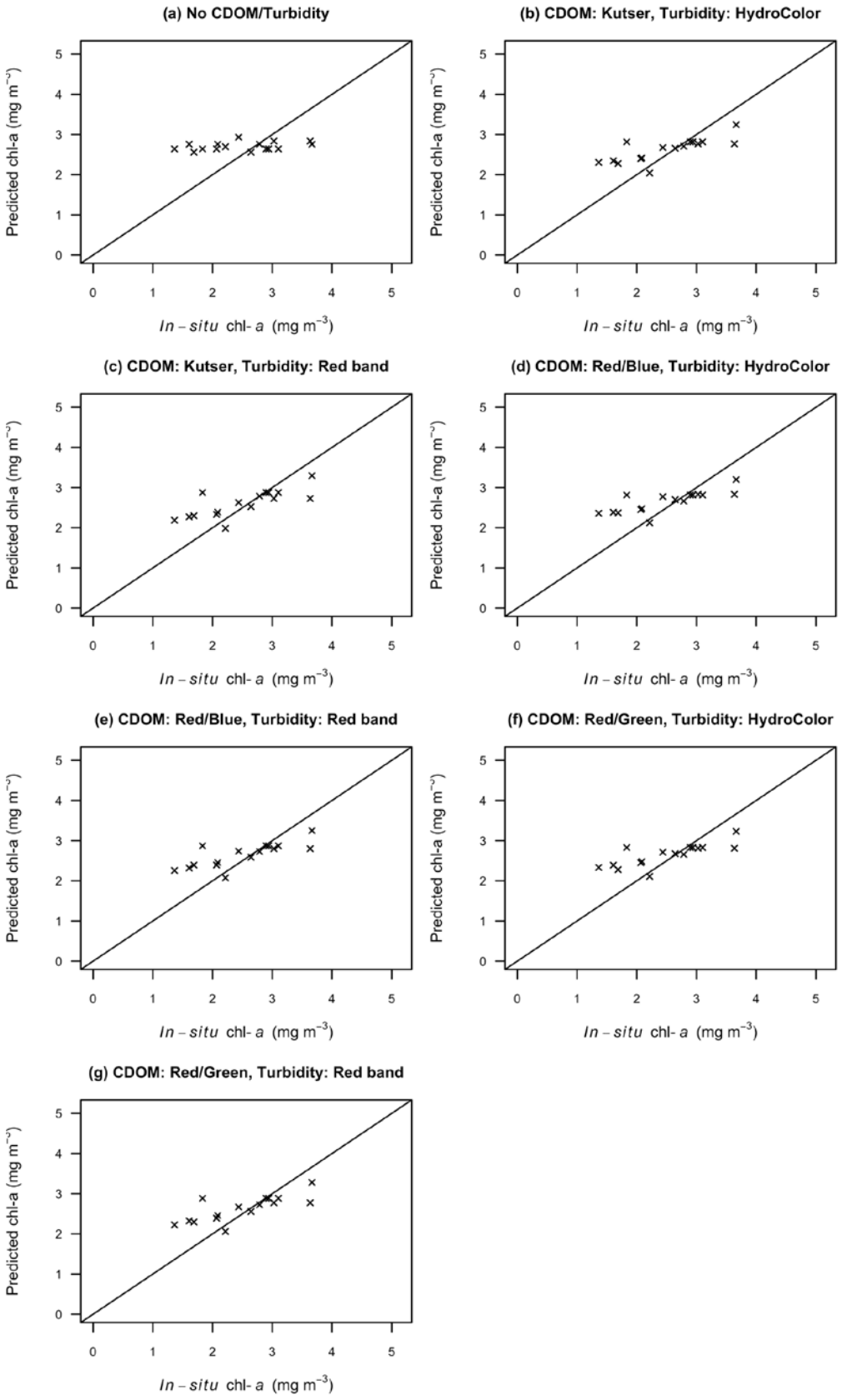

Figure 5-4: Validation plots for models. All models use the ratio R_{rs}(blue)/R_{rs}(green) for chl-a with different inputs to represent a_{cdom} and turbidity. The straight line in each graph is the 1:1 line.

It was not possible to make a meaningful comparison with the initial chl-a algorithm (equations 5-13 and 5-14) as for 10 of 16 samples in the validation dataset, remote sensing reflectance in the red and green bands were equal resulting in division by zero. For the remaining 6 samples, Pearson's coefficient of correlation between algorithm output and in-situ chl-a, r = 0.07.

5.5 Discussion

The weak correlation, r = 0.13, between *in-situ* chl-a and *in-situ* turbidity (Figure 5-2) suggests that the water leaving optical signal is unlikely to vary with chl-a alone and that the study areas can be classified as case two waters (Morel and Prieur, 1977). The complexity of these waters in turn explain the inability of the ratio $R_{rs}(blue)/R_{rs}(green)$ alone to usefully predict any variation in chl-a.

The similar performance between the HydroColor turbidity algorithm (equation 5-15) and $R_{rs}(red)$ as indicators of turbidity is likely due to the low range of *in-situ* turbidity encountered in the sampling process. *In-situ* turbidity, measured in formazin nephelometric units (FNU), did not exceed 20 FNU (Figure 5-3a). The HydroColor algorithm derives turbidity in nephelometric turbidity units (NTU), however within the range measured in this study the two units can be considered equivalent (Mylvaganam and Jakobsen, 1998). The resulting range of remote sensing reflectance in the red band, $0 < R_{rs}(red) < 0.015\ ^{sr-1}$ (Figure 5-3b,c) was in the region of the HydroColor model where relationship between equation 5-15 and $R_{rs}(red)$ remains linear (Figure 5-3d). Use of the HydroColor turbidity algorithm would not be expected to be beneficial until turbidity increased to the point where the relationship became non-linear.

Attempts to compare inputs representing a_{cdom} were similarly confounded although in this case in-situ data on CDOM was not available. The rationale for using $R_{rs}(red)/R_{rs}(blue)$ as an indicator of a_{cdom} was based two studies that suggested a linear relationship between a_{cdom} and $R_{rs}(red)/R_{rs}(blue)$. In the first, *in-situ* $a_{cdom}(440)$ ranged from 0.1 m^{-1} to 2.8 m^{-1} (Goddijn-Murphy et al., 2009) and in the second $a_{cdom}(400)$ ranged from 1.29 m^{-1} to 2.61 m^{-1} (Koponen et al., 2007). The power function utilising $R_{rs}(red)/R_{rs}(green)$ (equation 5-16) was derived from *in-situ* $a_{cdom}(420)$ ranging from 0.68 m^{-1} to 11.13 m^{-1} (Kutser et al., 2005). After factoring in the change in a_{cdom} from 400 nm to 440 nm (Kutser et al., 2005), it is clear that the latter study was validated against a wider range of *in-situ* values. Given that the results of this study are equivocal the use of an a_{cdom} indicator based on $R_{rs}(red)/R_{rs}(green)$ seems most logical although both types of a_{cdom} model have been shown to break down in the presence of high levels of inorganic sediment (Olmanson et al., 2016).

It was hoped that conducting multiple sampling trips over the course of more than a year would result in a suitably varied *in*-situ dataset for modelling. However, the low range of chl-a concentration, from 1.36 mg m^{-3} to 5.30 mg m^{-3}, proved challenging. Many algorithms perform worst at such concentrations as this is where chl-a specific absorption coefficient, a property that links optical absorption to chl-a concentration, is most variable (Bricaud et al., 1998; Gilerson et al., 2010; Gons et al., 2002; Moses et al., 2012). The fluorescence line height algorithm is sensitive to lower chl-a concentrations but requires three spectral bands adjacent to the chl-a fluorescence peak near 680 nm (Gower et al., 1999) and therefore is not suitable for use with standard digital cameras. Given the difficulties in remote sensing of chl-a concentrations at these levels in complex waters, a tempered, but somewhat optimistic view of the results might be taken: while the preceding results are not helpful in determining which inputs

best account for variations in turbidity and a_{cdom}, they do suggest that including such inputs can allow a ubiquitous device such as a mobile phone to detect relative changes in chl-a concentration. It is also likely that when applied to a dataset containing a wider range of chl-a concentrations and turbidity measurements, performance would improve. Future work should also measure *in-situ* absorption due to CDOM so that the effectiveness of each input can be fully evaluated.

The appeal of the HydroColor app is that it guides the user through established methods of capturing remote sensing reflectance (Mobley, 1999), allowing field workers or citizen scientists to capture relative measurements (Yang et al., 2018). Further development of a chl-a retrieval algorithm will enable rapid point sampling of a wider range of water quality parameters. Such algorithms could be adapted to unmanned aerial vehicles in order to give spatial coverage of smaller water bodies.

5.6 Conclusions

The results presented here suggest that the HydroColor app has the spectral capability to detect broad relative changes in chl-a concentration. However, given the narrow range of water quality parameters in the *in-situ* dataset, the extent to which these capabilities are useful is unclear and will need to be investigated further. Further, we have demonstrated that the performance of blue/green algorithms can be greatly improved in complex waters by adding inputs for CDOM and turbidity using even broad bands in the visible part of the spectrum.

5.7 Acknowledgments

Funding for instrumentation was provided by Sense-T, a partnership between the CSIRO, the University of Tasmania and the Australian government.

5.8 References

Anderson, D.M., Boerlage, S.F.E., Dixon, M.B., 2017. Harmful Algal Blooms (HABs) and Desalination : A Guide to Impacts, Monitoring , and Management.

Anderson, D.M., Cembella, A.D., Hallegraeff, G.M., 2012. Progress in Understanding Harmful Algal Blooms: Paradigm Shifts and New Technologies for Research, Monitoring, and Management. Ann. Rev. Mar. Sci. 4, 143–176. https://doi.org/doi:10.1146/annurev-marine-120308-081121

Bailey, S.W., Werdell, P.J., 2006. A multi-sensor approach for the on-orbit validation of ocean color satellite data products. Remote Sens. Environ. 102, 12–23.

Berra, E., Gibson-Poole, S., MacArthur, A., Gaulton, R., Hamilton, A., 2015. Estimation of the spectral sensitivity functions of un-modified and modified commercial off-the-shelf digital cameras to enable their use as a multispectral imaging system for UAVs. Int. Arch. Photogramm. Remote Sens. Spat. Inf. Sci. - ISPRS Arch. 40, 207–214. https://doi.org/10.5194/isprsarchives-XL-1-W4-207-2015

Bramich, J.M., Bolch, C.J.S., Fischer, A.M., 2018. Evaluation of atmospheric correction and high-resolution processing on SeaDAS-derived chlorophyll-a: an example from mid-latitude mesotrophic waters. Int. J. Remote Sens. 39, 2119–2138. https://doi.org/10.1080/01431161.2017.1420930

Bresciani, M., Cazzaniga, I., Austoni, M., Sforzi, T., Buzzi, F., Morabito, G., Giardino, C., 2018. Mapping phytoplankton blooms in deep subalpine lakes from Sentinel-2A and Landsat-8. Hydrobiologia 824, 197–214. https://doi.org/10.1007/s10750-017-3462-2

Bricaud, A., Morel, A., Babin, M., Allali, K., Claustre, H., 1998. Variations of light absorption by suspended particles with chlorophyll a concentration in oceanic (case 1) waters : Analysis and implications for bio-optical models Abstract . Spectral absorption coefficients of total particulate matter mg m-3). As pre. J. Geophys. Res. 103, 31033–31044.

Clark, J.M., Schaeffer, B.A., Darling, J.A., Urquhart, E.A., Johnston, J.M., Ignatius,

A.R., Myer, M.H., Loftin, K.A., Werdell, P.J., Stumpf, R.P., 2017. Satellite monitoring of cyanobacterial harmful algal bloom frequency in recreational waters and drinking water sources. Ecol. Indic. 80, 84–95. https://doi.org/10.1016/j.ecolind.2017.04.046

Dall'Olmo, G., Gitelson, A.A., 2005. Effect of bio-optical parameter variability on the remote estimation of chlorophyll-a concentration in turbid productive waters: experimental results. Appl. Opt. 44, 412–422.

Dall'Olmo, G., Gitelson, A.A., Rundquist, D.C., Leavitt, B., Barrow, T., Holz, J.C., 2005. Assessing the potential of SeaWiFS and MODIS for estimating chlorophyll concentration in turbid productive waters using red and near-infrared bands. Remote Sens. Environ. 96, 176–187. https://doi.org/10.1016/j.rse.2005.02.007

DPIF, 1997. Algal Biodiversity in Tasmanian Farm Dams and Reservoirs. Department of Primary Industry and Fisheries, Hobart.

Falconer, I.R., 2001. Toxic cyanobacterial bloom problems in Australian waters: risks and impacts on human health. Phycologia 40, 228–233. https://doi.org/10.2216/i0031-8884-40-3-228.1

Gilerson, A.A., Gitelson, A.A., Zhou, J., Gurlin, D., Moses, W.J., Ioannou, I., Ahmed, S.A., 2010. Algorithms for remote estimation of chlorophyll-a in coastal and inland waters using red and near infrared bands. Opt. Express 18, 24109–24125. https://doi.org/10.1364/OE.18.024109

Goddijn-Murphy, L., Dailloux, D., White, M., Bowers, D., Sciences, O., Sciences, L., Kaia, H., Bridge, M., 2009. Fundamentals of in Situ Digital Camera Methodology for Water Quality Monitoring of Coast and Ocean. Sensors 9, 5825–5843. https://doi.org/10.3390/s90705825

Gons, H.J., 1999. Optical teledetection of chlorophyll a in turbid inland waters. Environ. Sci. Technol. 33, 1127–1132.

Gons, H.J., Auer, M.T., Effler, S.W., Ef, S.W., 2008. MERIS satellite chlorophyll mapping of oligotrophic and eutrophic waters in the Laurentian Great Lakes. Remote Sens. Environ. 112, 4098–4106.

https://doi.org/http://dx.doi.org/10.1016/j.rse.2007.06.029

Gons, H.J., Rijkeboer, M., Ruddick, K.G., 2002. A chlorophyll-retrieval algorithm for satellite imagery (Medium Resolution Imaging Spectrometer) of inland and coastal waters. J. Plankton Res. 24, 947–951.

Gower, J., King, S., Borstad, G., Brown, L., 2005. Detection of intense plankton blooms using the 709 nm band of the MERIS imaging spectrometer. Int. J. Remote Sens. 26, 2005–2012. https://doi.org/10.1080/01431160500075857

Gower, J.F.R.R., Doerffer, R., Borstad, G.A., 1999. Interpretation of the 685 nm peak in water-leaving radiance spectra in terms of fluorescence, absorption and scattering, and its observation by MERIS. Int. J. Remote Sens. 20, 1771–1786. https://doi.org/10.1080/014311699212470

Ibelings, B.W., Backer, L.C., Kardinaal, W.E.A., Chorus, I., 2014. Current approaches to cyanotoxin risk assessment and risk management around the globe. Harmful Algae 40, 63–74. https://doi.org/10.1016/j.hal.2014.10.002

Klemas, V., 2012. Remote Sensing of Algal Blooms: An Overview with Case Studies. J. Coast. Res. 28, 34–43.

Koponen, S., Attila, J., Pulliainen, J., Kallio, K., Pyhälahti, T., Lindfors, A., Rasmus, K., Hallikainen, M., 2007. A case study of airborne and satellite remote sensing of a spring bloom event in the Gulf of Finland. Cont. Shelf Res. 27, 228–244. https://doi.org/10.1016/j.csr.2006.10.006

Krause, P., Boyle, D.P., Bäse, F., 2005. Comparison of different efficiency criteria for hydrological model assessment. Adv. Geosci. 5, 89–97. https://doi.org/10.5194/adgeo-5-89-2005

Kuhn, M., 2008. Building Predictive Models in R Using the caret Package. J. Stat. Softw. 28, 1–26. https://doi.org/10.1053/j.sodo.2009.03.002

Kutser, T., 2009. Passive optical remote sensing of cyanobacteria and other intense phytoplankton blooms in coastal and inland waters. Int. J. Remote Sens. 30, 4401–4425. https://doi.org/10.1080/01431160802562305

Kutser, T., Pierson, D.C., Kallio, K.Y., Reinart, A., Sobek, S., 2005. Mapping lake CDOM by satellite remote sensing. Remote Sens. Environ. 94, 535–540. https://doi.org/10.1016/j.rse.2004.11.009

Leeuw, T., 2014. Crowdsourcing Water Quality Data Using the iPhone Camera. Electron. Theses Diss. - Univ. Maine Paper 2118. https://doi.org/Paper 2118

Leeuw, T., Boss, E., 2018. The HydroColor app: Above water measurements of remote sensing reflectance and turbidity using a smartphone camera. Sensors (Switzerland) 18. https://doi.org/10.3390/s18010256

Matasaru, C., 2014. Mobile Phone Camera Possibilities for Spectral Imaging. Univ. East. Finland2014.

Mevik, B.-H., Wehrens, R., 2007. The pls Package: Principle Component and Partial Least Squares Regression in R. J. Stat. Softw. 18, 1–24. https://doi.org/10.1002/wics.10

Mishra, S., Mishra, D.R., 2012. Normalized difference chlorophyll index : A novel model for remote estimation of chlorophyll- a concentration in turbid productive waters. Remote Sens. Environ. 117, 394–406. https://doi.org/10.1016/j.rse.2011.10.016

Mobley, C.D., 1999. Estimation of the remote-sensing reflectance from above-surface measurements. Appl. Opt. 38, 7442–7455.

Morel, A., Prieur, L., 1977. Analysis of Variations in Ocean Color. Limnol. Oceanogr. 22, 709–722. https://doi.org/10.2307/2835253

Moses, W.J., Gitelson, A.A., Berdnikov, S., Saprygin, V., Povazhnyi, V., 2012. Operational MERIS-based NIR-red algorithms for estimating chlorophyll-a concentrations in coastal waters - The Azov Sea case study. Remote Sens. Environ. 121, 118–124. https://doi.org/10.1016/j.rse.2012.01.024

Mylvaganam, S., Jakobsen, T., 1998. Turbidity sensor for underwater applications. IEEE Ocean. Eng. Soc. Ocean. Conf. Proc. (Cat. No.98CH36259), Ocean. ’98 Conf. Proc. VO - 1 158. https://doi.org/10.1109/OCEANS.1998.725727

O'Reilly, J.E., Maritorena, S., Siegel, D.A., O'Brien, M.C., Toole, D., Mitchell, B.G., Kahru, M., Chavez, F.P., Strutton, P., Cota, G.F., 2000. Ocean color chlorophyll a algorithms for SeaWiFS, OC2, and OC4: Version 4. SeaWiFS postlaunch calibration Valid. Anal. Part 3, 9–23.

Olmanson, L.G.L.G., Brezonik, P.L.P.L., Finlay, J.C., Bauer, M.E.M.E., 2016. Comparison of Landsat 8 and Landsat 7 for regional measurements of CDOM and water clarity in lakes. Remote Sens. Environ. 185, 119–128. https://doi.org/10.1016/j.rse.2016.01.007

Palmer, S.C.J., Kutser, T., Hunter, P.D., 2015. Remote sensing of inland waters: Challenges, progress and future directions. Remote Sens. Environ. 157, 1–8. https://doi.org/10.1016/j.rse.2014.09.021

Tasmanian Irrigation, 2019. South East Stage 1 [WWW Document]. URL https://www.tasmanianirrigation.com.au/schemes/south-east-stage-1 (accessed 2.1.19).

World Health Organization, 1999. Toxic Cyanobacteria in Water: A guide to their public health consequences, monitoring and management, Retrieved March. https://doi.org/10.1046/j.1365-2427.2003.01107.x

Yang, Y., Cowen, L.L.E., Costa, M., 2018. Is ocean reflectance acquired by citizen scientists robust for science applications? Remote Sens. 10, 1–18. https://doi.org/10.3390/rs10060835

6 Synthesis

6.1 Thesis Outcomes

Chl-a is an indicator of algal biomass and as such, remote sensing of chl-a can aid in the monitoring and detection of high biomass harmful algal blooms (HAB). HAB events can have high spatial variability (Foster et al., 2017; Kutser, 2009) and the use of satellite remote sensing to complement existing *in-situ* and manual detection and monitoring has been suggested (Anderson et al., 2017; Klemas, 2012; Kutser, 2009; Palmer et al., 2015; Urquhart et al., 2017). However, satellite platforms designed for maritime applications are limited in terms of spatial resolution (Clark et al., 2017; Palmer et al., 2015). The preceding chapters have examined the capability of different sensor platforms to provide remote estimates of chl-a at a variety of spatial resolutions.

In chapter 2, the effect of the SeaDAS high resolution processing mode on chl-a retrievals was examined for a variety of atmospheric correction methods and chl-a algorithms in Tasmanian coastal waters. Spatial resolution, clouds and atmospheric correction were all identified as challenges to monitoring these socially and economically important waters using the MODIS platform. Attempts to improve the native spatial resolution to a pixel size of 250 metres using the high-resolution processing had a negative effect on chl-a retrievals and resulted in more negative reflectances, pointing to more problematic atmospheric correction. The sensor platforms examined in the subsequent chapters make some progress towards meeting these challenges.

Chapter 3 and chapter 4 evaluated two medium resolution satellite platforms, the Sentinel 2 MSI and the Landsat 8 OLI for chl-a retrievals. These platforms are not primarily designed for water monitoring but with spatial resolutions of 10 to 60 m and 30 m respectively, they are an appealing alternative for smaller water bodies. The

Sentinel 2 MSI was superior to the Landsat 8 OLI for chl-a retrievals. From Sentinel 2 imagery, the three band semi-analytic algorithm (Gons et al., 2005) modified with a dynamic model for chl-a specific absorption coefficient (Gilerson et al., 2010) achieved a NRMSEP of 7.5% and a NSE of 0.90 compared to NRMSEP of 21.6% and an NSE of 0.53 for the PLSR model with band ratio inputs from Landsat 8 imagery. This is not surprising given the lack an OLI band around 700 nm in wavelength. Ratios of bands either side of 700 nm have been shown to be well correlated with chl-a (Song et al., 2013). Given that the Sentinel 2 constellation offers better spatial resolution in the relevant bands and a revisit time of 5 days (ESA, 2018a), compared to 16 days for Landsat 8 (USGS, 2016), it is hard to find a compelling reason to recommend OLI for active bloom detection and monitoring.

In chapter 5, PLSR was used to develop a chl-a algorithm for the HydroColor mobile device app (Leeuw and Boss, 2018). Use of the remote sensing reflectances derived by the HydroColor app for chl-a retrievals were only moderately encouraging. The relatively narrow range of chl-a concentrations in the *in-situ* dataset proved challenging to detect using the three broad visible bands available. Given the range of chl-a concentrations encountered is where the chl-a specific absorption coefficient is most variable (Bricaud et al., 1995; Gilerson et al., 2010), it is reasonable to expect that a greater range of *in-situ* values would lead to improved modelling. Benefits of pursuing such algorithm development include speed of detection and an increase in monitoring capacity. The cost of even high-end digital cameras is small compared to that of sondes such as the EXO2, or hyperspectral cameras.

6.2 Implications of results

HABs pose risks to human and animal health (Anderson et al., 2012; Ibelings et al., 2014; World Health Organization, 1999) and the economic costs associated with detection, monitoring and managing the impacts HAB events is billions of United States dollars globally (Sanseverino et al., 2016). Recent years have seen HAB events increase in both coastal waters and inland waters (Anderson et al., 2012; Paerl and Otten, 2013) and this is likely to continue, aided by a globally changing climate (Paerl et al., 2011). While remote sensing of chl-a alone cannot determine if an algal bloom is harmful or not, improved accuracy and spatial resolution of chl-a retrievals will improve an important tool in assisting water managers in the detection and monitoring of such threats (Beck et al., 2016).

The improved semi-analytical algorithm (Gons, 1999; Gons et al., 2008, 2005, 2002) developed for Sentinel 2 MSI imagery could be extended to any platform with appropriate band positioning. The ocean and land colour instrument (OLCI) on the Sentinel 3 satellites has bands centred at 665 nm, 708 nm and several bands located between 750 nm and 780nm. The bandwidths of these bands in the order of half that of the equivalent MSI bands (ESA, 2018b, 2018a) and it is reasonable to expect the improved algorithm to also deliver good results on that platform. Whilst the 300 m spatial resolution of OLCI is inferior to the MSI, it has a revisit time of less than two days which would allow improved temporal coverage of waters where the lower spatial resolution was sufficient. Finally, OLCI has a narrow red band centred at 620 nm which raises the potential for remote sensing of phycocyanin, an accessory pigment found in cyanobacteria (Mishra et al., 2013; Ogashawara et al., 2013; Randolph et al., 2008).

The ability to use a single platform for the estimation of both chl-a and phycocyanin could enable differentiation of cyanobacteria blooms from those of other algal types.

An effective chl-a algorithm for use with digital cameras would lead to the ability to monitor water bodies with UAV mounted cameras. This would potentially allow sufficient spatial resolution for the coverage of virtually any water body of interest. UAVs have the computational power to acquire imagery at the correct geometry. Some camera sensors now include a white pixel (Kim and Kang, 2018), which should allow relative reflectance to be calculated without the need for a skyward facing image. Camera imagery would require adjustments for the effects of vignetting and atmosphere (Aasen et al., 2018) however these effects would be small compared to those encountered by satellite mounted sensors.

Regardless of the platform, remote sensing of chl-a does not represent a replacement for traditional *in-situ* monitoring regimes. There are still challenges in determining the algal type and toxicity from satellite data (Kutser, 2009): it is difficult to distinguish between phytoplankton taxa (Dierssen et al., 2006), toxin producing species may be present but in a non-toxic state and some species may be toxic at levels below remote detection thresholds (Stumpf and Tomlinson, 2005). Rather, the creation of integrated networks that include remote sensing data alongside in-situ observations of water quality and environmental parameters have been suggested (Anderson et al., 2017; Jochens et al., 2010; Shen et al., 2012). Remote sensing data could make manual sampling regimes more responsive and efficient by identifying locations of high priority. Long term patterns could inform the positioning of *in-situ* instrumentation. Such integrated networks could in turn allow for a continuous revalidation, if needed, recalibration of remote sensing models.

6.3 Recommendations for future research

The outcomes discussed in previous sections, in particular the improved semi-analytical algorithm and the potential of the PLSR chl-a algorithm for the HydroColor app would benefit from additional research.

The chl-a specific absorption coefficient model (Gilerson et al., 2010) selected in chapter 4 resulted in improved performance of the semi-analytic chl-a retrieval algorithm (Gons, 1999) when used in place of the default fixed value. While this model generalised well to a third location, the ubiquity of this relationship should be further evaluated. Given the variable nature of chl-a specific absorption (Ahn et al., 1992; Bricaud et al., 1995; Sathyendranath et al., 1987) the extent of its applicability must be further evaluated. If multiple models are found to be optimal, for example between marine and inland waters, then it may be possible to determine from the spectral signatures of the water which model to apply.

The PLSR algorithm used in chapter 5 relied on the assumption, as assumed in semi-analytical algorithm development (Dall'Olmo and Gitelson, 2005; Gons, 1999), that the primary optically active constituents in water, aside from water itself, were phytoplankton, CDOM and suspended sediments (Gordon et al., 1988). Adding explanatory variables for phytoplankton (chl-a), CDOM and suspended sediments (turbidity) moderately improved performance when compared to use of the ratio of blue to green reflectances alone. However, it is not clear as to whether the performance of this approach was limited by the explanatory power of the inputs selected, or the lack of variability in the *in-situ* dataset. If the latter were the limiting factor on performance, then this approach is worthy of further investigation on an expanded dataset. Additionally, inexpensive cameras are available that do not block infrared light from

the sensor (Raspberry Pi Foundation, 2019) which raise the potential of using a pair of cameras and a narrow pass filter to obtain in addition to red, blue and green, a NIR channel which seems so useful in chl-a retrievals (Song et al., 2013).

6.4 References

Aasen, H., Honkavaara, E., Lucieer, A., Zarco-Tejada, P.J., 2018. Quantitative remote sensing at ultra-high resolution with UAV spectroscopy: A review of sensor technology, measurement procedures, and data correctionworkflows. Remote Sens. 10, 1–42. https://doi.org/10.3390/rs10071091

Ahn, Y.-H.H., Bricaud, A., Morel, A., 1992. Light backscattering efficiency and related properties of some phytoplankters. Deep Sea Res. Part A, Oceanogr. Res. Pap. 39, 1835–1855. https://doi.org/10.1016/0198-0149(92)90002-B

Anderson, D.M., Boerlage, S.F.E., Dixon, M.B., 2017. Harmful Algal Blooms (HABs) and Desalination : A Guide to Impacts, Monitoring , and Management.

Anderson, D.M., Cembella, A.D., Hallegraeff, G.M., 2012. Progress in Understanding Harmful Algal Blooms: Paradigm Shifts and New Technologies for Research, Monitoring, and Management. Ann. Rev. Mar. Sci. 4, 143–176. https://doi.org/doi:10.1146/annurev-marine-120308-081121

Beck, R., Zhan, S., Liu, H., Tong, S., Yang, B., Xu, M., Ye, Z., Huang, Y., Shu, S., Wu, Q., Wang, S., Berling, K., Murray, A., Emery, E., Reif, M., Harwood, J., Young, J., Nietch, C., Macke, D., Martin, M., Stillings, G., Stump, R., Su, H., 2016. Comparison of satellite reflectance algorithms for estimating chlorophyll-a in a temperate reservoir using coincident hyperspectral aircraft imagery and dense

coincident surface observations. Remote Sens. Environ. 178, 15–30. https://doi.org/10.1016/j.rse.2016.03.002

Bricaud, A., Babin, M., Morel, A., Claustre, H., 1995. Variability in the chlorophyll-specific absorption coefficients of natural phytoplankton: Analysis and parameterization. J. Geophys. Res. 100, 332,13313-13321.

Clark, J.M., Schaeffer, B.A., Darling, J.A., Urquhart, E.A., Johnston, J.M., Ignatius, A.R., Myer, M.H., Loftin, K.A., Werdell, P.J., Stumpf, R.P., 2017. Satellite monitoring of cyanobacterial harmful algal bloom frequency in recreational waters and drinking water sources. Ecol. Indic. 80, 84–95. https://doi.org/10.1016/j.ecolind.2017.04.046

Dall'Olmo, G., Gitelson, A.A., 2005. Effect of bio-optical parameter variability on the remote estimation of chlorophyll-a concentration in turbid productive waters: experimental results. Appl. Opt. 44, 412–422.

Dierssen, H.M., Kudela, R.M., Ryan, J.P., Zimmerman, R.C., 2006. Red and black tides: Quantitative analysis of water-leaving radiance and perceived color for phytoplankton, colored dissolved organic matter, and suspended sediments. Limnol. Oceanogr. 51, 2646–2659. https://doi.org/10.4319/lo.2006.51.6.2646

ESA, 2018a. SENTINEL-2 User Guide [WWW Document]. URL https://sentinel.esa.int/web/sentinel/user-guides/sentinel-2-msi (accessed 12.4.18).

ESA, 2018b. User Guides - Sentinel 3 OLCI [WWW Document]. URL https://sentinel.esa.int/web/sentinel/user-guides/sentinel-3-olci (accessed 9.14.18).

Foster, G.M., Graham, J.L., Stiles, T.C., Boyer, M.G., King, L.R., Loftin, K.A., 2017.

Spatial variability of harmful algal blooms in Milford Lake, Kansas, July and August 2015. US Geological Survey. https://doi.org/https://doi.org/10.3133/sir20165168

Gilerson, A.A., Gitelson, A.A., Zhou, J., Gurlin, D., Moses, W.J., Ioannou, I., Ahmed, S.A., 2010. Algorithms for remote estimation of chlorophyll-a in coastal and inland waters using red and near infrared bands. Opt. Express 18, 24109–24125. https://doi.org/10.1364/OE.18.024109

Gons, H.J., 1999. Optical teledetection of chlorophyll a in turbid inland waters. Environ. Sci. Technol. 33, 1127–1132.

Gons, H.J., Auer, M.T., Effler, S.W., Ef, S.W., 2008. MERIS satellite chlorophyll mapping of oligotrophic and eutrophic waters in the Laurentian Great Lakes. Remote Sens. Environ. 112, 4098–4106. https://doi.org/http://dx.doi.org/10.1016/j.rse.2007.06.029

Gons, H.J., Rijkeboer, M., Ruddick, K.G., 2005. Effect of a waveband shift on chlorophyll retrieval from MERIS imagery of inland and coastal waters. J. Plankton Res. 27, 125–127. https://doi.org/10.1093/plankt/fbh151

Gons, H.J., Rijkeboer, M., Ruddick, K.G., 2002. A chlorophyll-retrieval algorithm for satellite imagery (Medium Resolution Imaging Spectrometer) of inland and coastal waters. J. Plankton Res. 24, 947–951.

Gordon, H.R., Brown, O.B., Evans, R.H., Brown, J.W., Smith, R.C., Baker, K.S., Clark, D.K., Herrine, S.K., Michael, B., Ma, W.L., Rossi, S., Dunn, S.R., Hyslop, T., 1988. A semianalytic radiance model of ocean color. J. Geophys. Res. Atmos. 93, 10909–10924. https://doi.org/10.1029/JD093iD09p10909

Ibelings, B.W., Backer, L.C., Kardinaal, W.E.A., Chorus, I., 2014. Current approaches to cyanotoxin risk assessment and risk management around the globe. Harmful Algae 40, 63–74. https://doi.org/10.1016/j.hal.2014.10.002

Jochens, A.E., Malone, T.C., Stumpf, R.P., Hickey, B.M., Morrison, R., Dyble, J., Jones, B., Trainer, V.L., Carter, M., Morrison, R., Dyble, J., Jones, B., Trainer, V.L., 2010. Integrated ocean observing system in support of forecasting harmful algal blooms. Mar. Technol. Soc. J. 44, 99–121.

Kim, J., Kang, M.G., 2018. Color Interpolation Algorithm for the Sony-RGBW Color Filter Array. Electron. Imaging 2018, 1–4. https://doi.org/10.2352/ISSN.2470-1173.2018.13.IPAS-439

Klemas, V., 2012. Remote Sensing of Algal Blooms: An Overview with Case Studies. J. Coast. Res. 28, 34–43.

Kutser, T., 2009. Passive optical remote sensing of cyanobacteria and other intense phytoplankton blooms in coastal and inland waters. Int. J. Remote Sens. 30, 4401–4425. https://doi.org/10.1080/01431160802562305

Leeuw, T., Boss, E., 2018. The HydroColor app: Above water measurements of remote sensing reflectance and turbidity using a smartphone camera. Sensors (Switzerland) 18. https://doi.org/10.3390/s18010256

Mishra, S., Mishra, D.R., Lee, Z., Tucker, C.S., 2013. Quantifying cyanobacterial phycocyanin concentration in turbid productive waters: A quasi-analytical approach. Remote Sens. Environ. 133, 141–151. https://doi.org/http://dx.doi.org/10.1016/j.rse.2013.02.004

Ogashawara, I., Mishra, D.R., Mishra, S., Curtarelli, M.P., Stech, J.L., 2013. A performance review of reflectance based algorithms for predicting phycocyanin concentrations in inland waters. Remote Sens. 5, 4774–4798.

Paerl, H.W., Hall, N.S., Calandrino, E.S., 2011. Controlling harmful cyanobacterial blooms in a world experiencing anthropogenic and climatic-induced change. Sci. Total Environ. 409, 1739–1745. https://doi.org/10.1016/j.scitotenv.2011.02.001

Paerl, H.W., Otten, T.G., 2013. Harmful Cyanobacterial Blooms: Causes, Consequences, and Controls. Microb. Ecol. 65, 995–1010. https://doi.org/10.1007/s00248-012-0159-y

Palmer, S.C.J., Kutser, T., Hunter, P.D., 2015. Remote sensing of inland waters: Challenges, progress and future directions. Remote Sens. Environ. 157, 1–8. https://doi.org/10.1016/j.rse.2014.09.021

Randolph, K., Wilson, J., Tedesco, L., Li, L., Pascual, D.L., Soyeux, E., 2008. Hyperspectral remote sensing of cyanobacteria in turbid productive water using optically active pigments, chlorophyll a and phycocyanin. Remote Sens. Environ. 112, 4009–4019. https://doi.org/http://dx.doi.org/10.1016/j.rse.2008.06.002

Raspberry Pi Foundation, 2019. Pi NoIR Camera V2 [WWW Document]. URL https://www.raspberrypi.org/products/pi-noir-camera-v2/ (accessed 2.12.19).

Sanseverino, I., Conduto, D., Pozzoli, L., Dobricic, S., Lettieri, T., 2016. Algal bloom and its economic impact. https://doi.org/10.2788/660478

Sathyendranath, S., Lazzara, L., Prieur, L., 1987. Variations in the spectral values of specific absorption of phytoplankton 32.

Shen, L., Xu, H., Guo, X., 2012. Satellite remote sensing of harmful algal blooms (HABs) and a potential synthesized framework. Sensors (Basel) 12, 7778–7803. https://doi.org/10.3390/s120607778

Song, K., Li, L., Tedesco, L.P., Li, S., Duan, H., Liu, D., Hall, B.E., Du, J., Li, Z., Shi, K., Zhao, Y., 2013. Remote estimation of chlorophyll-a in turbid inland waters: Three-band model versus GA-PLS model. Remote Sens. Environ. 136, 342–357. https://doi.org/10.1016/j.rse.2013.05.017

Stumpf, R.P., Tomlinson, M.C., 2005. Remote sensing of harmful algal blooms, in: Remote Sensing of Coastal Aquatic Environments. Springer, pp. 277–296.

Urquhart, E.A., Schaeffer, B.A., Stumpf, R.P., Loftin, K.A., Werdell, P.J., 2017. A method for examining temporal changes in cyanobacterial harmful algal bloom spatial extent using satellite remote sensing. Harmful Algae 67, 144–152. https://doi.org/10.1016/j.hal.2017.06.001

USGS, 2016. Landsat 8 (L8) Data Users Handbook, America.

World Health Organization, 1999. Toxic Cyanobacteria in Water: A guide to their public health consequences, monitoring and management, Retrieved March. https://doi.org/10.1046/j.1365-2427.2003.01107.x

Appendix A:

Published version of chapter 2

Bramich, J. M., Bolch, C. J. S., Fischer, A. M., 2018. Evaluation of atmospheric correction and high-resolution processing on SeaDAS-derived chlorophyll-a: an example from mid-latitude mesotrophic waters. International Journal of remote sensing, 39(8), 2119-2138